GEMS & GEMOLOGY

WINTER 2012
VOLUME XLVIII

THE QUARTERLY JOURNAL OF THE GEMOLOGICAL INSTITUTE OF AMERICA

Natural, Cultured *Pinctada Maxima* Pearls

Magnetism of HPHT Synthetic Diamond

Color Origin of Lavender Jadeite

GEMS & GEMOLOGY

Winter 2012
VOLUME 48, No. 4

pg. 247

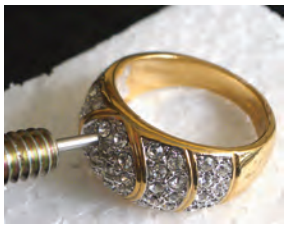

pg. 268

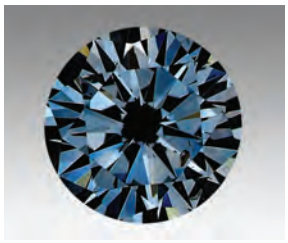

pg. 305

Editorial

Feature Articles

Notes and New Techniques

Regular Features

GEMS & GEMOLOGY

gia.edu/gandg

Subscriptions
Copies of the current issue may be purchased for $29.95 plus shipping. Subscriptions are $79.99 for one year (4 issues) in the U.S. and $99.99 elsewhere. Canadian subscribers should add GST. Discounts are available for group subscriptions, GIA alumni, and current GIA students. For institutional rates, contact the Managing Editor. Subscriptions include *G&G*'s monthly gemological e-newsletter, the *G&G eBrief*.

To purchase subscriptions and single issues (print or PDF), visit store.gia.edu or contact Customer Service.

PDF versions of individual articles and sections from Spring 1981 forward can be purchased at gia.metapress.com for $12 each. Visit gia.edu/gandg for free online access to the 1934–2011 subject and author indexes and all 1934–1980 issues.

Database Coverage
Gems & Gemology is abstracted in Thomson Reuters products (Current Contents: Physical, Chemical & Earth Sciences and Science Citation Index—Expanded, including the Web of Knowledge) and other databases. For a complete list of sources abstracting *G&G*, go to gia.edu/gandg.

Manuscript Submissions
Gems & Gemology welcomes the submission of articles on all aspects of the field. Please see the Guidelines for Authors at gia.edu/gandg or contact the Managing Editor. Letters on articles published in *Gems & Gemology* are also welcome.

Gems & Gemology is published quarterly by the Gemological Institute of America, a nonprofit educational organization for the gem and jewelry industry.

Postmaster: Return undeliverable copies of *Gems & Gemology* to GIA, The Robert Mouawad Campus, 5345 Armada Drive, Carlsbad, CA 92008.

Our Canadian goods and service registration number is 126142892RT.

About the Cover

The lead article in this issue, by Kenneth Scarratt and coauthors, reviews the colorful history of natural pearling in Australian waters. The second part of the article examines methods to differentiate between natural pearls from the Pinctada maxima *mollusk and those that are accidental by-products of the culturing process. Shown on the cover are the eight natural pearls from* P. maxima *examined for this study, set against mother-of-pearl from one of the shell specimens. Courtesy of Paspaley Pearling Co. Photos by Robert Weldon.*

Printing is by Allen Press, Lawrence, Kansas.
GIA World Headquarters The Robert Mouawad Campus 5345 Armada Drive Carlsbad, CA 92008 USA

ISSN 0016-626X

Thank You

In our final issue for 2012, I'd like to take a moment to say "Thank you" to our readers, contributors, and manuscript reviewers for another successful year of *Gems & Gemology*—we could not have done it without you!

Pearls are the headliners for this winter issue. In the lead article, Kenneth Scarratt, managing director of GIA in Thailand and a noted pearl expert, explores the fascinating history of pearling in Australian waters for the prized natural pearls from the *Pinctada maxima* mollusk. The second part of the article looks at the properties of those natural gems that might separate them from samples accidentally produced during the culturing process. This is followed by a pair of articles on South Sea cultured pearls, which also come from the *Pinctada maxima* mollusk. Youngchool Kim offers a study on identifying silver irradiated South Sea cultured pearls using electron spin resonance spectroscopy, while Chunhui Zhou investigates dye treatment in the yellow or "golden" variety.

In other articles: Kirk Feral tests the effectiveness of a handheld magnet in detecting HPHT-grown synthetic diamonds, and Ren Lu examines the color origin of lavender jadeite using quantitative spectroscopy and trace-element analysis.

I look forward to another year of presenting the latest research in the fascinating world of gemology...

And as with every issue, our team of Lab Notes and Gem News International correspondents from around the world report on the latest discoveries and developments.

With that, I look forward to another year of presenting the latest research in the fascinating world of gemology, both in this familiar printed form of G&G and as we continue to build our presence in the digital realm.

Cheers,

Jan Iverson | Editor-in-Chief | jan.iverson@gia.edu

NATURAL PEARLS FROM AUSTRALIAN *PINCTADA MAXIMA*

Kenneth Scarratt, Peter Bracher, Michael Bracher, Ali Attawi, Ali Safar, Sudarat Saeseaw, Artitaya Homkrajae, and Nicholas Sturman

The fascinating and colorful history of natural pearling in Australian waters is presented, from the early six-man luggers to the large ships in modern fleets where pearl culture has been the focus for the past several decades. For the scientific investigation of this paper, the authors retrieved natural pearls from wild *Pinctada maxima* in Australian waters and recorded the various properties that might help to differentiate between natural pearls from this mollusk and those that are accidental by-products of the culturing process. Three distinct categories of host *Pinctada maxima* shells and mantle pearls were collected and examined by the authors: (1) from wild shell prior to any pearl culturing operation, (2) from wild shell after pearl culturing and approximately two years on the farm, and (3) from hatchery-reared shell prior to pearl culturing. Data were collected from microscopy, X-rays of internal structures (using real-time microradiography and X-ray computed microtomography, various forms of spectroscopy, and LA-ICP-MS chemical analysis. The results showed that microradiographic structures previously considered indicative of an accidentally cultured *P. maxima* pearl may not be conclusive, and that such criteria should only be applied with the utmost caution by an experienced technician.

According to Cilento (1959), natural pearls have been found off the western and northern coasts of Australia since well before European settlement in the early 19th century. Coastal-dwelling Aborigines and fishermen from Sulawesi had collected and traded pearl shell for possibly hundreds of years.

> The pearling industry in Queensland dates from 1868, when Captain William Banner, of the Sydney brig Julia Percy fished the first cargo of pearl shell from Warrior Reef. Captain Banner noticed the natives preparing for a dance, and saw they had big mother-of-pearl pendants round their necks. He made a bargain with Kebisu, mamoose (chief) of the headhunters of Tutu, who, for generations, raided the islands of Torres Strait in their great war canoes.
>
> Perhaps the menace of Banner's shotted fore and aft guns, which could far outrange the eight-foot bows and barbed arrows of the black bowmen of Tutu, had something to do with the friendliness of the blood-thirsty and crafty Kebisu and his headhunters. In return for tomahawks and iron—the most valuable things in their eyes—they gave Capt. Banner as much as he wanted of what they considered the common and relatively valueless pearl shell and pearls.
>
> Capt. Banner and his crew won a rich harvest from the coral sea, for pearl shell was then worth £150 a ton in Sydney; and Banner collected many large pearls. (Cilento, 1959)

Pearling, particularly for the recovery of natural pearls from the most remarkable of all pearl oysters—*Pinctada maxima*—in the adventure-strewn waters off the Australian coast, has a diverse and fascinating history. This history may be eyed through the literary skills of authors such as E.W. Streeter and Louis Kornitzer, who hailed from a time when natural pearls were objects of great value and wrote about them with passion and wonder.

As one delves into the history of pearling in this region, it is difficult not to become wrapped up in a wondrous web of adventure and intrigue, danger from every conceivable corner, and the ecstasy of the ultimate find: a lustrous sphere, perhaps with that smoothly flattened side that gives it the shape of a button, or slightly elongated to form a teardrop, exposed within the mantle with the gills glinting behind it, the curtained backdrop to this pearl's debut on the world's stage (figure 1).

See end of article for About the Authors and Acknowledgments.
GEMS & GEMOLOGY, Vol. 48, No. 4, pp. 236–261,
http://dx.doi.org/10.5741/GEMS.48.4.236.

Figure 1. A natural round 6.04 × 5.93 mm pearl sits within the mantle of a P. maxima *pearl oyster, whose gills provide a dramatic backdrop to one of nature's great miracles. Photo by K. Scarratt.*

Kornitzer takes us on a helter-skelter ride through his journeys from Singapore down through the island realms that encase the Java, Banda, Celebes, and Timor Seas and ultimately into those wild waters that run from Exmouth Gulf and up through Broome and on to Darwin. His stories are the very epitome of boyhood adventure dreams, leaping from the pages to convince the reader that "a pearling he must go":

> It was as a humble young dealer in Hatton Garden that the urge to adventure came to me, that strong, compelling urge like a kick in the pants, which is produced by the fact that one's family is hungry and growing. I had a chance to go pearl-hunting in the tough pearling grounds in North-Western Australia, and I took it. From Australia the chase for pearls led me in half a lifetime all around the world, but I was a stone that rolled slowly enough to gather a minute quantity of moss. At any rate, I have never regretted it. One looks back with a strange satisfaction on the lonely and risky periods of one's life.
>
> As I was the first white trader ever to penetrate into the pearl fisheries of the Sulu Seas, I still have a proprietary feeling about that part of the world. (Kornitzer, 1947a)

These stories are eloquently told and retold in books such as Hurley's *Pearls and Savages* (1924), Berge and Lanier's *Pearl Diver* (1930), Benham's *Diver's Luck* (1949), and Bartlett's *The Pearl Seekers* (1954). Each work adds yet another layer of intrigue to an incredible adventure.

Lately, other highly informative and passionate accounts of Australian pearling have emerged. Two of particular note are *The Last Pearling Lugger: A Pearl Diver's Story* (Dodd, 2011) and *The Pearls of Broome: The Story of TB Ellies* (Ellies, 2010). Dodd's book brings the reader up to the early 1980s, when the luggers (figure 2) left service in favor of the much larger vessels in use today. The latter work recounts the incredible story of the Sri Lankan immigrant T.B. Ellies, who was one of the world's finest "pearl doctors" of the late 19th century. Practitioners of this lost art enhanced the appearance of a pearl by carefully removing blemishes on the outer layers.

Like many others in the Australian pearling industry, Ellies made his home in the town of Broome (figure 3). Activity had initially centered around Nickol

Figure 2. The men on deck of this lugger, at anchor in Darwin harbor in 1897, give scale to the small size of the vessel, which had cramped quarters for a six-man crew at sea for weeks at a time. Courtesy of Paspaley Pearling Co.

Figure 3. An early 20th century dealer in Broome sorts his natural pearls. Courtesy of Paspaley Pearling Co.

Bay and Exmouth Gulf, but by 1910 Broome was the largest pearling center in the world. Indeed, pearling remains an important part of the Western Australian economy, albeit largely through the cultured market.

In the mid-1880s, the famed English jeweler, entrepreneur, and author E.W. Streeter moved to Broome with his son (G.S. Streeter, a prolific author in his own right) and became heavily involved in pearling. By 1890, the elder Streeter had acquired significant property on the outskirts of the town, establishing a general store and owning one-eighth of the pearling fleet. Renowned for his great work *Pearls and Pearling Life* (1886) among others, he is also credited with the introduction of hard-hat diving. Indeed, the Streeter name is indelibly linked with the chronicles of this great pearling town (figure 4; Smith and Devereux, 1999).

Lennon (1934) describes hard-hat diving as one of the "world's most dangerous occupations." He notes, "Divers may work up to 30 fathoms [180 ft], but 22 fathoms is the average depth to which they descend. After bottoming the diver is pulled up a couple of feet and permits himself to be towed along by the lugger. Sighting shell, he signals to his tender, who lets him drop." Wearing an extremely cumbersome helmet and boots, the diver "works kneeling on his right knee and gathering with his right hand, taking good care to keep his head erect. If his head gets down, the air in his dress may shift and he would shoot aloft, feet first." Not recommended, as the normal method of ascending is to haul up the diver very gradually before surfacing, thus avoiding potentially fatal divers' paralysis, commonly known as "the bends."

Beyond the romance of the written word, early pearling in the region may somewhat be likened to the American "Wild West," as witnessed by fisheries inspector Pemberton Walcott. In his report covering the period from April 15 to June 30, 1881, he writes

> I have on good private information the following, which will require immediate investigation. During last pearling season, the majority of the fleet being at anchor in or near LaGrange Bay, three bush natives were killed by some De Grey River pearling natives; some time, days after, the bush natives retaliated by killing some De Grey pearlers (two or three), when the latter mustered in force, and in fact seem to have organized an expedition and followed the natives up, slaying all they surprised. I have reason to believe twenty to thirty were killed.

His report concludes

> It frequently occurs that, in holding any communication with the shore, a vessel has to run up creeks and is left high and dry at low water, so at the mercy of the natives, and no white man should land without means of protecting himself, for it may and does frequently happen that however friendly natives be at one time they maybe [*sic*] found hostile and troublesome at another, in consequence perhaps of some act which they may consider themselves bound to avenge. (Walcott, 1881)

The data provided in a report on North Western

Figure 4. This photo shows Streeter's Jetty, where the pearling luggers would unload their haul and scrape the keels of barnacles at low tide. The jetty was restored and reopened in 2001 as a community project to preserve the heritage of Broome. Photo by K. Scarratt.

TABLE 1. Value of pearl shell recovered from Western Australia, 1889–1898 (from Gale, 1901).

Year	Weight of mother-of-pearl (*P. maxima* shell) gathered		Value
	Tons	CWT (Hundredweight)	Pounds (sterling)
1889	744	10	74,450
1890	702	10	70,250
1891	749	-	89,880
1892	781	9	78,471
1893	540	17	35,499
1894	422	15	57,997
1895	352	14	26,258
1896	362	8	30,160
1897	366	-	38,630
1898	538	6	76,586
Shell total	5,556		578,181
Pearl total			**300,000**
Shell + Pearl total value at 1910			**878,181**
Shell + Pearl adjusted total £ value at 2011			**£82,259,214**
Shell + Pearl adjusted total US$ value at 2011			**US$127,273,557**

Australia's pearling industry to the attorney general by the chief inspector of fisheries (Gale, 1901) explain why intrepid adventurers came to such remote and often inhospitable places. Between 1889 and 1898, some 5,556 tons of pearl shell with a value of £587,181 were "declared" (table 1). While the annual haul fell between the beginning and end dates, the actual monetary amount rose slightly.

Gale's report also provides some insight into the pearling industry of the time. He noted that during the year from June 30, 1900, 177 boats were officially licensed. This represented a total tonnage of 2,480 tons, with the 159 luggers averaging 10 tons each. The 18 schooners, employed mainly as supply vessels and as storage for shell haul, ranged from 30 to 100 tons. Gale noted that each lugger carried a crew of six, with the diver in command. He added that a large amount of capital had been invested in each lugger: an average of £550 (£51,500 or approximately US$80,000 in 2011, adjusted for inflation) for a fully outfitted vessel. The approximate value of the fleet was £8.19 million, or US$12.7 million today.

Gale also provides us with some interesting asides concerning the value of pearls recovered during this period. He notes (as did other authors of the period) the difficulty of estimating this value from the quantity of pearl collected, due to heavy illicit trading of *snide*.[1] But taking figures from the statistical register for the previous 10 years, he estimates the value to be £300,000, or £28,101,000 today. He comments that these large numbers were somewhat offset by the costly expenditures involved: The average amount paid to the crew of each lugger was about £220, not including a £20 bonus to the diver for every ton of shell collected.

Kornitzer (1937) brings to vivid life the world of snide pearl trading in Broome in recounting one of his experiences. While fishing off the "long Wooden Pier" (probably referring to what is now known as Streeter's Jetty; figure 4), he is approached by a smuggler named Da Silva, who tells him:

> *Master, you buy fifty-grain round pearl, oh such a beautiful thing – you got thousand pounds in your pockit? If not I trust you. Master, you can sell it for two thousand for sure. I've got her here, you like to see?*

To control the shady business of snide, one P. Percy designed a box (patented in 1910) to securely hold any pearls found by the shell openers onboard the luggers. Pearls were placed in the box (figure 5) through a round hole in the top. The pearls went into the box along a "bent tube." The bend in the tube ensured that even if the box were tipped upside-down, the pearls would remain inside. All pearls recovered would be placed in the locked box for delivery to the owner upon docking.

In reality, the skipper had little time for monitoring what went into the box and what did not. His primary concerns were the navigation of the vessel and the safety of the divers. It was therefore more of an

Figure 5. Percy's patented box is used to store recovered natural pearls on the deck of this pearling lugger. Note the red cap over the opening and the padlock on the door at the front of the box. Photo courtesy of Paspaley Pearling Co.

[1]The term for pearls that were smuggled from the lugger, usually by shell openers, and then sold clandestinely.

Figure 6. The Japanese cemetery in Broome, as seen in 2011. Photo by K. Scarratt.

"honesty box" than a true deterrent. Judging from the many texts that have alluded to it, a brisk business in snide pearls was prevalent in Broome.

Broome was indeed the Wild West of Australia, and just like any frontier settlement it was full of intrigue and character. One cannot write about the history of Broome without mentioning its Japanese cemetery (figure 6), the largest in Australia. More than 900 Japanese pearl divers are buried here in over 700 graves. The site testifies to Broome's close ties with the people of Japan and the enormous importance of pearling in the region.

The first interment was recorded in 1896, and a plaque at the entrance to the cemetery acknowledges the great many men lost to drowning or divers' paralysis. A large stone obelisk bears testimony to those who perished in the 1908 cyclone. It records the 1887 and 1935 cyclones, each of which caused 140 deaths. In 1914 alone, decompression sickness claimed the lives of 33 men. Not mentioned are victims of scurvy, the disease caused by vitamin deficiency, which was brought on by subsisting on fish and rice for many weeks aboard the luggers.

HISTORIC PEARLS

Given the region's long history of natural pearling, there can be little doubt that the vaults of important dealers worldwide, including those in Europe and the Arabian Gulf, contain a large number of treasures gained from Australian waters. *Pinctada maxima* in these waters indeed produce some of the finest known natural pearls in all sizes and shapes (e.g., figure 7). But as production emphasis shifted to the highly successful "South Sea" cultured pearls, the casual observer began to overlook the natural pearl. And over the last few decades, the natural pearl even strayed from the minds of those most closely associated with the fishing of this incredible mollusk. Indeed, it had become economically unimportant to them.

Thankfully, the focus is shifting again, and natural pearls from *Pinctada maxima* are now edging their way back into the minds of those who love all that is rare and beautiful (N. Paspaley, pers. comm., 2011). Perhaps due to the prevalence of snide, few records exist of notable natural specimens from Australian waters, even though it can be assumed that most, if not all, of the largest nacreous natural pearls have been the product of *Pinctada maxima* rather than a smaller pearl oyster[2].

In P.O. Lennon's interesting account of the Australian pearl industry, a plate illustrates several "empire" pearls and five "Indian" pearls (three drops and two rounds) weighing 9.32–48.92 grains. There are also six somewhat larger "Australian" pearls: one near-perfect round weighing 110 grains, two off-rounds (18 and 20.80 grains), and three drops (a pair totaling 62.80 grains and a single weighing 86.80 grains).

In August 1949, an account of a major pearl find was reported in the *Northern Standard*:

> More than five tones [*sic*] of pearl shell brought back to Darwin this week has been declared by local shell experts to be of the finest quality ever to be taken in Darwin waters, either before or since the war. The shell represents the catch of two luggers belonging to Mr. Nicholas Paspaley, who said it prom-

Figure 7. This historical photo shows an array of natural pearls on the desk of a dealer in Broome. Photo courtesy of Paspaley Pearling Co.

[2]Pearl oysters include marine bivalves classified in the family Pteriidae and the genera *Pinctada* and *Pteria*, such as *Pinctada maxima*, *Pinctada margaritifera*, *Pinctada mazatlanica*, *Pinctada fucata* (*martensii*) and *Pinctada imbricata*, *Pinctada radiata*, *Pinctada maculata*, *Pteria penguin*, and *Pteria sterna*.

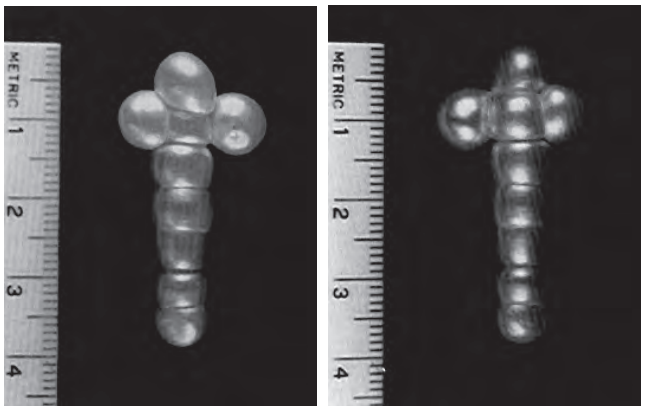

Figure 8. The back of the Southern Cross (left) reveals a very slightly flattened surface. The front of the cross is seen in the middle. The line drawing on the right shows the only two remaining joints (A and B) that were completely natural at the time of examination in 1981. Joint A is supported by some adhesive, while the other joints are now artificial (Scarratt, 1986b).

> ised well for future operations of his fleet.
>
> In addition to the shell, the luggers brought back a perfect drop shaped pearl estimated to weigh between 50 and 60 grains. Local authorities say it is the best pearl taken in Darwin since operations commenced after the war. Mr. Paspaley said that last year he had taken a pearl weighing 106 grains but its quality was much inferior to the one brought in this week. ("Pearl shell," 1949)

In 1917, a Japanese diver working for James Clark (the "Pearl King") discovered the Star of the West, a 100-grain beauty also known as the Broome pearl. This specimen was described in the July 1918 edition of *The Colonizer* as a "perfect drop with a skin of iridescent luster diffused with a pinkish glow." Other pearls of similar size are loosely recorded as the A. G. Russel, a 100-grain perfect round; the Eacott, a large drop; the Bardwell, a double button; the Rodriquez, a 92-grain perfect round; the 100-grain Hawke and Male; and the E. G. Archer, a 76-grain drop.

But the most storied Australian pearl is unquestionably the Southern Cross (figure 8). Kunz and Stevenson (1908) describe its history with both fascination and some disdain:

> The "Southern Cross" is an unusual pearl or rather cluster of pearls which attracted much attention twenty years ago. It consists of nine attached pearls forming a Roman cross about one and one half inches in length, seven pearls constituting the shaft or standard, while the arms are formed by one pearl on each side of the second one from the upper end. The luster is good, but the individual pearls are not perfect spheres, being mutually compressed at the point of juncture and considerably flattened at the back. If separated, the aggregate value of the individual pearls would be small, and the celebrity of the ornament is due almost exclusively to its form. This striking formation was exhibited at the Colonial and Indian Exhibition at London in 1886, and later at the Paris Exhibition in 1889, where it was the center of interest, and obtained a gold medal for the exhibitors. It is reported that an effort was made to bring about its sale at £10,000, the owners suggesting that it was especially appropriate for presentation to Leo XIII, on the occasion of his jubilee in 1896. The writers have been unable to obtain information as to its present location.

Henry Taunton (1903) offered further details on the Southern Cross in a very interesting account of his Australian wanderings. He presents apparently reliable statements showing that it was found on March 26, 1883, at Baldwin Creek, off the coast between Broome and Derby (figure 9). It was discovered by a boy named Clark, in the employ of master pearler James W. S. Kelly. It was delivered to Kelly in three distinct pieces, though the boy reported that he found it in one piece a few hours earlier. Kelly sold it in three pieces, receiving £10 from a fellow pearler named Roy. Roy sold it for £40 to a man named

Figure 9. Eighty Mile Beach runs from Broome down to Port Hedland and is bounded inland by the Great Sandy Desert. The famed Southern Cross was found off the coast between Broome and Derby.

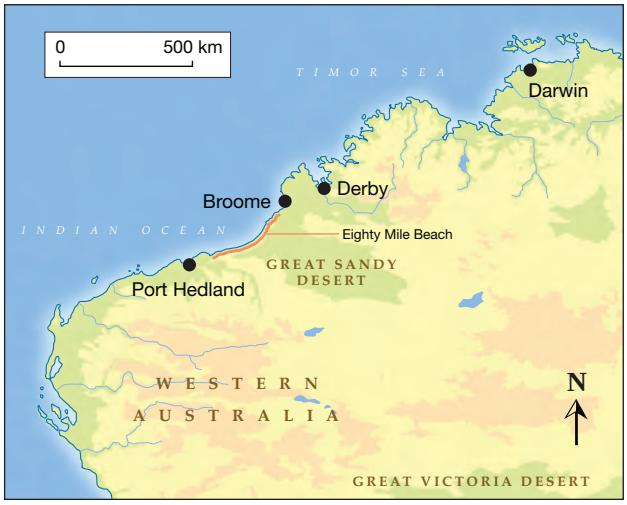

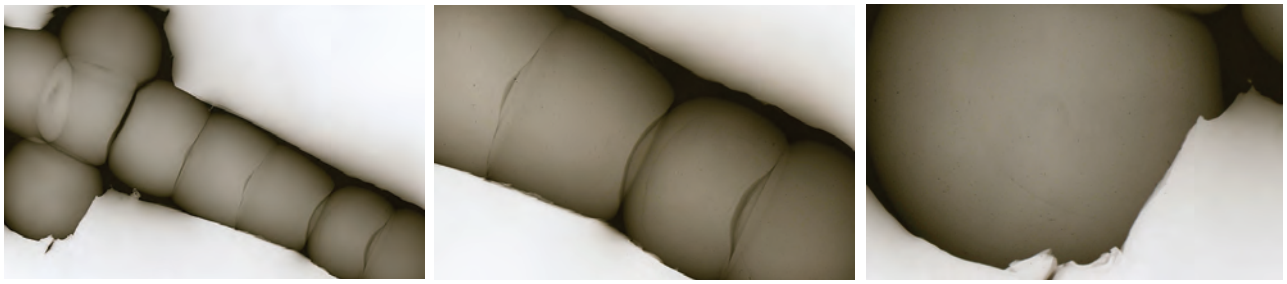

Figure 10. The microradiograph of the Southern Cross on the left was taken in 1981. The white surrounding area is a lead template used to absorb scattered X-rays. The image clearly shows the junctions between each of the pearls forming this unique cluster. A closer view of the microradiograph (center) shows the two lower pearls in the Southern Cross and the natural growth structures (black lines). An even closer view (right) shows the natural growth structures (black lines) in the lower arm of the cross.

Craig, who in turn dealt the pearl to an Australian syndicate.

According to Taunton, there were only eight pearls in the cluster when it was sold by Kelly in 1883. To make it resemble a well-proportioned cross—the right arm being absent—another pearl of suitable size and shape was subsequently secured in the town of Cossack and attached in the proper place. In the meantime, the other pearls had been refastened together by diamond cement, for a total of three artificial joints in the cluster:

> As if to assist in the deception, nature had fashioned a hollow in the side of the central pearl just where the added pearl would have to be fitted; and the whole pearling fleet with their pearls and shells coming into Cossack about this time, it was no difficult matter to select a pearl of the right size and with the convexity required. The holder paid some ten or twelve pounds for the option of selecting a pearl within given limits; and then once more, with the aid of diamond cement and that of a skillful "faker," this celebrated gem was transformed into a perfect cross. (Taunton, 1903)

When it was examined by one of the authors in 1981 (Scarratt, 1986b), the Southern Cross weighed 99.16 grains (24.79 ct), measuring 37.2 mm long and 18.3 mm wide. The length was similar to that reported by Kunz and Stevenson (1908), while the general shape matched the photo from a 1940s exhibit.

Scarratt examined the cluster for both its natural origin as well as the natural formation of the cross. He clearly determined that the pearls were natural, though by that time only two of the joints (A and B in figure 8, right) remained entirely natural.

The microradiograph of the cluster[3] (figure 10) clearly shows dark junction lines representing varying degrees of organic material or simply voids between each pearl, indicating the fragility of each junction and going some way toward validating Clark's statement that the cluster was discovered intact and broke shortly afterward. It may also be noted that the arms of the cross are created by pearls of unequal size and shape, which brings into question Taunton's "positive statement" that one of the arms was added by a "skillful faker," for surely that person would have chosen a closer match.

This examination of the Southern Cross also highlights just how fine the growth structures can be in pearls from *P. maxima*. Figure 10 (center and right) shows magnified microradiographic views of sections from the Southern Cross, which reveal only a very few organic (line) structures, demonstrating how "tight" the crystalline component is for each of the pearls in the cluster. This structural characteristic, while not universal for pearls from *P. maxima*, may certainly be regarded as common to them.

In Brief

- Historically, Australia has given the world an untold but significant volume of natural pearls, some of which have been quite notable.
- For several decades, the commercial importance of natural *Pinctada maxima* pearls has declined as the cultured pearl industry has matured.
- A newly rekindled market for natural pearls has generated interest in natural *P. maxima* pearls from Australian waters.
- Microradiographic structures previously used to distinguish between natural *P. maxima* pearls and accidentally cultured specimens are not necessarily conclusive.

[3]This microradiograph was obtained using fine-grained X-ray film in conjunction with an X-ray unit, designed specifically for the London Laboratory, that used a Machlett tube with a water-cooled molybdenum target and beryllium windows.

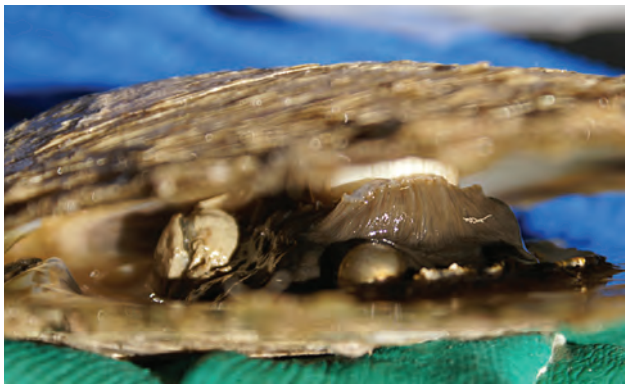

Figure 11. A pea crab (left) scurries around within a P. maxima*, while a natural pearl (center) sits in the mantle against the backdrop of the gills and adductor muscle. Photo by K. Scarratt.*

THE MOLLUSK

P. maxima (described in Jameson, 1901) is the largest species of the Pinctada genus and indeed the largest of the "pearl oysters," reaching sizes that may exceed 40 cm. The species has an extraordinary life span of up to 40 years or longer. It occupies a wide-ranging area of the Pacific, from Burma to the Solomon Islands, with Australian, Papua New Guinean, and Philippine waters the traditional habitats. Indeed, it may still have prolific shell beds in these areas. The range extends from Hainan, off the coast of China, down to the eastern and western coasts of Australia. The mollusk lives at depths of up to 90 meters, but growth rates are optimized if the depth is limited to 30–40 meters.

P. maxima have a light beige color externally, though variants do occur, and radial markings are absent. Internally, the nacre is thick and has a high luster, with the outer border having a gold or silver band, the reason why *P. maxima* is popularly known as the golden- or silver-lipped pearl oyster. The left valve is convex and the right valve only slightly so.

Pea crabs, *Pinnotheres villosulus*, live in symbiotic harmony with some 85% of *Pinctada maxima*, both wild and hatchery-grown (figure 11). Such close associations between various mollusks and pea crabs are common. Upon opening *P. maxima*, one is often treated to the extraordinary sight of a small crab scurrying around within the mantle cavity, as if the lower portion were a bed on which to lay its weary head while the upper portion holds the comforting blankets to its shell cradle.

As natural pearls may form within *P. maxima* as the result of some trauma to the mantle, it is interesting to speculate on the possible role of intruding crustaceans in producing these magnificent wonders. The animal certainly does wander in the region of the gills (which filter water and exchange oxygen), and by all accounts this appears to be the area of the mollusk where most natural pearls form. Figure 12 shows this position to be typically within the mantle and in front of the gills, close to the widest point of the adductor muscle.

Natural blister pearls that encase dead pea crabs

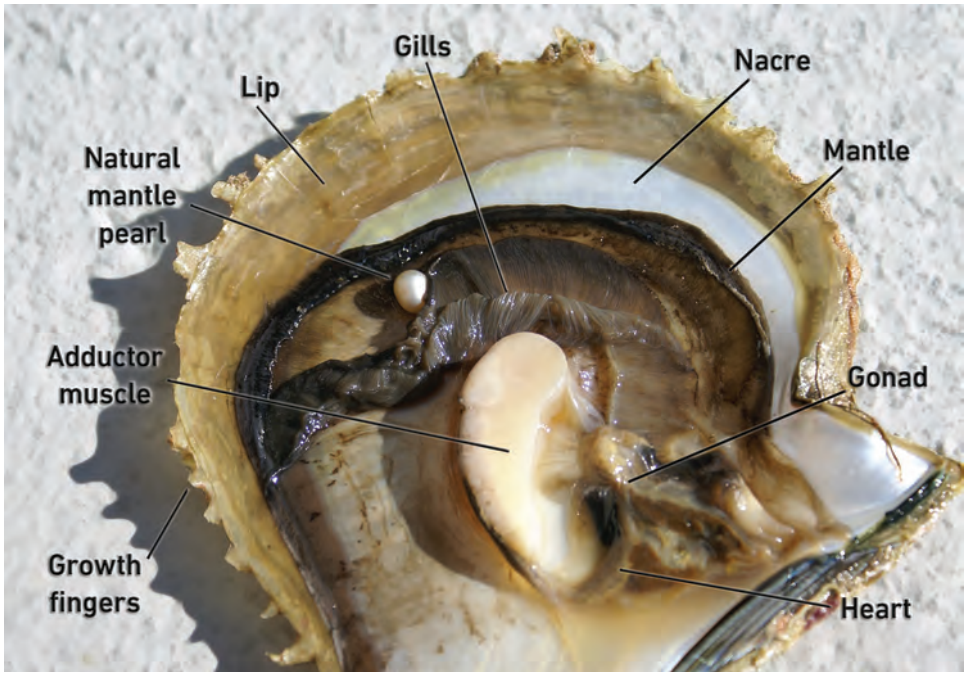

Figure 12. A partial anatomy of P. maxima *is shown here using an opened shell that also contains a natural mantle pearl. These pearls are typically positioned near the gills. Photo by K. Scarratt.*

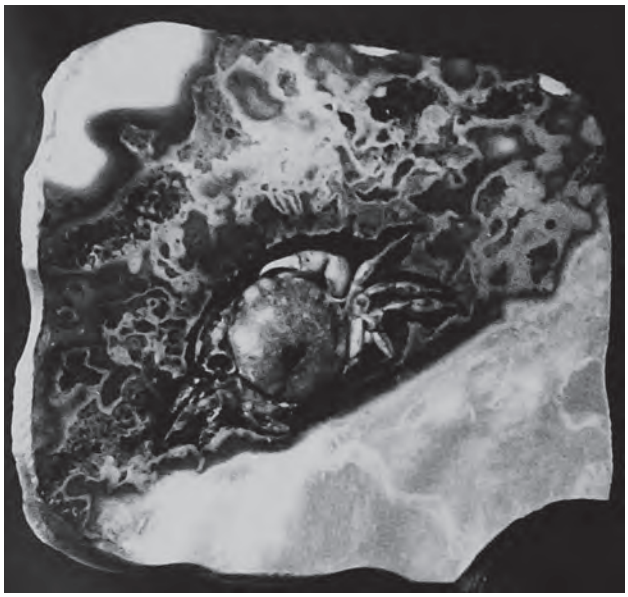

Figure 13. "Buried in a pearly mausoleum. The end of a small inquisitive crab in a pearl blister." This photo is from the archives of E. Hopkins.

inside the shell have been noted on several occasions, not only in *P. maxima* but also in other shells (Edwards, 1913; Hedegaard, 1996; PearlMan, 2011; figure 13). There have also been reports of "pearlfish" (slim, eel-shaped marine fishes of the Carapidae family) and other cohabiters of this wonderfully protective pearl shell dying inside *P. maxima* and providing the basis for the formation of other incredibly interesting blister pearls (Smith, 2003; Hochstrasser, 2011).

A supreme example examined by one of the authors (KS) in recent years is shown in figure 14. Here a blister pearl–encrusted pearlfish is attached to the shell, not far from where the heart and gonad would have been in the living mollusk. This attests to the symbiotic harmony of the fish living within the protective valves of the *P. maxima*.

As one ponders the lengthy life cycle of this mollusk and considers many decades of examining microradiographs of the natural pearls produced within its slender and near transparent mantle, it is surprising to find there is still debate over what initiates the growth of a natural pearl. It is clear that within the valves, life is not motionless. Apart from invading life forms, another potential trigger is the tremendous amount of ocean floor debris that likely finds its way over the mantle and onto the mollusk's gills.

There is no convenient single initiator but rather a wealth of possibilities that make the growth process even more intriguing. Of the hundreds of thousands of microradiographs examined by the authors, very few definitively show what caused a particular pearl's formation. Two spectacular examples that come to mind appear in figures 15–17.

In figures 16 and 17, the *Pectinidae* shell is extraordinarily clear. The owner understood the uniqueness of the pearl and stored it safely in his collection, which has allowed us to reexamine the specimen several times as imaging technology has improved. The images in figure 17 were obtained via X-ray computed micro-tomography and further manipulated to obtain the vividly detailed images presented here.

With these two pearls in particular, plus a few others we have documented that are not quite as spectacular, we were particularly lucky to have obtained them from reliable sources. In recent years, a variety of foreign bodies, including natural pearls and even shells, have been artificially inserted into cultured pearl sacs (produced from a graft of mantle tissue, or from mantle damage due to human handling) to further coat them with nacre. These practices, by deceiving gem laboratories and consequently the industry, have placed a question mark over all natural pearls.

Figure 14. A blister-encrusted fish can be observed toward the hinge of this 220 × 210 mm P. maxima *shell (left). An enlarged view (center) more clearly shows the blister pearl–encrusted fish; the blister measures 63 × 13.91 mm. A partial microradiographic image (right) clearly displays the fish's skull and vertebrae.*

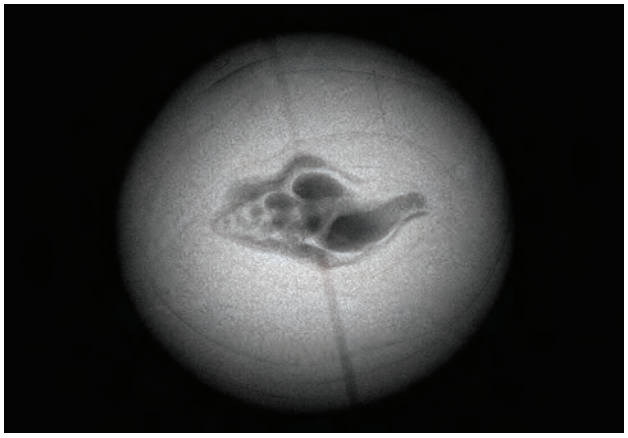

Figure 15. This microradiograph shows a shell, with chambers that appear to indicate a Strombidae, situated at the center of a natural pearl. Examined in GIA's Carlsbad laboratory circa 2002, the specimen was identified as natural. The pearl's current whereabouts are unknown. Note that the pearl has been drilled, as indicated by the dark broad line running slightly off vertical. The microradiograph was taken using X-ray film rather than real-time computerized imaging. The producing mollusk is unknown.

OTHER *P. MAXIMA* PRODUCTS

There is little if anything wasted by those who farm *P. maxima*. The mollusk provides us with not only pearls, both natural and cultured, but also very high quality mother-of-pearl and an edible delicacy.

Pearl shell (figures 18 and 19) is used today, as it has been for the last two centuries, in the manufacture of luxury utensils, as inlays in jewelry and furniture, and in various art forms. In fact, the value of the shell fished in toward the end of the 19th century often exceeded that of the natural pearls (table 1). Today, with the main use of the oyster (both wild and hatchery) being the production of large South Sea cultured pearls, the shell has a lower proportional value. Nevertheless, it remains an important element in the value stream of pearling companies.

It may be appropriate to quote Kornitzer again, for never have the writer's words been bettered in any works concerning this great bivalve:

> A shell it was, as large as a soup-plate, no more. A brilliantly nacreous thing with a natural polish, smooth as a mirror and reflecting not only my still youthful features, but also, it seemed, some of the things the future promised to hold for me.
>
> How interesting, and how foolish, to believe that one can see into the future at the magic touch of some alien thing and vaguely guess one's destiny in a waking dream!
>
> It happened in the prosaic London Docks, that staid businesslike place with its background of romance. As the man lifted the pearl shell out of the open case for me to admire its unusual size and weight, I did what probably nine women out of ten would have done in similar circumstances. I eyed myself carefully in the smooth and shining surface. Presently the reflection of my own face seemed gradually to fade, and even as I looked there took shape in my mind the vision of a life oddly governed by the moon-fired stones of my future love.

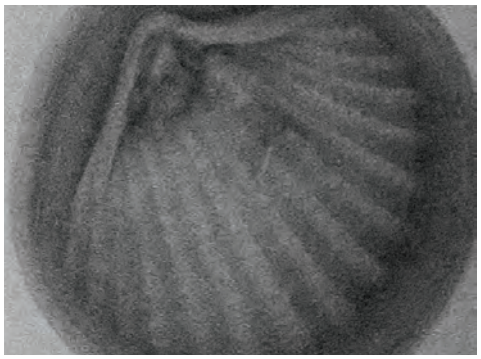

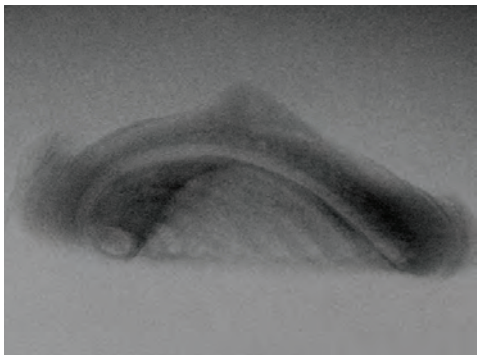

Figure 16. These top and side view microradiograph are of a 19.06-grain, 9.66 × 9.62 × 7.60 mm button-shaped natural pearl from a P. maxima *discovered in Australian waters in 2007. At its heart lies one of the most incredible sights: a perfectly preserved shell of the Pectinidae family, just 3.5 mm across.*

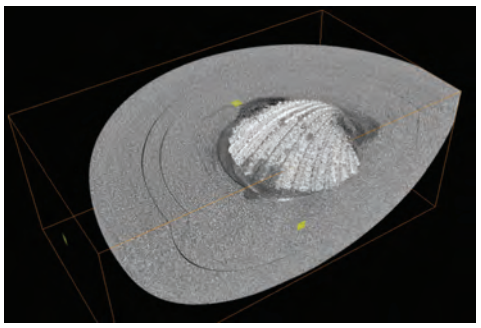

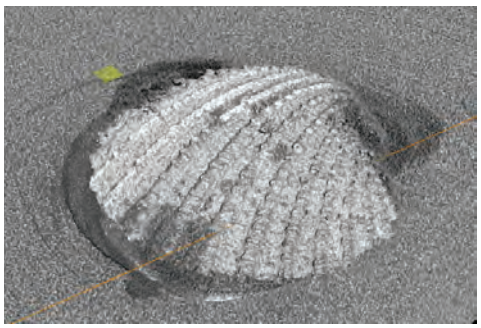

Figure 17. Images constructed using X-ray microtomography show the pearl-encrusted shell from figure 16. The computerized image on the left shows the shell and concentric growth structure. The enlarged image is on the right. Courtesy of Nick Hadland, Hadland Technologies.

Figure 18. These large P. maxima *shells display high-quality nacre (mother-of-pearl). Courtesy of Paspaley Pearling Co.*

Figure 20. Fresh pearl meat from the P. maxima *adductor muscles is regarded as a delicacy, particularly in China. Photo by K. Scarratt.*

> The vision faded. I stood like a ninny with the shell in my hand. The man nudged me and said, "Trying to drill holes into this shell with your eyes?"
>
> "No," I said apologetically. "I've been dreaming. These outlandish things seem to awaken in me the desire to travel, that's all." (Kornitzer, 1937)

Pearl meat from the *P. maxima* adductor muscle is a delicacy, particularly in China but also to anyone fortunate enough to experience this gastronomic delight (figure 20). Eaten raw or quickly flash-seared in a hot pan for just a few seconds or slowly braised, it will excite the taste buds of any dissenter.

It is estimated that 60% of all pearl meat harvested in Western Australia makes its way to Asian markets after drying and packing. It sells for Aus$100–$150 per kg. The rest is monopolized by top chefs in Sydney and Perth, as well as Broome, which is why very little pearl meat can be found in the shops (Broadfield, 2010).

Figure 19. Searching P. maxima *for natural pearls aboard a lugger. Courtesy of Paspaley Pearling Co.*

Chef Matt Stone of Perth says, "What I love about it most is the texture: It's halfway between a scallop and an abalone. It's got a bit of chew to it, but not so much as abalone" (Broadfield, 2010). All of the authors who have tasted the meat of *P. maxima* are in full agreement.

WILD SHELL COLLECTION TODAY

The pearl culturing industry is one of Australia's most valuable aquaculture industries, with a value estimated at Aus$120–160 million (Hart and Friedman, 2004). Considering the natural as well as manmade challenges, this is truly a significant statistic. Clearly, one important factor behind the industry's success is the reliance on hatchery-grown mollusks that offer more control over production processes. Interestingly, the Paspaley Pearling Company, whose operations are focused on the waters of the Northern Territory and Western Australia, still fish for wild shell and use them for much of their culturing operations[4].

To protect the species, the harvesting of mother–of-pearl (MOP) in Western Australia was virtually phased out by the late 1980s, and strict quota controls were placed on sizes suitable for pearl culturing. Hart and Friedman (2004) point out that the fishing for *P. maxima* targets smaller shell (120–165 mm dorso-ventral measurement, or DVM; see figure 21) that are more suitable for pearl culture, leaving larger (175 mm+) MOP on the pearling grounds. They add that in 2004, the shell were protected by the "gauntlet" strat-

[4]Australia still has a predominantly wild oyster industry. The current Australian quotas are set at 1,342 units, made up of 992 units of wild shell and 350 units of hatchery shell; wild shell thus accounts for 74% of the quota. The number of shell permitted per quota unit is set each year by the Fisheries Department, depending upon the availability of shell.

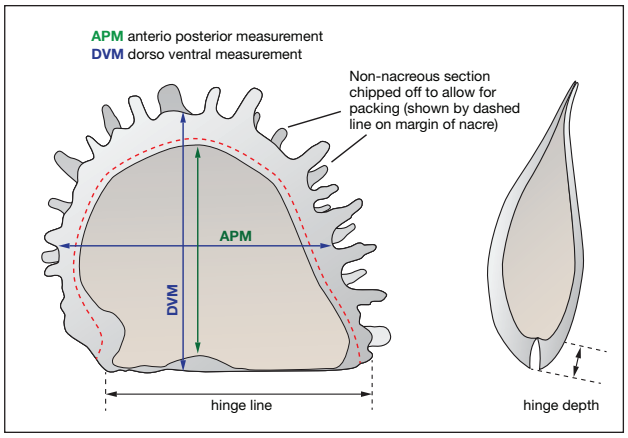

Figure 21. Common measurements applied to the morphology of P. maxima*. After Hart and Friedman (2004).*

egy adopted by the Fisheries Department, and that "with almost 20 years of protection from fishing mortality, there has been a buildup of MOP on some pearling grounds, leading to proposals to commercialize (again) this component of the fishery." The quota system has been so effective that the fisheries sector is now the "only remaining significant natural source of large *P. maxima* MOP left worldwide." As wild stocks fluctuate, however, historic norms are the most likely outcome.

The wild shell collected by Paspaley are kept separate from their hatchery shell via a strict stock control system that begins the moment a specimen is brought aboard the vessel. Collection of the wild shell occurs mostly off Western Australia's Eighty Mile Beach (between Broome and Port Hedland in figure 9), but the company also has a quota in Northern Territory waters. Although divers now operate from modern, specially designed vessels (figure 22), the principles are similar to those used in the days of the lugger. With today's larger ships, up to six divers are pulled along the seabed as the ship plows a slow-moving grid at the surface. Divers are still connected to the vessels by safety lines and air hoses, but they wear modern wetsuits and are not constrained by the hard-hat environment once used aboard the luggers.

As they move along the seabed, the divers trail below them a rope basket for the shells (figure 23). Once the basket is full, the diver ascends to a shallower depth where a large storage container awaits. He transfers the shells from his basket and returns down to the seabed to continue collecting. He may repeat this process several times before the dive ends. There is great rivalry between divers, with "scores" being eagerly awaited once back onboard the vessel.

While the practice is unquestionably safer now than it was in the days of the luggers, the everyday dangers of such a remote environment remain just as real today.

It takes a very special type of person to be a diver on a pearling vessel. Spending up to eight hours a day in the deep and unforgiving waters off Western Australia, the diver needs to be adventurous, but calm and to some extent fearless, while maintaining a focused approach to the task. Decompression sickness, sharks, saltwater crocodiles, jellyfish, sea snakes, tangled air

Figure 22. A Paspaley diving vessel operates off Eighty Mile Beach. The lines running from the stern of the vessel are the divers' air hoses and safety lines. Photo by K. Scarratt.

Figure 23. A Paspaley diver collects wild shell off Eighty Mile Beach. The diver's air hose and safety lines are connected to the vessel on the surface, which slowly pulls him along the ocean floor. Photo courtesy of Paspaley Pearling Co.

TABLE 2. Shell and pearls obtained off the Western Australian coast aboard Paspaley Pearling Co. vessels, July 26–29, 2011.

Specimen no.	Type	Wild/hatchery Operated/unoperated	Relationships	DVM x APM x Thickness (mm)	Length x Width x Depth (mm)	Weight	Shape
1WU	Pearl	Wild unoperated	Found in shell 1WU		6.04 x 5.93	6.128 grains	Round
2WU	Pearl	Wild unoperated	Found in shell 2WU		8.34 x 8.20 x 6.62	13.596 grains	Button
3WU	Pearl	Wild unoperated	Found in shell 3WU		7.87 x 6.46	9.984 grains	Oval
1WU	Shell	Wild unoperated	Pearl 1WU	138.64 x 126.13 x 31.54		242.8 grams	
2WU	Shell	Wild unoperated	Pearl 2WU	132.96 x 118.78 x 31.86		250.2 grams	
3WU	Shell	Wild unoperated	Pearl 3WU	138.57 x 129.19 x 31.37		258.8 grams	
1WO	Pearl	Wild operated	Found in shell 1WO		11.74 x 11.24 x 9.18	35.04 grains	Button
1WO	Shell	Wild operated	Pearl 1WO	200 x 170 x 45.93		775.6 grams	
1HU	Pearl	Hatchery unoperated	2HU and 3HU found in same shell		6.55 x 6.40 x 5.58	6.784 grains	Round
2HU	Pearl	Hatchery unoperated	1HU and 3HU found in same shell		6.06 x 5.90 x 5.11	6.04 grains	High button
3HU	Pearl	Hatchery unoperated	1HU and 2HU found in same shell		4.96 x 4.61	2.904 grains	Round—slight drop
4HU	Pearl	Hatchery unoperated	None		3.10 x 2.43	0.74 grains	Round

lines, and low visibility are just a few of the very real dangers. These dangers are difficult to convey unless the reader is a seafarer with knowledge of Australia's rugged western coast. Needless to say, few people who lead the pearling life do not know of someone who has been taken by a shark or nearly died following a sting from the thumbnail-size Irukandji jellyfish.

COLLECTION AND EXAMINATION OF PEARLS FROM WILD AND HATCHERY SHELL

Whenever natural nacreous pearls are spoken of, the tendency is to think of pearls from the Gulf region, which are produced mainly by *Pinctada radiata*. Indeed, one young European dealer was overheard saying that the only natural pearls are "Basra" pearls. Many are surprised to discover that high-quality natural pearls are also being produced by *Pinctada maxima*—or at all. Hopefully this paper will serve to address trade misconceptions.

Recently, questions have been raised in some gem laboratories concerning nacreous pearls from *Pinctada maxima*. These questions are related to the difficulty in some instances of determining whether a pearl from this mollusk is natural, non-bead cultured, or even bead-cultured using a natural or non-bead cultured (atypical) bead. Indeed, some laboratories may have taken, for a time, the extreme measure of not issuing identification reports on any nacreous pearls from *Pinctada maxima*.

An understanding of the *Pinctada maxima* has therefore become vital to the health of the natural pearl trade; the alternative is for the pearl business to become relevant only to the antiques market, with questions hanging even over these. Further, as the

Pinctada radiata mollusk begins to be used in the Gulf for pearl culture, so too will the same questions need to be addressed with regard to this mollusk

MATERIALS AND METHODS

Assuring sample integrity has always been a challenge within the gemological community. For the most part, gemologists have proceeded with research based on samples that have been donated or loaned rather than attempting to secure a higher degree of reliability concerning their origin. With gemstones, the highest degree of integrity is assured when a member of the research team collects samples *in situ* at the mine site, records the find/extraction in precise detail, and secures these samples in such a manner as to avoid any contamination.

With pearling, the challenges are often at least equal. We addressed sample integrity by first observing the thoroughness of Paspaley's stock control systems for both wild and hatchery shell and then working with them in a spirit of complete openness. Over several years, as wild shell were fished and "relaxed" aboard the vessel, the mantle in the area of the opening was inspected for likely natural pearls prior to putting them on the production line. The authors asked that video be taken of any pearls found still in the mantle of these wild shells. As more were eventually discovered, we were invited onboard to record them ourselves and retrieve the pearls and shell for examination in the laboratory.

Between July 26 and 29, 2011, the authors achieved their goal and left Western Australia with a clear understanding of how natural pearls are discovered within *P. maxima* shell, along with a small but suitable group of samples for laboratory examination (table 2).

From the tens of thousands of wild shell fished just prior to the team's arrival aboard the Paspaley vessel, three were discovered to have natural pearls still present within their sacs in the mantle, positioned in front of the gills and closest to the widest part of the adductor muscle (again, see figure 12). Upon inspection, we found that these shell had not been opened beyond the normal "natural relaxed" position. All three shells, and indeed all other wild shell aboard the vessel, were in the size range allowed for fishing wild shell for pearl culture (120–165 mm DVM; again, see figure 21). The three containing natural pearls ranged from 132.96 to 138.64 mm DVM and weighed (after cleaning) between 242.8 and 258.8 grams. The opening of the shell and the extraction of the pearls were witnessed by all members of the team. Both video and still images were recorded, and neither the shell nor the pearls have left the full control of the team since that time.

Figure 24. Three natural pearls (6.128–13.596 grains) extracted from three separate wild shells are shown together in one of the shells. Photo by K. Scarratt.

The three natural pearls extracted (figure 24) weighed between 6.128 and 13.596 grains, with minimum to maximum dimensions of 5.93 and 8.20 mm. Their shapes were near round, button, and near oval. The control numbers for each of these three shell and pearls are 1WU, 2WU, and 3WU. None of these three shells had been operated on for pearl culture or any other purpose prior to the discovery of the pearls.

A pearl weighing 35.04 grains was found in another wild shell, but in this instance the shell had previously been operated on and had been on the farm for more than a year (figures 25 and 26). As with the three previous discoveries, the pearl was found within the mantle, positioned in front of the gills and near the

Figure 25. A 35.04-grain button-shaped pearl is discovered within a wild P. maxima *shell that had previously been operated on for culturing. Photo by K. Scarratt.*

Figure 26. The 35.04 grain button-shaped pearl is removed from the wild P. maxima *shell. The upper mantle has been folded back to reveal the pearl more clearly. Photo by K. Scarratt.*

widest part of the adductor muscle. The shell was considerably larger than the three unoperated shells, with a DVM of 200 mm and a cleaned weight of 775.6 grams, nearly three times the weight of the largest wild unoperated shell. The pearl was almost 2.6 times the size of the largest specimen found in the wild unoperated shells. The control number for this pearl and shell is 1WO.

Four other pearls were discovered during this investigation. The technicians aboard the vessels were aware of our interest and were on the lookout for anything unusual. In the first instance, one of the staff emerged from the operating room with a small dark pearl that had just been extracted from a hatchery shell that had yet to be operated upon. This pearl (4HU; figure 27) was rather small, measuring 3.10 × 2.43 mm and weighing only 0.74 grains.

Figure 27. Pearl 4HU was from a hatchery shell that had not been operated on. Photo by K. Scarratt.

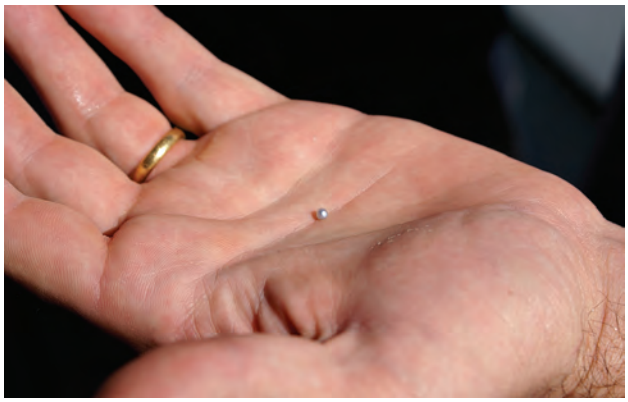

In the second occurrence a hatchery shell, also yet to be operated upon, was brought out with three pearls in the mantle. This time the pearls were located close to the heel of the shell rather than in front of the gills, as with the wild shell. The three pearls—one round, another round but with a slight drop shape, and the other a high button—weighed 6.784, 6.04, and 2.904 grains, respectively (figure 28). The control numbers for these pearls were 1HU, 2HU, and 3HU.

All microradiographic images from the examination of the pearls and shells were obtained with the Faxitron CS-100, a high-resolution real-time 2D X-ray unit installed in GIA's Bangkok laboratory. The samples were also examined using X-ray computed microtomography with a Procon X-rays CT-Mini model, also in the Bangkok laboratory.

The pearls and shell were examined using Gemolite microscopes at 10×–60× magnification. Photomicrographs were recorded digitally using a Nikon system SMZ1500 with a Nikon Digital Sight Capture System and at various magnifications up to 176×.

The chemical composition of the pearls and shell were determined with a Thermo X Series II laser ablation–inductively coupled plasma–mass spectrometry (LA-ICP-MS) system equipped with an attached New Wave Research UP-213 laser. UV-visible reflectance spectra for all samples were obtained with a Perkin-Elmer Lambda 950 UV-Vis-NIR spectrometer using a reflectance accessory bench fitted with an integrating sphere to capture data. Both Raman and PL data were recorded using a Renishaw inVia Raman microscope system incorporating a 512 nm argon ion laser. All instruments are installed in GIA's Bangkok laboratory.

Figure 28. Pearls 1HU, 2HU, and 3HU were found in the mantle but close to the heel of this hatchery shell, which had not been operated on. Photo by K. Scarratt.

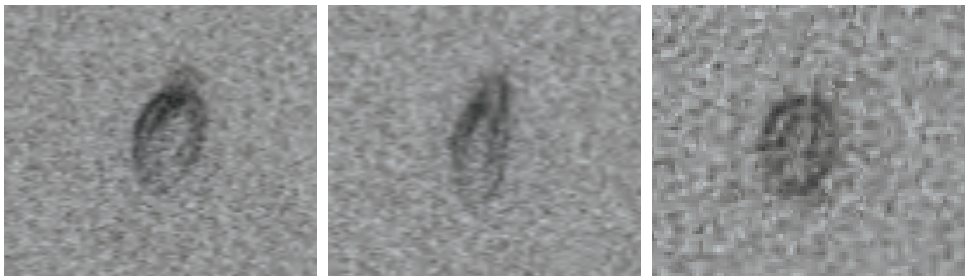

Figure 29. These micro-CT images show (left to right) X-, Y-, and Z-direction slices of pearl 1WU, zoomed center.

OBSERVATIONS AND RESULTS

Microscopy. Selected microscopic images are shown in tables 3–7. As expected, the horny exterior of the shells hosted many foreign life forms taking the shapes of calcified undulating tubes (table 5F) coral exoskeletons (tables 3F, 4F, and 5E), or other unknown forms. We noted that the hinge of one shell also acted as the sarcophagus of a shrimp-like encrustation (table 6F), while a worm-like blister was apparent in shell 2WU (see table 4E).

In each case, the shell had three major components: the non-nacreous edge, the nacreous inner core, and the hinge (tables 3A-3B, 4A-4B, 5A-5B and 6A-6B), all of which were characteristic in their appearance. The non-nacreous edge under magnification revealed a clear prismatic growth in cross-section when viewed directly from above; the appearance differed slightly between reflected and transmitted light (tables 3D, 4D, 5D, and 6D). The nacreous central region, which was solid and had a naturally high luster, revealed the expected structure of overlapping platelets (tables 3C, 4C, 5C and 6C) when viewed at high magnification and in the ideal reflective lighting.

Magnification of each pearl, regardless of the source (wild or hatchery), revealed the expected overlapping platelet structures typical of nacreous pearls, both natural and cultured (tables 3I-3J, 4I–4J, 5I–5J, 6I–6J, 7B–7C, 7H–7I, 7J–7K, and 7P–7Q). In these instances, though, the structures observed in the pearls from hatchery shell (table 7) appeared somewhat coarser than those produced in wild shell.

Microradiography and Micro-CT. Dubois (1901) suggested the use of X-rays (radiography) for detecting pearls in oysters and ably demonstrated the technique a decade later (Dubois, 1913). But it was not until the introduction of the round cultured pearl (Mikimoto, 1922) that the importance of X-rays as a gem identification tool was realized. Three X-ray techniques were applied to pearl identification. One in particular, microradiography, proved the most versatile (Alexander, 1941).

Since the advent of X-rays in pearl testing, there have been many technical advances, particularly in the areas of imaging and computerization. While film photography is still used as a backup, many gem laboratories today employ the more convenient high-resolution 2-D real-time options, along with 3-D X-ray computed microtomography (micro-CT).

Both real-time microradiographs and micro-CT images were recorded for pearls 1WU, 2WU, and 3WU (from wild unoperated shell). For the first sample, microradiographs recorded only the vague appearance of an organic area toward the center of the pearl in one direction but a clearer image of this small centralized structure revealing micro "growth rings" was produced from another direction (table 3L). This sample was otherwise free of growth structures when microradiographs were taken in any direction. 3-D micro-CT scans revealed structures similar to those seen in the 2-D microradiographs. Zoomed-in areas of selected slices from the X, Y, and Z directions are shown in figure 29.

For pearl 2WU, the microradiographic detail was

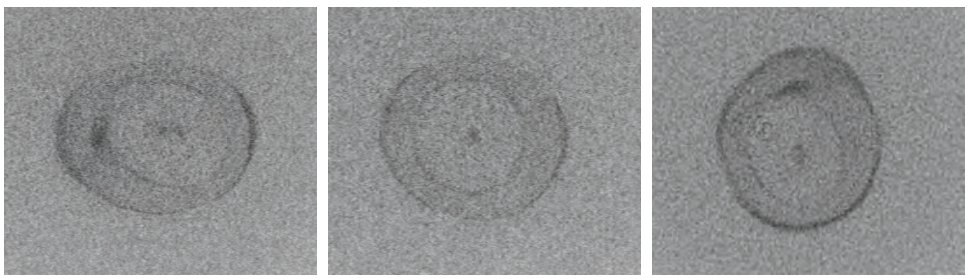

Figure 30. These micro-CT images show (left to right) X-, Y-, and Z-direction slices of pearl 2WU, zoomed center.

TABLE 3. Detail of shell and pearl 1WU (wild unoperated *P. maxima*).

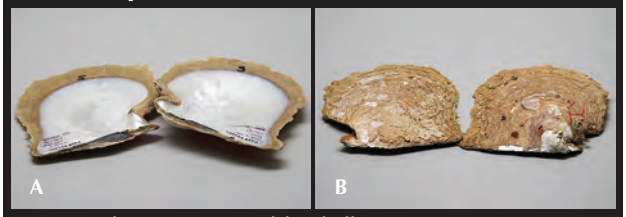

Interior and exterior views of the shell.

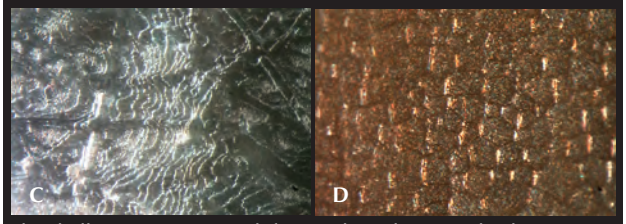

The shell's nacreous areas (left) reveal overlapping platelets. Non-nacreous areas (right) show cross sections of prismatic columns.

The exterior of the shell, seen at 10x magnification, also had a red material attached to it.

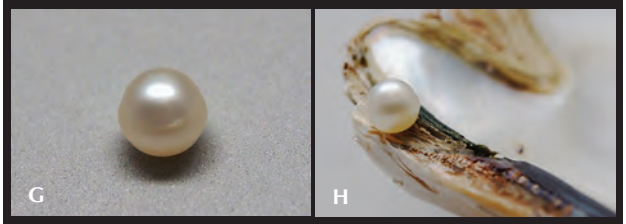

Pearl 1WU (left) is set against the shell in which it was discovered.

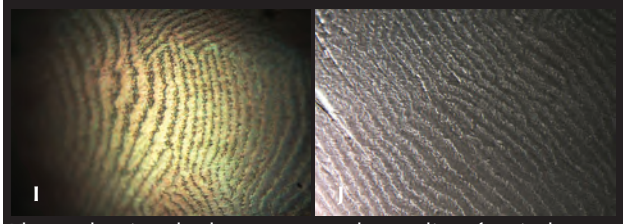

The overlapping platelet structure on the pearl's surface is shown in different lighting conditions. Magnified 176x.

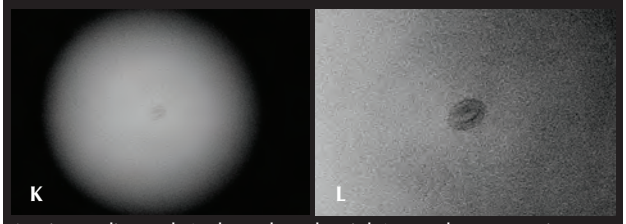

A microradiograph (enlarged on the right) reveals an organic growth structure toward the center of the pearl, which was otherwise relatively free of growth structures.

TABLE 4. Detail of shell and pearl 2WU (wild unoperated *P. maxima*).

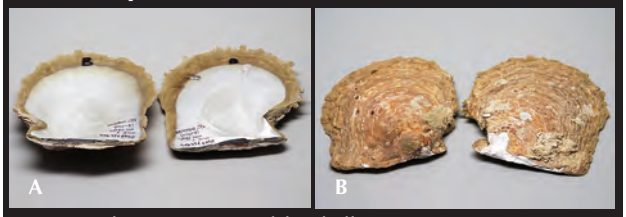

Interior and exterior views of the shell.

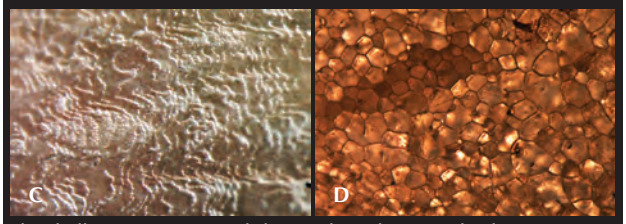

The shell's nacreous areas (left) reveal overlapping platelets. Non-nacreous areas (right) show cross sections of prismatic columns.

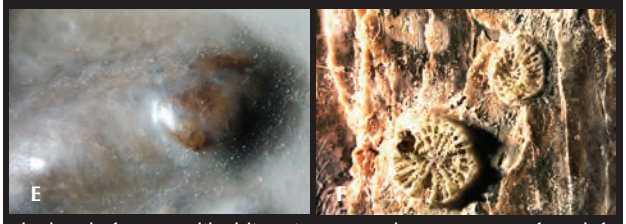

The head of a worm-like blister is seen on the nacreous surface (left). Small coral-like structures were attached to the outer surface (right).

Pearl 2WU (left) is set against the shell in which it was discovered.

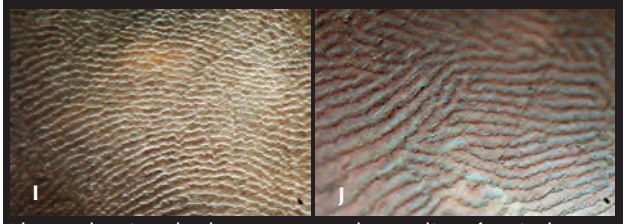

The overlapping platelet structure on the pearl's surface is shown in different lighting conditions. Magnified 176x.

A microradiograph (enlarged on the right) reveals a near-symmetric organic area toward the center of the pearl, which was otherwise relatively free of growth structures.

TABLE 5. Detail of shell and pearl 3WU (wild unoperated *P. maxima*).

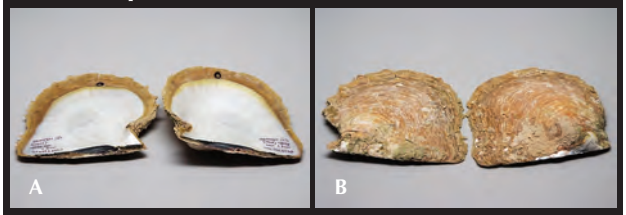

Interior and exterior views of the shell.

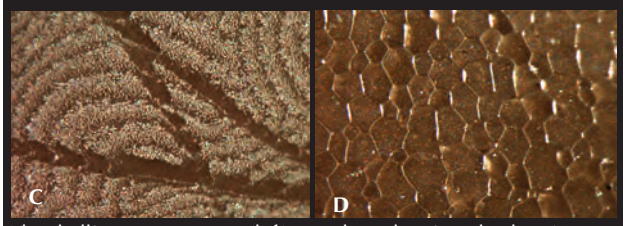

The shell's nacreous areas (left) reveal overlapping platelets. Non-nacreous areas (right) show cross sections of prismatic columns.

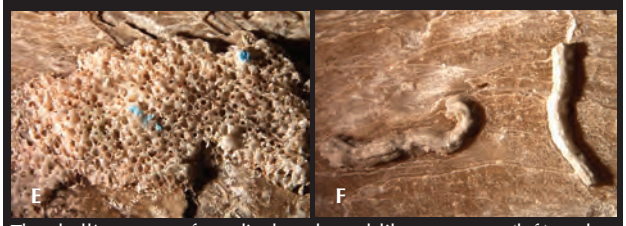

The shell's outer surface displayed coral-like structures (left) and tubeworm-like calcareous structures (right).

Pearl 3WU (left) is set against the shell in which it was discovered.

The overlapping platelet structure on the surface of the pearl is shown in different lighting conditions. Magnified 176x.

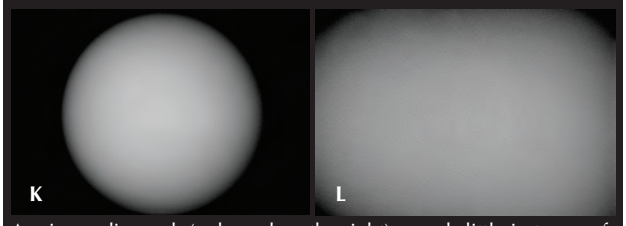

A microradiograph (enlarged on the right) reveals little in terms of organic growth.

pronounced. A relatively large area of organic growth extended from the center of this 8.34 mm button-shaped pearl to encompass about one third of the sample's apparent volume. Within the dominant organic core, additional ringed growth structures could be observed toward the center of the pearl. Overall, the microradiographic structures revealed a great deal of organic material toward the center, while the outer portions appeared tightly crystalline with negligible organic material (table 4K–4L). 3-D micro-CT scans revealed structures similar to those seen in the 2-D microradiographs, but in slightly more detail. Zoomed areas of selected slices from the X, Y, and Z directions are seen in figure 30.

Pearl 3WU revealed little in terms of internal organic growth using 2-D microradiography (table 5K–5L). Under normal circumstances, therefore, one would regard this natural *P. maxima* pearl as "solid" throughout. Yet 3-D micro-CT scans revealed two tiny points of organic accumulation not seen in the 2-D microradiographs. Figure 31 represents three slices, from the X, Y, and Z directions, that show these two dark spots quite clearly.

Pearl 1WO, which weighs 35.04 grains and measures 11.74 × 11.24 × 9.18 mm, was recovered from an older and larger wild shell than shells 1WU, 2WU, and 3WU described above. This shell had already been (gonad-) operated on for pearl cultivation and had been on the farm for about two years. The pearl was recovered from the mantle in a similar area to that of the other three.

2-D microradiography (table 6K–6L) revealed a slightly off-center area of patchy organic material in a *P. maxima* pearl that otherwise seems to be "solid" throughout. 3-D micro-CT scans revealed images similar to those obtained in 2-D, but in greater detail. While it is impossible to adequately reproduce the 3-D aspect of the micro-CT scans in the two-dimensional medium of this article, figure 32 presents three slices each from the X, Y, and Z directions. Viewing these, one may surmise that the off-center area of patchy organic material is composed of many very small organic areas, both connected and unconnected with each other.

In table 7A, pearls 1HU, 2HU, 3HU, and 4HU present an interesting nomenclature dilemma: While they were found in mollusks that had not been operated on, these were hatchery-reared *P. maxima*. One school of thought suggests that as the host is "cultured" (i.e., hatchery-reared), anything that host produces should also be considered a product of culturing—i.e., a cultured pearl. As shown by the se-

TABLE 6. Detail of shell and pearl 1WO (wild operated *P. maxima*).

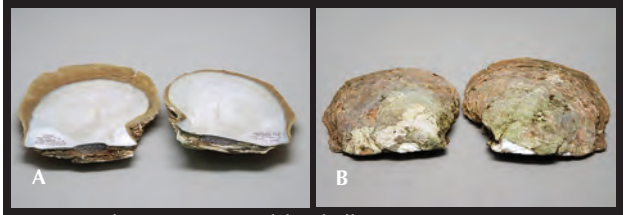

Interior and exterior views of the shell.

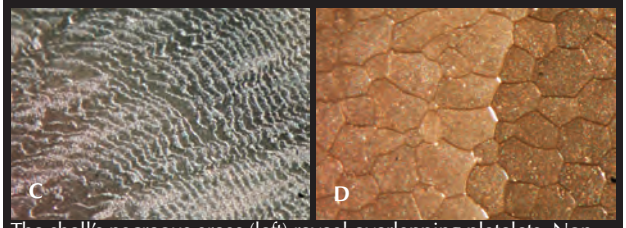

The shell's nacreous areas (left) reveal overlapping platelets. Non-nacreous areas (right) show cross sections of prismatic columns.

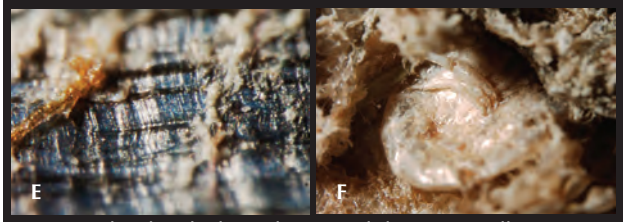

Discovered within the hinge ligament (left) was a small crustacean (right).

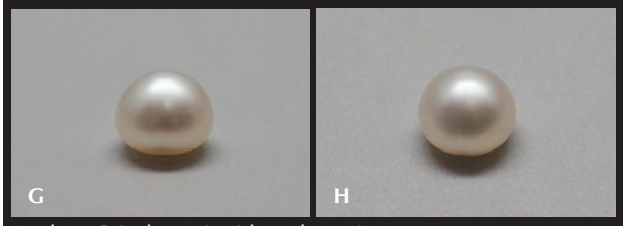

Pearl 1WO is shown in side and top views.

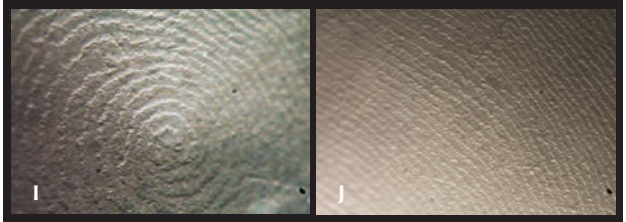

These images show the pearl's overlapping platelet structure. Magnified 176x.

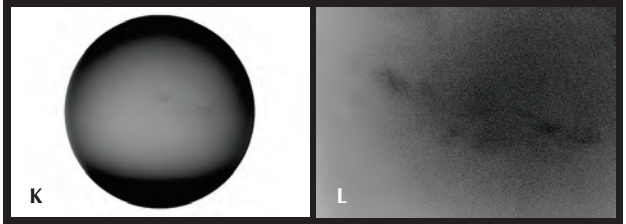

A side-view 2-D microradiograph (enlarged on the right) reveals a slightly off-center area of patchy organic material.

ries of microradiographic images in table 7, however, nothing in their growth structures indicates a cultured origin. Indeed, all microradiographic indications point toward these pearls as being natural.

Not surprisingly, the microradiograph for pearl 4HU (which has a distinctly gray color) reveals the greatest amount of organic growth (table 7D–7E), and the pearl appears to have entirely natural growth structures.

The microradiographs for pearls 1HU and 3HU (table 7L–7M and 7N–7O) reveal virtually nothing in terms of growth structures, which is expected for natural *P. maxima* pearls. Yet there were no indications that they were a product of culturing, either.

Some of the microradiographs for pearl 2HU (table 7E–7G) did indicate a slight "shadowing." As with pearls 1HU and 3HU, however, the growth appears to be tight and crystalline. There is insufficient organic growth to appear on a microradiograph as diagnostic data. The same was also true for the micro-CT scans performed on each of these pearls.

Fluorescence. Viewed under long-wave ultraviolet light, the pearls listed in table 2 showed a strong, fairly even chalky green fluorescence, and a much weaker chalky green under short-wave UV. The pearls were also examined using the DiamondView imaging system, which can produce a fluorescence image of the pearl in real time. The system uses a very short wavelength (below 230 nm) light source to excite fluorescence close to the surface of the pearl. These images have proved very useful in the detection of treatments, particularly coatings that are not visible under the microscope. The DiamondView images shown here (figure 33) will provide valuable reference data in future cases of treatment uncertainty. All three pearl types showed a distinctly blue fluorescence, sometimes slightly mottled, with no phosphorescence.

Raman and PL Spectra. Raman spectroscopy is a technique in which photons of light from a laser interact with a material and produce scattered light of slightly different wavelengths. Every material produces a characteristic series of scattered light wavelengths, and measuring these can identify a material. The light of a particular wavelength from a laser beam (or other light source) is used to illuminate the gem. Because this laser light is aligned along the optical path of a microscope, the operator can focus it onto a gem to obtain a Raman spectrum (Kiefert et al., 2001). Light emitted by the sample is collected and analyzed by the spectrophotometer to produce a spectrum, which is compared to an extensive mineral database assembled by GIA over the past two decades.

TABLE 7. Detail of pearls from hatchery unoperated *P. maxima*.

Left to right: 4HU, 1HU, 3HU, and 2HU were discovered in hatchery-reared shells prior to surgery.

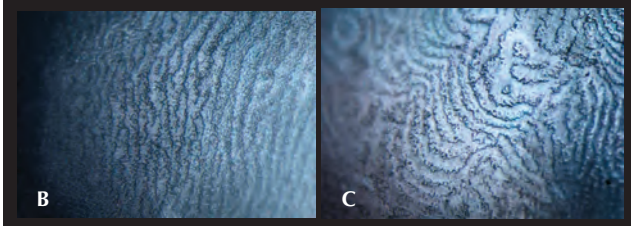

These images show the overlapping platelet structure on pearl 1HU. Magnified 176x.

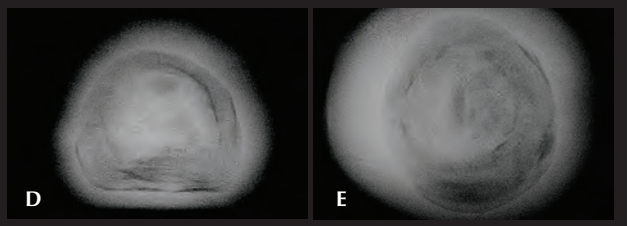

Microradiographs of pearl 4HU.

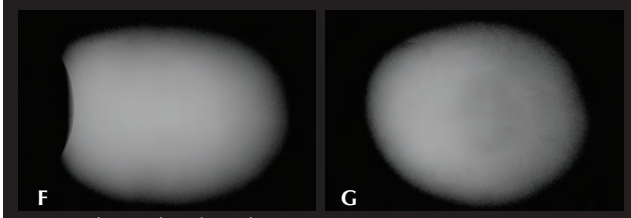

Microradiographs of pearl 2HU.

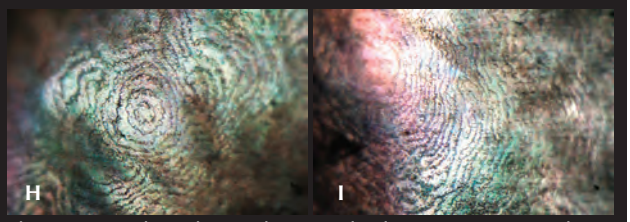

These images show the overlapping platelet structure on pearl 4HU. Magnified 176x.

These images show the overlapping platelet structure on pearl 2HU. Magnified 176x.

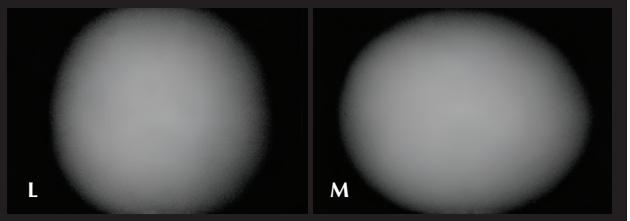

Microradiographs of pearl 1HU.

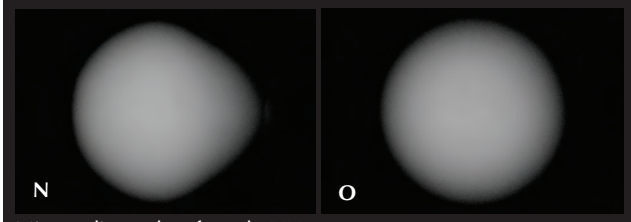

Microradiographs of pearl 3HU.

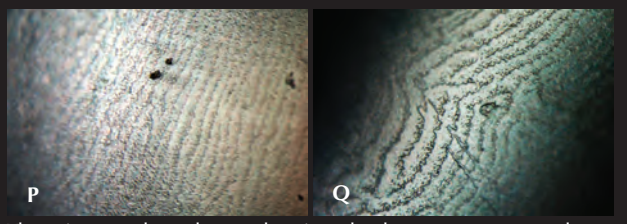

These images show the overlapping platelet structure on pearl 3HU. Magnified 176x.

Raman spectra recorded for the pearls listed in table 2 revealed two weak peaks located at 702 and 706 cm^{-1} (a doublet) and a strong peak at 1085 cm^{-1} (figure 34). These peaks are typical for aragonite, the crystalline material normally associated with pearls from *P. maxima*. No peaks associated with carotenoids or polyenes were recorded. No differences in the Raman spectra were noted between the three "types" of *P. maxima* pearls examined: from wild shell (unoperated), wild shell (operated), and hatchery-reared shell.

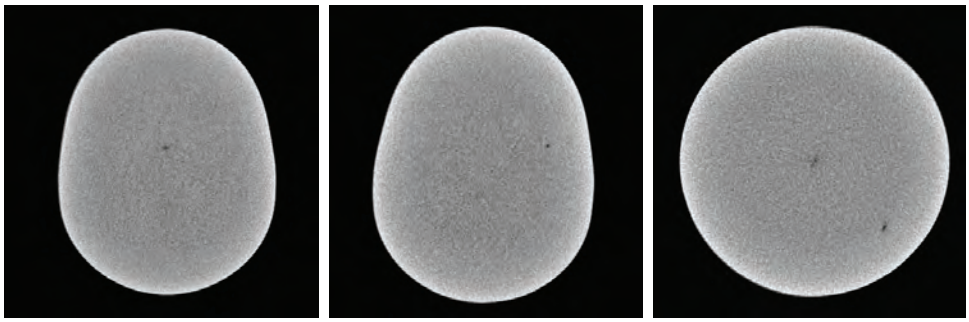

Figure 31. These micro-CT images show (left to right) X-, Y-, and Z-direction slices of pearl 3WU, zoomed center.

PL (photoluminescence) spectroscopy is a noncontact and nondestructive method used to probe the electronic structure of materials. In this process, a substance absorbs and re-radiates photons. It can be described as an excitation (in this study by a 514 nm argon ion laser) to a higher energy state, followed by a return to a lower energy state with the simultaneous emission of a photon (figure 35). The PL spectra can be collected and analyzed to provide information about the excited states, in this case by using the same system used to collect Raman spectra. No differences in the PL spectra were noted between *P. maxima* pearls from wild shell (operated or unoperated) and hatchery-reared shell.

UV-Visible Spectroscopy. UV-Vis-NIR spectroscopy is a complementary technique to EDXRF for examining the trace-element composition of gems, particularly when detailed in absorption coefficient. UV-Vis-NIR spectroscopy may provide information about the portions of the visible spectrum that are absorbed by these trace elements to create the gem's color. Given

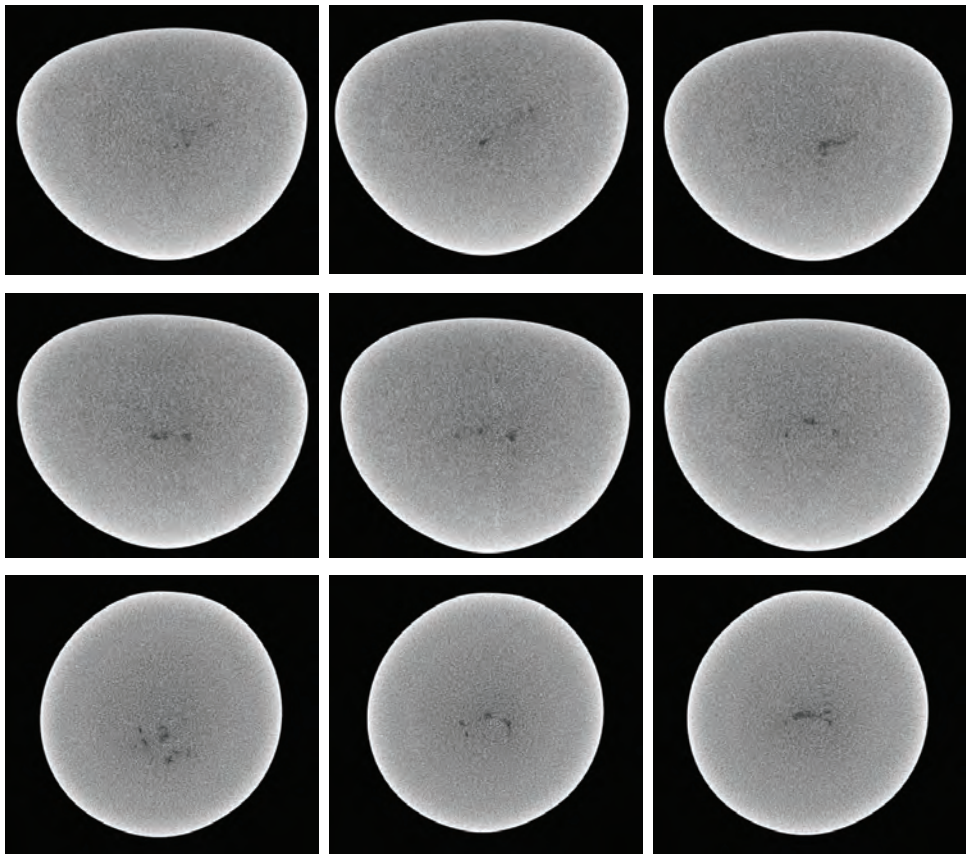

Figure 32. Each row (left to right) shows X-, Y-, and Z-direction slices from micro-CT scans of pearl 1WO.

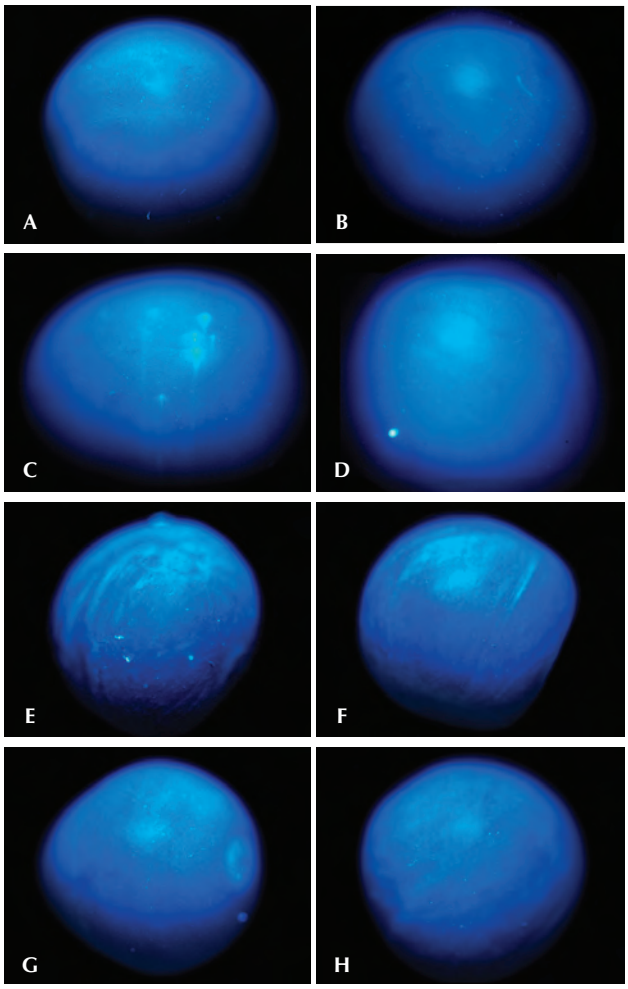

Figure 33. DiamondView images of pearls (A) 1WU, (B) 2WU, (C) 3WU, (D) 1WO, (E) 4HU, (F) 2HU, (G) 3HU, and (H) 1HU reveal blue fluorescence, occasionally mottled, and no phosphorescence.

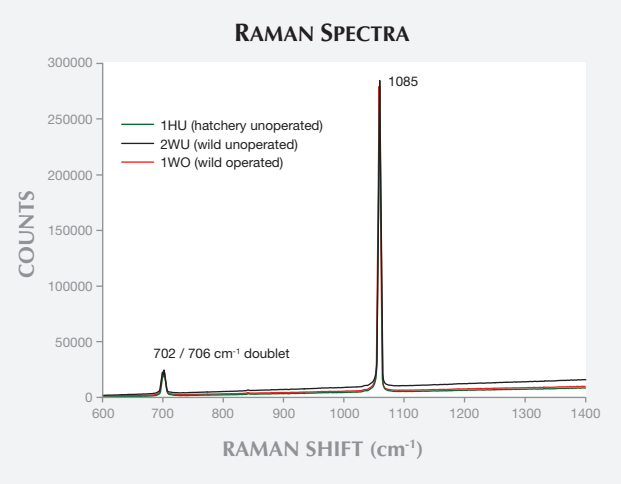

Figure 34. Three representative Raman spectra were gained from pearls produced by a P. maxima *hatchery-reared shell, a wild unoperated* P. maxima *shell, and a wild operated* P. maxima *shell. Each showed virtually identical spectral features that were consistent with aragonite. The representative samples are the same as those used for the PL spectra (figure 35).*

the opaque nature of pearls, such spectra must be recorded in a percentage reflectance. These spectra are important in defining some species and in some cases whether or not a treatment has been applied.

The white pearls in this group for which spectra were recorded (table 2) revealed curves that differed only in the reflectance at given wavelengths (figure 36). The only exception was 2WU, where there appears to be a slight difference in shape throughout the visible range (nominally 400–700 nm). The percentage reflectance throughout the visible region for each of the other samples decreases slightly toward the longer wavelengths. For sample 2HU, this translates to a percentage reflectance of 77.2 at 400 nm to 72.7 at 700 nm. For 1WO, this translates to a percentage reflectance of 84.65 at 400 nm and 78.41 at 700 nm.

A reflectance trough at 278 nm is common to all the spectra for these pearls, as is a peak at 253 nm and a percentage reflectance drop to between 32 and 34 at 200 nm.

Chemical Composition. LA-ICP-MS provides qualitative and quantitative data of chemical elements. The laser sampling area (5 µm) can be focused on very small color and other surface zones. The ablation mark is less than the width of a human hair, visible only under magnification. The ablated particles are carried by helium gas to the plasma torch and mass spectrometer for analysis. The plasma unit atomizes and ionizes the atoms. The mass spectrometer measures the mass of each element for identification according to mass-to-charge ratio. LA-ICP-MS is a powerful method in the separation between saltwater and freshwater pearls and the detection of some treatments.

All of the pearls listed in table 2 were analyzed by LA-ICP-MS, and the results are presented in table 8. The pearls show great similarity in trace-element levels, with only 1WO trending toward the high end for Mn, Sr, Ba, La, Ce, and Pb. Many more examples of each type will need to be analyzed to determine if any significant trends exist.

TABLE 8. Trace-element composition recorded by LA-ICP-MS (figures are in ppmw).[a]

	Specimen	^{7}Li	^{11}B	^{23}Na	^{24}Mg	^{31}P	^{39}K	^{45}Sc	^{55}Mn	^{57}Fe	^{66}Zn	^{69}Ga	^{88}Sr	^{137}Ba	^{139}La	^{140}Ce	^{208}Pb	^{209}Bi
Wild unoperated	1WU	bdl	22.1	7177.0	136.2	bdl	123.9	bdl	2.3	179.4	1.1	bdl	1327	0.52	0.02	0.00	0.10	0.00
	2WU	bdl	19.6	9017.0	98.9	bdl	194.2	bdl	2.3	168.3	0.3	bdl	1440	0.76	0.03	0.09	0.30	0.04
	3WU	bdl	21.6	7708.0	139.8	28.3	162.2	bdl	3.5	158.0	1.0	bdl	1093	0.36	0.00	0.00	0.06	0.01
Wild operated	1WO	bdl	18.3	7749.0	166.1	bdl	133.9	bdl	17.9	158.2	3.4	bdl	1719	1.43	0.20	0.26	0.44	0.04
Hatchery	1HU	bdl	25.7	8329.0	183.2	23.0	147.2	bdl	7.2	164.9	0.7	bdl	1461	0.95	0.03	0.06	0.18	0.02
	2HU	bdl	26.9	7486.0	176.3	bdl	115.2	bdl	2.8	161.6	2.6	bdl	1414	1.15	0.06	0.07	0.13	0.02
	3HU	bdl	20.7	6918.0	146.0	29.0	81.3	bdl	1.5	165.3	1.0	bdl	1321	0.67	0.07	0.07	0.08	0.02
	4HU	bdl	19.6	6492.0	124.2	28.6	78.8	bdl	2.5	153.1	2.5	bdl	1318	0.71	0.01	0.01	0.02	0.03
Detection Limit		1.36	1.50	22.87	0.89	22	9.12	1.46	0.75	43.88	0.65	0.17	0.36	0.32	0.012	0.02	0.04	0.01

[a] *Abbreviations: bdl= below detection limit*

CONCLUSIONS

The foregoing text and images clearly establish the ongoing recovery of natural pearls from *P. maxima* in Australian waters, a region with a significant pearling tradition stretching back to the 19th century and earlier (figure 37). The historical evidence is contained within official records as well as personal experiences related by respected authors of the time, such as Kornitzer (1937) and Kunz and Stevenson (1908).

Many gemologists have written excellent papers on the separation of cultured from natural pearls using various techniques (see Recommended Reading list), but few have been wholly educational or all-encompassing in terms of the microradiographic structures one might expect from natural pearls. This may be because of the exceedingly wide variation of possibilities, the difficulty of gaining sufficiently high-resolution images, or the research time to devote to a project that produces a large volume of data. Moreover, the journals would have to be willing to publish the extraordinary numbers of images necessary to convey the scope of the data. Web publishing is beginning to provide a greater volume of microradiographic structural images, which were and are beyond the scope of printed jour-

Figure 35. Three representative PL spectra obtained from pearls produced by a hatchery-reared shell, a wild unoperated shell, and a wild operated shell. Each showed virtually identical spectral features that were consistent with pearls produced by P. maxima. *The representative samples are the same as those used for the Raman spectra (figure 34).*

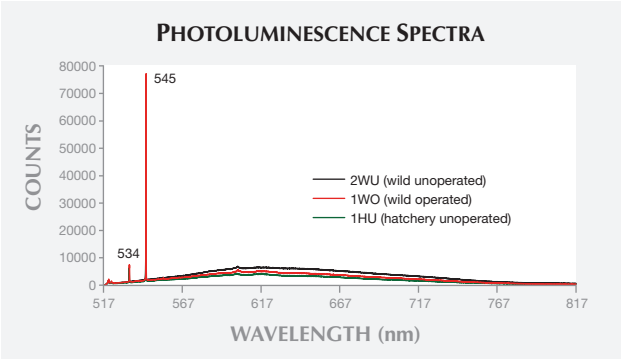

Figure 36. The reflectance spectra for the pearl samples. Note that the lamp switch point at 319 nm and a filter change at 373 nm create slight anomalous shifts in the recorded spectra.

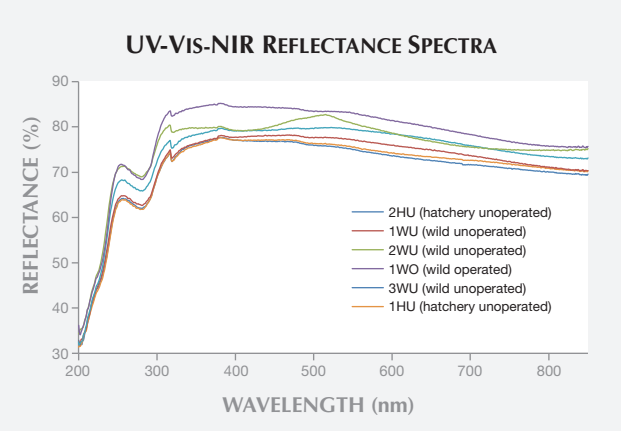

Figure 37. Australia's natural pearling tradition continues today, exemplified by this 11.74 × 11.24 × 9.18 mm pearl (weighs 35.04 grains) atop the shell of a P. maxima *oyster, discovered in July 2011. Photo by K. Scarratt.*

nals or books. An example of this is the document authored by N. Sturman (2009).

Sturman (2009) shows through a series of microradiographs both obvious and subtle examples of internal structures recorded for non-bead (intentional or unintentional) cultured pearls. The paper also presents a few historical microradiographs for both natural and bead cultured pearls.

Of the eight natural pearls collected during this project, samples 4HU (found in a hatchery unoperated shell), 1WU (taken from the mantle of a wild unoperated shell), and 2WU (from the mantle of a wild unoperated shell) may have sufficient internal growth structures to be identified as natural in a "blind" test.

Pearl 1WO (from the mantle of a wild operated shell) may not have a classic microradiographic structure for a natural or nonbead-cultured pearl, which might result in some debate concerning its nature given that the mollusk had been on a farm. Nevertheless, a blind test would conclude that the pearl was of natural origin, a result that would be consistent with the data collected.

Returning to 3WU, the microradiographic structure recorded may easily misinterpreted as that of a nonbead-cultured pearl, and herein lies the first dilemma for those involved in both the pearling industry and pearl testing.

Over the past decade or so, the type of structure observed in pearl 3WU has been assumed to be an indicator of non-bead cultured growth. This assumption probably resulted from the structure's resemblance to the "classic" nonbead-cultured pearl structure (see Sturman, 2009). This pearl challenges that assumption.

The second dilemma concerns more the pearling industry. In industry discussions, it has often been suggested that anything produced by a mollusk on a pearl farm is cultured—and that a pearl produced by a hatchery-raised mollusk should also be considered cultured. Yet the very basis of a pearl culturing operation lies in the ability of technicians to create a "sac" for the cultured pearl. It is not the host mollusk but the creation of this sac that defines the process. Pearls produced within a sac that is a product of human intervention are clearly cultured. But if a sac is a creation of nature, without human intervention, then logic dictates that anything it produces is "of nature." Even if one opposes this logic, the fact remains that pearls 1HU, 2HU, 3HU, and 4HU, the products of pearl sacs formed by nature within hatchery-reared shell, are virtually indistinguishable from natural pearls and could not be identified as cultured.

This examination of a small number of definitive samples has therefore produced what may appear to be

unexpected results that may add further to the challenges faced with pearl identification. Clearly, many more samples from each of the types discussed will need to be collected and examined before a clearer picture emerges. In the meantime, the authors will conduct ongoing expeditions and research. In late November 2012, some of the authors were able to extract another 30 natural pearls from Australian *Pinctada maxima*, and the technical data from these will be the subject of another report.

ABOUT THE AUTHORS

Mr. Scarratt is GIA's managing director of Southeast Asia and director of its Bangkok laboratory. Peter and Michael Bracher are executive directors of the Paspaley Group of Companies. Mr. Attawi is a gemologist, and Mr. Safar is director, of the Gem and Pearl Testing Laboratory of Bahrain. Ms. Saesaw is analytical lead, Ms. Homkrajae is a staff gemologist, and Mr. Sturman is supervisor of the pearl identification department at GIA's Bangkok laboratory.

ACKNOWLEDGMENTS

The authors gratefully acknowledge the enthusiastic assistance of the Paspaley pilots, skippers, and crews, especially the team of divers who collected many thousands of shell during the season leading up to our expedition. We truly appreciate the assistance of David Mills, lead scientist/biologist at the Paspaley Pearling Company, and we unquestionably owe thanks to Nick Paspaley, who has been incredibly supportive over many years. We also owe the manuscript reviewers a note of thanks for their efforts to ensure the readability and presentation of this paper. The Australian National Museum is thanked for access to the available fine historic photography of pearling in Australia.

REFERENCES

Alexander A.E. (1941) Natural and cultured pearl differentiation (parts 1 and 2). *G&G*, Vol. 3, No. 11/12, pp. 169–172, 184–188.

Bartlett N. (1954) *The Pearl Seekers*. Andrew Melrose Limited, London, 309 pp.

Bauer M. (1904) *Precious Stones*. Charles Griffin and Co., London, 647 pp.

Benham C. (1949) *Diver's Luck: A Story of Pearling Days.* Angus and Robertson, Sydney, 258 pp.

Berge V., Lanier H.W. (1930) *Pearl Diver: Adventuring Over and Under Southern Seas*. Doubleday, Doran & Company Inc., New York, 368 pp.

Broadfield R. (2010) Pearl meat the new gem on menus. *The West Australian*, http://au.news.yahoo.com/thewest/lifestyle/a/-/lifestyle/7110030/pearl-meat-the-new-gem-on-menus/.

Cilento R. (1959) *Triumph in the Tropics: An Historical Sketch of Queensland*. Smith & Paterson Pty. Ltd., Brisbane.

Dodd M. (2011) *The Last Pearling Lugger: A Pearl Diver's Story*. Macmillan, Sydney, 240 pp.

Doelter C.A. (1896) Verhalten der Mineralien zu den "Röntgen'schen" X-Strahlen. *Neues Jahrbuch für Mineralogie*, Vol. 2, pp. 87–106.

Dubois R. (1901) Sur la mode de formationdes perles dans Myt.ed, *Compte Rendu des Séances de L'Académie des Sciences*.

Dubois R. (1913) La Perle et L'huitre Perliere. *La Science et la Vie*, Vol. 11, No. 8. p. 15.

Edwards C.L. (1913) The abalones of California. *Popular Science*, Vol. 83, No. 36, pp. 533–550.

Ellies A. (2010) *The Pearls of Broome*. CopyRight Publishing, Brisbane, 978 pp.

Gale C.F. (1901) Report on Pearling and Turtle Industry in the North-West. Oct. 1, 3 pp.

Hart A.M., Friedman K.J. (2004) Mother-of-pearl shell (*Pinctada maxima*): Stock evaluation for management and future harvesting in Western Australia. FRDC Project No. 1998/153, Fisheries, P., Western Australia. November 2004, www.fish.wa.gov.au/res.

Hedegaard C. (1996) Formation and composition of gems from the sea: Pearls from American waters. *In Proceedings of Gemmologia Europa VI: Gemmologists of the World on Gems from the Sea,* CISGEM, Milan, pp. 106–129.

Hainschwang T., Hochstrasser T. (2011) Gem News International: A most unusual blister pearl. *G&G*, Vol. 45, No. 4, pp. 300–301.

Hurley F. (1924) *Pearls and Savages: Adventures in the Air, on Land and Sea—in New Guinea*. G.P. Putnam's Sons, London, 414 pp.

Jameson H.L. (1901) On the identity and distribution of the mother of pearl oysters; with a revision of the subgenus *Margaritifera*. *Proceedings of the Zoological Society of London*, Vol. 70, No. 2, pp. 372–394.

Kiefert L., Hänni H.A., Ostertag T. (2001) Raman spectroscopic applications to gemmology. In I.R. Lewis and H.G.M. Edwards, Eds., *Handbook of Raman Spectroscopy: From the Research Laboratory to the Process Line*. Marcel Dekker, New York, pp. 469–489.

Kornitzer L. (1937) *The Pearl Trader*. Sheridan House, New York, 359 pp.

——— (1947a) Pearls and men: First steps in a difficult art. *The Gemmologist*, Vol. 16, No. 195, pp. 285–290.

Kunz G.F., Stevenson C.H. (1908) *The Book of the Pearl*. The Century Co., New York, 548 pp.

Lennon, P. O. (1934) Knapping Flints, the Oldest Industry. *Sands, Clays and Minerals,* Vol. 2, No. 1, pp. 67–71.

Mikimoto K. (1922) *Processes for Causing Oysters to Produce Pearls*. United Kingdom Patent GB157788, issued April 10.

Pearl shell (1949) *Northern Standard*, Darwin, August 26.

PearlMan (2011) Speaking of natural pearls, Part 2, Sea Cortez Pearl Blog, http://www.perlas.com.mx/blog/tag/pea-crab/.

Scarratt K. (1986b) Notes from the Laboratory: The Southern Cross. *Journal of Gemmology*, Vol. 20, No. 3, pp. 145–146.

Smith G.F.H. (1905) An improved form of refractometer. *Mineralogical Magazine*, Vol. 14, No. 64, pp. 83–86.

Smith M.M., Heemstra P.C., Eds. (2003) *Smiths' Sea Fishes*. Struik Publishers, Cape Town, 1047 pp.

Smith P.A., Devereux L. (1999) Streeter's Jetty, Broome, Western Australia: An example of a heritage icon moving from private ownership to community control. *Australasian Historical Archaeology*, Vol. 17, pp. 116–120.

Streeter E.W. (1886) *Pearls and Pearling Life*. George Bell & Sons, London.

Sturman N. (2009) The microradiographic structures of non-bead cultured pearls, http://www.giathai.net/pdf/The_Microradiographic_structures_in_NBCP.pdf.

Taunton H. (1903) *Australind: Wanderings in Western Australia and the Malay East*. Edward Arnold, London.

Walcott P. (1881) Western Australia Report by the Inspector of Pearl Shell fisheries of his proceedings on the North-West Coast.

ADDITIONAL READING

Akamatsu S., Li T.Z., Moses T.M., Scarratt K. (2001) The current status of Chinese freshwater cultured pearls. *G&G*, Vol. 37, No. 2, pp. 96–113, http://dx.doi.org/10.5741/GEMS.37.2.96.

Anderson B.W. (1961) Cultured pearls with split nuclei. *The Gemmologist*, Vol. 30, No. 358, p. 86.

Anderson B.W., Payne C.J. (1953) The density of pearls and cultured pearls. *The Gemmologist*, Vol. 22, No. 262, pp. 81–86.

Gutmannsbauer W., Hänni H.A. (1994) Structural and chemical investigations on shells and pearls of nacre forming salt- and fresh-water bivalve molluscs. *Journal of Gemmology*, Vol. 24, No. 4, pp. 241–252.

Hänni H.A. (1983) The influence of the internal structure of pearls on Lauegrams. *Journal of Gemmology*, Vol. 18, No. 5, pp. 386–400.

Hänni H.A. (1996) A short synopsis of pearls: Natural, cultured, imitation. *Journal of the Gemmological Association of Hong Kong*, Vol. 18, pp. 43–46.

Hänni H.A. (1999) Sur la formation de nacre et de perles. *Revue de Gemmologie a.f.g.*, No. 137, pp. 30–35.

Hänni H.A., Kiefert L., Giese P. (2004) Ein notwendiger Test in der Perlenuntersuchung. *Zeitschrift der Deutschen Gemmologischen Gesellschaft*, Vol. 53, No. 1. pp. 39–42.

Kornitzer L. (1947b) Pearls and men: On the valuation of pearls. *The Gemmologist*, Vol. 16, No. 197, pp. 339–344.

——— (1947c) Pearls and men: Pearls are expensive. *The Gemmologist*, Vol. 16. No. 193, pp. 231–235.

——— (1947d) Pearls and men: Seed pearls. *The Gemmologist*, Vol. 16, No. 188, pp. 91–95.

——— (1947e) Pearls and men: The advent of the cultured pearl. *The Gemmologist*, Vol. 16, No. 196, pp. 312–316.

——— (1947f) Pearls and men: The gentle art of being a rogue. *The Gemmologist*, Vol. 16, No. 191, pp. 207–211.

——— (1947g) Pearls and men: The lore of the pearl. *The Gemmologist*, Vol. 16, No. 189, pp. 120–124.

——— (1947h) Pearls and men: The pearls birth certificate. *The Gemmologist*, Vol. 16, No. 192, pp. 207–211.

Scarratt K. (1984a) Natural pearls. *Journal of Gemmology*, Vol. 19, No. 2, pp. 107–108.

——— (1984b) Notes from the Laboratory: A filled pearl. *Journal of Gemmology*, Vol. 19, No. 2, pp. 113–114.

——— (1984c) Notes from the Laboratory: Large non-nucleated cultured pearls. *Journal of Gemmology*, Vol. 19, No. 2, pp. 114–115.

——— (1984d) Notes from the Laboratory: Mauve freshwater natural pearls. *Journal of Gemmology*, Vol. 19, No. 2, pp. 119–121.

——— (1984e) Notes from the Laboratory: Stained mottled brown cultured pearls. *Journal of Gemmology*, Vol. 19, No. 2, pp. 107–108.

——— (1986a) Notes from the Laboratory: Natural pearl necklace with a bead-like centre. *Journal of Gemmology*, Vol. 20, No. 2, p. 95.

——— (1989a) Notes from the Laboratory: Double nucleated cultured pearls. *Journal of Gemmology*, Vol. 21, No. 5, pp. 294–295.

——— (1989b) Notes from the Laboratory: Repaired and filled pearls. *Journal of Gemmology*, Vol. 21, No. 5, pp. 294–296.

Scarratt K., Moses T., Akamatsu S. (2000) Characteristics of nuclei In Chinese freshwater cultured pearls. *G&G*, Vol. 36, No. 2, pp. 98–109, http://dx.doi.org/10.5741/GEMS.36.2.98.

Streeter E.W. (1882) *The Great Diamonds of the World*. George Bell & Sons, London, 321 pp.

——— (1892) *Precious Stones and Gems*. Bell, London, 355 pp.

——— (1895) *The Koh-i-Nûr Diamond: Its Romance & History*. George Bell & Sons, London.

Wang W., Scarratt K., Hyatt A., Shen A.H.-T., Hall M. (2006) Identification of "Chocolate Pearls" treated by Ballerina Pearl Co. *G&G*, Vol. 42, No. 4, pp. 222–235, http://dx.doi.org/10.5741/GEMS.42.4.222.

Webster R. (1949) Stained pearls and x-rays. *Journal of Gemmology*, Vol. 2, No. 2, pp. 51–54.

——— (1950) London laboratory's new x-ray equipment. *G&G*, Vol. 6, No. 9, pp. 279–281.

——— (1954) Some unusual structures in pearls and cultured pearls. *Journal of Gemmology*, Vol. 4, No. 8, pp. 325–334.

——— (1955a) X-rays and their use in gemmology: Part II: Friedrich and Knipping experiment. *The Gemmologist*, Vol. 24, No. 286, pp. 87–91.

——— (1955b) X-rays and their use in gemmology: Part IV: Skiagram method for pearl testing. *The Gemmologist*, Vol. 24, No. 288, pp. 131–135.

——— (1955c) X-rays and their use in gemmology: Part V: Laue patterns. *The Gemmologist*, Vol. 24, No. 289, pp. 148–151.

——— (1957a) Cultured pearls: Part III: Cultivating the oyster. *The Gemmologist*, Vol. 26, No. 314, pp. 158–163.

——— (1957b) The detection of cultured pearls: Part 1: How it started. *The Gemmologist*, Vol. 26, No. 315, pp. 178–184.

——— (1957c) The detection of cultured pearls: Part 2: Further identification methods. *The Gemmologist*, Vol. 26, No. 316, pp. 200–207.

——— (1966) X-rays in the testing of gems. *X-Ray Focus*, Vol. 7, No. 1, pp. 2–5.

Webster R., Anderson B.W. (1983) *Gems: Their Sources, Description and Identification*, 4th ed. Butterworths, London, 1006 pp.

DETECTING HPHT SYNTHETIC DIAMOND USING A HANDHELD MAGNET

Kirk Feral

This study investigated the effectiveness of a handheld magnet in detecting synthetic diamonds. A total of 104 synthetic diamonds from nine different manufacturing sources were tested. Of the HPHT-grown synthetic samples tested, 58% registered a detectable magnetic response. Strong N52-grade neodymium magnets were able to detect 35% more HPHT synthetics than traditional ferrite and alnico magnets. CVD-grown synthetic diamonds showed no magnetic attraction. A set of 168 natural diamonds, including HPHT-treated natural diamonds, was tested as a control group. None of the natural transparent diamond samples showed attraction to a neodymium magnet, but two heavily included translucent specimens with unusually large opaque inclusions were strongly magnetic. A new magnetic testing method is presented for detecting small magnetic inclusions in loose HPHT-grown products, and for identifying small synthetic diamonds mounted in jewelry.

Instruments used by gem testing labs to identify synthetic diamonds, such as the DiamondView and DiamondSure, are specialized and costly. Electronic diamond testers that measure a gem's thermal conductivity to detect imitations are readily available to consumers, but these instruments cannot distinguish natural from lab-grown diamonds. Spectrometers, microscopes, polariscopes, and UV lamps are standard gemological tools that can be effective in detecting signs of synthetic origin, but only if one knows how to use them and interpret the results. For those without training or access to such equipment, a handheld magnet can serve as a practical and inexpensive tool (Matlins and Bonano, 2008). This study attempts to evaluate the effectiveness of magnetic testing for separating natural from synthetic diamonds.

For decades, gemologists have known that synthetic diamonds grown under high-temperature, high-pressure (HPHT) conditions often contain iron-rich flux particles that are sufficiently large and abundant to cause visible attraction to a magnet (Webster, 1970, p. 332; Koivula, 1984, figure 1). Since natural

Figure 1. Magnetic attraction is an almost certain indication of HPHT synthetic diamond. In this photo, a blue 0.22 ct HPHT synthetic diamond is being picked up by a 1/16 in. diameter neodymium magnet at the site of a flux inclusion located below the surface of the pavilion facets. Photo by K. Feral.

See end of article for About the Author and Acknowledgments.
GEMS & GEMOLOGY, Vol. 48, No. 4, pp. 262–272,
http://dx.doi.org/10.5741/GEMS.48.4.262.

diamonds normally show no magnetic attraction, any positive response is generally considered an indicator of synthetic origin.

This distinction is critical for determining value, as a synthetic diamond sells for considerably less than a natural stone of similar quality. Melee-size goods (under 0.20 ct) are of particular concern, as these generally go untested and their origins may be unknown to the appraiser, gem dealer, or buyer. A study by Kitawaki et al. (2008) identified nearly 10% of the loose yellow melee-size diamonds tested as HPHT-grown synthetics. In that same study, tests on fine jewelry containing yellow melee diamonds showed that half of the pieces each contained an average of 10% HPHT-grown samples.

Laser inscriptions used by most manufacturers to brand their products are seldom applied to melee-size goods. In the current study, loose melee comprised half of the HPHT synthetic diamonds tested, and half of these small samples could be detected with a magnet. Techniques developed during this study provide a means to test individual diamonds mounted in jewelry for synthetic origin, including melee-size goods.

Figure 2. Five magnets of different sizes and strengths were compared in testing HPHT-grown synthetic diamonds for magnetic response. Left to right: a ½ in. diameter ferrite disc wand, a 1 in. wide alnico horseshoe magnet, a ⅕ in. diameter Hanneman wand, a ½ in. diameter N52 neodymium wand, and a 1/16 in. diameter N52 neodymium pinpoint wand. Photo by K. Feral.

BACKGROUND

Test samples were obtained from all major manufacturers of gem-quality synthetic diamonds, as well as two manufacturers of industrial-grade synthetics (DeBeers and Sumitomo). Table 1 shows how HPHT-grown samples responded to a handheld magnet. Direct responses are further classified as either "Pickup" or "Drag" responses. Fewer than half of the samples showed this type of obvious response. Weaker responses, made visible by floating the individual sample on a small raft in water, are noted as Strong, Weak, or Diamagnetic (repelled).

Relative to the total mining output of gem-quality diamonds each year, synthetic diamond production is still quite small, but their presence in the jewelry trade is growing. Until recently, most gem-quality synthetics were grown using the HPHT process, which has a production time of several days and involves ferromagnetic flux metals such as iron, nickel, and (to a lesser extent) cobalt. Yellow is the most common bodycolor encountered in HPHT-grown synthetic diamonds.

Newer to the trade are synthetic diamonds grown by chemical vapor deposition (CVD) without flux metals or high pressure. This process generally takes longer than HPHT growth, and most CVD synthetics are currently limited to sizes less than 1 ct. At the present time, CVD products are generally colorless, although pink and a number of other colors can be induced after CVD growth by processes such as HPHT treatment, low-temperature annealing, and irradiation (Kitawaki et al., 2010). Methods of synthesis continue to evolve, and some industry observers estimate that the annual production of gem-quality CVD-grown synthetic diamonds now significantly exceeds that of HPHT-grown material (A. Grizenko and S. Pope, pers. comm., 2012).

Published reports that mention magnetic testing of synthetic diamonds often do not specify the type, size, or strength of the magnets used, or the rate of detection achieved. Traditional magnets such as ferrite refrigerator magnets (containing iron oxides) and alnico (aluminum-nickel-cobalt) horseshoe magnets have been employed by gemological researchers, as well as Dr. William Hanneman's neodymium magnetic wand. The Hanneman wand, introduced as a synthetic diamond tester in 1995, contains a 5 mm diameter neodymium-iron-boron magnet of unspecified grade.

The effect of magnet strength on the rate of detection has not been investigated until now, nor has there been an attempt to standardize testing procedures to the strongest permanent magnet available today, the N52-grade neodymium magnet. This study compares alnico, ferrite, and neodymium magnets as testing tools (figure 2), and looks at the rele-

TABLE 1. Magnetic responses for 85 HPHT synthetic diamonds.

Sample	Weight (ct)	Color	Cut	Response	Sample	Weight (ct)	Color	Cut	Response
DeB 21301	0.06	Colorless	Round brilliant	Diamagnetic	Chat PR13	0.85	Pink	Round brilliant	Pickup
GTL 30580	2.42	Yellow	Rough	Pickup	Chat PR14	0.55	Pink	Round brilliant	Weak
GTL 30579	3.66	Yellow	Rough	Pickup	Chat PR15	0.07	Pink	Round brilliant	Diamagnetic
GTL 30578	3.81	Yellow	Rough	Pickup	Chat PR16	0.06	Pink	Round brilliant	Diamagnetic
Sum 28756	0.37	Yellow	Partially faceted	Diamagnetic	Chat PR17	0.06	Pink	Round brilliant	Diamagnetic
Sum 28753	0.17	Yellow	Square	Diamagnetic	Chat PR18	0.06	Pink	Round brilliant	Diamagnetic
Sum 28521	0.18	Red	Square	Diamagnetic	Chat PR19	0.05	Pink	Round brilliant	Diamagnetic
Sum 28518	0.36	Yellow	Tabular	Pickup	Chat PR20	0.06	Pink	Round brilliant	Diamagnetic
Sum 28516	0.35	Red	Tabular	Diamagnetic	Chat PR21	0.06	Pink	Round brilliant	Diamagnetic
Sum 28513	0.19	Yellow	Round brilliant	Weak	GDC LG7401	0.33	Yellow	Radiant	Diamagnetic
Sum 28507	0.12	Yellow	Tabular	Diamagnetic	GDC LG7402	0.34	Yellow	Radiant	Diamagnetic
Sum 17729	0.80	Yellow	Partially faceted	Diamagnetic	GDC LG8314	0.32	Yellow	Emerald	Diamagnetic
TCG 21892	0.12	Red	Hexagon	Diamagnetic	GDC LG8118	0.34	Yellow	Princess	Diamagnetic
TCG 21891	0.13	Yellow	Hexagon	Weak	GDC LG8203	0.34	Yellow	Princess	Weak
TCG 21006	0.61	Yellow	Partially faceted	Pickup	AOTC YB84	1.10	Yellow	Round brilliant	Drag
UIM 21500	0.17	Yellow	Round brilliant	Pickup	AOTC BB414	0.77	Blue	Round brilliant	Pickup
UIM 21305	0.08	Colorless	Round brilliant	Pickup	AOTC YB136	0.62	Yellow	Round brilliant	Diamagnetic
UIM 21304	0.23	Colorless	Partially faceted	Diamagnetic	AOTC B407	0.56	Blue	Round brilliant	Pickup
UIM 21303	0.06	Blue	Round brilliant	Pickup	AOTC B192	0.51	Blue	Round brilliant	Diamagnetic
UIM 21300	0.17	Colorless	Square	Diamagnetic	AOTC BB242	0.30	Blue	Round brilliant	Diamagnetic
UIM 20490	0.50	Brown	Partially faceted	Pickup	AOTC BB79	0.28	Blue	Round brilliant	Diamagnetic
UIM 20489	0.55	Brown	Partially faceted	Pickup	NAD YR001	0.47	Yellow	Rough	Pickup
UIM 20488	0.68	Brown	Partially faceted	Strong	NAD YR002	0.54	Yellow	Rough	Pickup
UIM 20426	0.16	Yellow	Tabular triangle	Weak	NAD YR003	0.61	Yellow	Rough	Weak
UIM 20425	0.17	Brown	Tabular triangle	Diamagnetic	NAD YR004	0.46	Yellow	Rough	Pickup
UIM 20423	0.46	Yellow	Tabular	Weak	NAD YR005	0.42	Yellow	Rough	Pickup
UIM 20201	0.17	Yellow	Tabular triangle	Diamagnetic	NAD YR006	0.30	Yellow	Rough	Pickup
UIM 20195	0.45	Yellow	Tabular	Diamagnetic	NAD YR007	0.24	Yellow	Rough	Pickup
UIM 20194	0.46	Yellow	Tabular	Diamagnetic	NAD YR008	0.29	Yellow	Rough	Pickup
UIM 20193	0.16	Yellow	Tabular triangle	Diamagnetic	NAD YR009	0.29	Yellow	Rough	Pickup
UIM 19368	0.09	Yellow	Cube	Diamagnetic	NAD YR0010	0.08	Yellow	Rough	Diamagnetic
UIM 17799	0.15	Yellow	Square	Diamagnetic	NAD YR0011	0.06	Yellow	Rough	Diamagnetic
UIM 17621	0.06	Colorless	Round brilliant	Diamagnetic	NAD YR0012	0.14	Yellow	Rough	Pickup
UIM 17620	0.19	Blue	Partially faceted	Pickup	NAD YR0013	0.07	Yellow	Rough	Pickup
UIM 17619	0.05	Colorless	Round brilliant	Pickup	NAD YR0014	0.04	Yellow	Rough	Pickup
UIM 21499	0.16	Yellow	Round brilliant	Weak	NAD BR001	0.16	Blue	Rough	Drag
UIM 24030	0.22	Blue	Round brilliant	Pickup	NAD BR002	0.09	Blue	Rough	Pickup
UIM 28754	0.19	Yellow	Baguette	Diamagnetic	NAD BR003	0.03	Blue	Rough	Pickup
UIM 23580	1.07	Yellow	Square	Strong	NAD BR004	0.04	Blue	Rough	Pickup
UIM 21501	0.14	Yellow	Round brilliant	Strong	NAD BR005	0.25	Blue	Rough	Pickup
UIM 28957	0.58	Yellow	Partially faceted	Pickup	NAD BR006	0.35	Blue	Rough	Pickup
UIM 0212	>0.50	Yellow	Faceted	Pickup	NAD BR007	0.02	Blue	Rough	Drag
Chat PR12	0.65	Pink	Round brilliant	Pickup					

Abbreviations: DeB=De Beers, TCG=Tairus Created Gems, GTL=Golden Triangle Ltd., Sum=Sumitomo Electric, Chat=Chatham Created Gems, GDC=Gemesis Diamond Company, AOTC=AOTC Group B.V., NAD=New Age Diamonds, UIM=Unidentified Manufacturer

BOX A: TERMINOLOGY OF MAGNETISM

1. **Magnetic:** In the context of this paper, referring to any material that displays visible attraction to a handheld magnet.
2. **Diamagnetic:** Having a temporary low magnetization that is opposed to the inducing field of a magnet and is consequently repelled by it. Using a strong neodymium magnet, we can clearly demonstrate this phenomenon by placing a diamagnetic material such as natural diamond on a raft floating in water. The raft moves away from the magnet.
3. **Paramagnetic:** Having a temporary magnetization that is induced when an external magnet is applied. Paramagnetic materials have a weaker magnetic response than ferromagnetic materials, and they cannot be permanently magnetized. Many colored gemstone materials (such as garnet) are paramagnetic, showing visible attraction to an N52-grade neodymium magnet.
4. **Ferromagnetic:** Referring to an element such as iron, nickel, and cobalt that retains permanent magnetization in the absence of an applied field. Such materials are picked up by a magnet, and their magnetic attraction is up to a million times stronger than that of paramagnetic materials.
5. **Ferrimagnetic:** Referring to a strong, permanent magnetization that occurs in materials where the magnetic fields associated with individual atoms align themselves—some in parallel (as with ferromagnetism) and others in opposite directions. Magnetite is a ferrimagnetic mineral.
6. **Antiferromagnetic:** A type of ordered magnetism that occurs in a material when electron spins are alternately opposed, resulting in almost no external magnetization. Like ferromagnetic and ferrimagnetic substances, antiferromagnetic materials exhibit strong, direct responses to a magnet.
7. **Magnetic Susceptibility:** The ratio of a material's induced magnetization to the applied field of a magnet, this represents how strongly or weakly a material responds to a magnetic field. The degree of magnetic susceptibility can be measured precisely with instruments such as a magnetometer or magnetic susceptibility balance (Hoover, 2007).

vance of magnet size and strength in separating synthetic diamond from natural.

Natural diamond is considered non-magnetic—or more precisely, diamagnetic (repelled by a magnet), as its primary component is carbon, a diamagnetic element. (See box A for explanations of magnetic terms used in this article.) Previous studies have shown that magnetic minerals are commonly found as inclusions in natural diamond. Yet the microscopic size of these inclusions renders them magnetically undetectable except by ultrasensitive instruments such as a SQUID magnetometer (Rossman and Kirschvink, 1984; Yelisseyev et al., 2008).

The most common magnetic mineral found in natural diamond is pyrrhotite, a ferromagnetic iron sulfide mineral that, like all natural diamond inclusions, generally measures less than 0.5 mm (Clement et al., 2008). Pyrrhotite inclusions are dark, opaque particles that can be mistaken for "carbon spots." Another relatively common magnetic inclusion in natural diamond is chrome pyrope garnet, a paramagnetic gem mineral that may appear as red transparent crystal inclusions.

Other magnetic inclusions such as chromite and hematite (both antiferromagnetic) and native iron (ferromagnetic) are only rarely encountered in diamond (Boyd and Meyer, 1979). It would be difficult to find a natural diamond with magnetic mineral inclusions of any kind large enough to be detected with a handheld magnet (Koivula, 2000, p. 134). Prior to this study, no such cases had been reported.

In Brief

- Simple testing methods using N52-grade neodymium magnets detect a significant percentage of HPHT synthetic diamonds. The detection rate with traditional magnets is substantially lower.
- CVD-grown synthetic diamonds contain no detectable metallic impurities and cannot be separated from natural diamonds using magnetic testing.
- This study documents the first case of a natural faceted diamond attracted to a handheld magnet due to natural mineral inclusions.
- Small diamonds mounted in jewelry, including melee-size gems, can be individually tested for synthetic origin using a small $^{1}/_{16}$ in. diameter N52 magnet in conjunction with flotation.

Aside from magnetic mineral inclusions, natural diamonds are subject to surface contamination from tiny amounts of iron deposited by a metal dop stick

or polishing wheel during the faceting process. Shen and Shigley (2004) documented a diamond that showed a visible magnetic response due to iron residue deposited inside cavities at the girdle and pavilion facets during polishing. One magnetic natural diamond in the current study was found to contain similar surface inclusions, which appeared to result from contamination during polishing.

Nevertheless, these metallic impurities in natural diamond are typically insignificant compared to those found in synthetic diamond, and normally they are not detectable with a magnet (Barnard, 2000, p. 94). The same applies to surface contamination of bruted (unpolished) girdles, where routine handling with tweezers can leave minute amounts of iron residue. No such contamination of bruted girdles was detected with a magnet during this study.

MATERIALS AND METHODS

Natural Diamonds. A total of 168 natural diamonds were tested as a control group, all ungraded as to type or clarity. The majority were colorless transparent rounds, but a few yellow and brown diamonds and an irradiated blue were among the test samples. All specimens, whether loose or mounted, were floated on a small raft in water to maximize the sensitivity of the magnetic tests.

GIA provided 50 untreated colorless natural diamonds ranging from 0.34 to 0.90 ct (figure 3, left). Most were eye-clean, while some had bruted girdles and one contained numerous black inclusions. GIA also supplied two gray/black carbonado rough diamonds from Sierra Leone (see box B).

Suncrest Diamonds provided 58 faceted HPHT-treated natural diamonds. They ranged from 0.05 to 0.70 ct and included colorless, yellow, pink, and green specimens (figure 3, right). Some of these samples may have been subjected to additional treatment by irradiation. Unlike the HPHT growth process, HPHT treatment of diamonds to enhance or alter color and improve clarity does not involve flux metals. Magnetic flux inclusions are not found in HPHT-treated diamonds.

A private collection of 48 natural diamonds mounted in vintage gold jewelry was also tested. This collection was assembled more than 30 years ago, prior to the use of synthetic diamonds in jewelry. These samples ranged from approximately 0.01 to 2 ct. Two contained microscopic red and orange-red crystal inclusions, possibly garnet. The vintage mounted diamonds and other natural diamond samples not provided by GIA or Suncrest were subjected to thermal conductivity testing, UV testing, and high-power magnification to verify their identity as natural diamonds rather than simulants or synthetics.

After a selective online search, two natural diamonds with exceptionally large opaque inclusions were acquired for this study. Theoretically, if para-

BOX B: NATURAL BLACK DIAMOND

The color of most natural black diamonds found in jewelry results from treatments such as irradiation, heat, or HPHT treatment. Naturally colored black diamond known as *carbonado* is mined in central Africa and Brazil for industrial purposes, but it is also occasionally faceted for jewelry use. These translucent to opaque gems are generally considered diamagnetic, as the black coloration is due primarily to numerous carbon inclusions in the form of graphite. Rough carbonado specimens tested in this study were not attracted to a magnet (figure B-1).

The only type of naturally colored black diamond that characteristically exhibits magnetic attraction is stewartite, a strictly industrial-grade bort from South Africa. This opaque polycrystalline diamond derives its strong magnetic properties from ferrimagnetic inclusions of magnetite (Bibby, 1982).

Figure B-1. This 3.11 ct rough carbonado diamond from Sierra Leone is diamagnetic. GIA Collection no. 5914; photo by K. Feral.

Figure 3. Untreated and treated natural diamonds were included in the study. On the left are three untreated samples provided by GIA: 0.64, 0.41, and 0.90 ct. On the right are four HPHT-treated natural diamonds from Suncrest Diamonds: a 0.43 ct colorless round, a 0.63 ct pink oval, a 0.66 ct green shield, and a 0.70 ct yellow round. Photos by K. Feral.

magnetic inclusions of garnet or ferromagnetic inclusions of pyrrhotite were large enough (over 0.5 mm) and concentrated close enough to the surface of a natural diamond, such a diamond could show visible attraction to an N52-grade neodymium magnet if the sensitive flotation method were applied. Both diamonds contained inclusions larger than 0.5 mm, and both exhibited magnetic attraction.

Synthetic Diamonds. A total of 85 HPHT-grown synthetic diamonds were examined, ranging from 0.02 to 3.81 ct. Faceted gems represented 51% of the sample set (figure 4), while the remainder were rough, partially faceted, or tabular in form. A few HPHT synthetic samples were completely colorless, but most showed various intensities of yellow, blue, pink, or red color.

Of the 85 HPHT-grown synthetics, 41 with unspecified acquisition dates were provided by the GIA Museum, 43 were recently supplied by the manufacturer, and one was recently made available by the Morion Company. Of the 41 GIA samples, 27 were from unidentified manufacturers and the remaining 14 were acquired from Sumitomo Electric (Japan), Tairus Created Gems (Russia), Golden Triangle (Russia), and De Beers (South Africa). The sources for the 43 HPHT diamonds recently loaned by the manufacturer were New Age Diamonds (Russia), AOTC Group B.V. (Netherlands), Chatham Created Gemstones (United States), and Gemesis Diamond Company (United States).

An additional 19 CVD-grown synthetic diamonds were tested. Scio Diamond Technology provided 14 colorless CVD-grown samples in the form of unpolished transparent wafers and blocks ranging from 0.25 to 0.57 ct, with 1–2 mm thicknesses. Gemesis Corp. provided five colorless faceted CVD synthetics in various shapes ranging from 0.27 to 0.30 ct.

Magnets. To determine whether magnet strength is a significant factor in detecting ferromagnetic inclusions in synthetic diamonds, HPHT synthetics were tested using five magnets of different strength. (Because they lack flux inclusions, the CVD samples were tested only with the two strongest magnets). The most powerful magnet, a ½ in. neodymium cylinder with a pull force of 18 pounds, was estimated to be more than 30 times stronger than the weakest magnet, a ½ in. ferrite disc. The five magnets are presented here in the order of weakest to strongest relative to pole surface area:

1. ½ in. diameter pole × 3⁄16 in. ferrite disc of unspecified grade
2. 1 in. alnico horseshoe magnet of unspecified grade with ¼ in. square poles
3. Hanneman wand with ⅛ in. diameter pole × 1⁄16 in. neodymium disc of unspecified grade

Figure 4. Magnetic attraction was observed in all three of these faceted HPHT synthetic diamonds, but only the 0.22 ct blue and 0.08 ct colorless samples were picked up by a magnet. Flotation was required to detect the weak magnetic attraction of the yellow 0.16 ct synthetic. Photo by K. Feral.

4. 1/16 in. diameter pole × ¼ in. N52-grade neodymium cylinder
5. ½ in. diameter pole × ½ in. N52-grade neodymium cylinder

Although the grade of the Hanneman wand was unknown, it exhibited a weaker pull force than an N42-grade neodymium magnet of the same dimensions. Other than the horseshoe magnet, the magnets were assembled as wands by attaching a handle.

Testing Methods. Three methods of magnetic testing were employed: the direct method, the flotation or floating method (Gumpesberger, 2006; see also www.gemstonemagnetism.com), and pinpoint testing. First, the magnet was placed directly against the surface of a sample to see if it would be picked up or dragged along a smooth dry surface. If no response was noted, the flotation method was employed. This test involved placing the sample on a foam raft floating in water, thereby reducing friction and greatly enhancing the sensitivity of the magnetic test. While the observer held the exposed pole end of the magnet near the surface of the sample, movement of the raft toward the magnet was noted as either weak or strong. Movement away from the magnet was noted as diamagnetic. Whenever a diamagnetic response was noted, the sample was subjected to the pinpoint method.

Flotation tests using a ½ in. diameter neodymium magnetic wand showed that the carbon body of a synthetic diamond could induce a diamagnetic (repelling) response that essentially masked localized ferromagnetism of small flux inclusions. Overcoming this problem required a wand that could be directed at specific areas of a sample where small inclusions were located. A 1/16 in. (1.5 mm) diameter neodymium magnet, the smallest diameter N52-grade magnet available today, was found suitable for that purpose. A pinpoint wand fashioned with this small magnet and used in conjunction with the flotation method proved effective in detecting small magnetic inclusions in HPHT synthetic diamonds that were not detectable by magnets with larger pole surfaces (see figure 5, left). Responses elicited by this method were at times extremely weak.

This study identified another important use for the pinpoint method. A pinpoint wand was effective in individually testing small diamonds (including melee size) mounted in jewelry for magnetic response. Jewelry pieces containing multiple diamonds were floated on a raft, and a pinpoint wand was directed at individual gems (figure 5, right). Fine jewelry castings of high-purity gold or silver are diamagnetic and therefore do not interfere with pinpoint testing. Because platinum is a paramagnetic metal, gems mounted in platinum castings are not suitable for magnetic testing.

RESULTS AND DISCUSSION

Natural Diamonds. Sensitive flotation and pinpoint testing with strong N52-grade neodymium magnets did not detect a positive magnetic response from any of the 166 transparent natural diamonds, including HPHT-treated natural diamonds and samples containing small inclusions. Any iron residue that might have been de-

Figure 5. Pinpoint testing with flotation may be required to detect magnetic attraction in synthetic diamonds containing tiny metallic inclusions, such as the 1.07 ct yellow HPHT-grown sample on the left. This method can also be used to test individual small diamonds mounted in jewelry, as depicted on the right with a gold and diamond ring undergoing flotation testing. The raft material is Styrofoam. Photos by K. Feral.

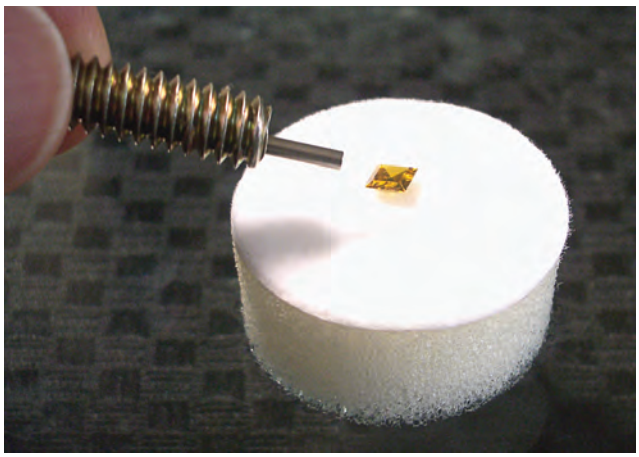


Figure 6. These are rare examples of magnetic natural diamond. The translucent 0.37 ct diamond on the left has a large metallic inclusion, likely surface residue from polishing, in and around a central pit in the table. The 0.61 ct translucent stone on the right contains very large natural mineral inclusions (likely pyrrhotite) that are strongly magnetic. Photos by Kevin Schumacher.

posited on the surfaces of these diamonds due to frequent handling with tweezers was not detected either.

The two heavily included translucent natural diamonds containing exceptionally large opaque inclusions (over 0.5 mm) were strongly magnetic. These inclusions were visible with the unaided eye and showed magnetic attraction to a pinpoint wand. Diamonds such as these, with large inclusions and low clarity, are not typically found in jewelry.

One of these magnetic natural diamonds was a translucent brownish red 0.37 ct round with numerous gray-black inclusions visible at the surface but not in the interior (figure 6, left). Several of these inclusions were situated in and around relatively large cavities on the table and pavilion surfaces. The largest one, centrally located on the table facet, measured 0.65 mm. When a ½ in. N52-grade magnet was applied, it dragged this diamond across a smooth, dry surface. A pinpoint wand revealed that only the inclusions were responsible for the magnetism. Alnico and ferrite magnets were not strong enough to elicit a direct response from this diamond. Although the composition of the magnetic inclusions is unknown, their appearance is consistent with that of iron residue from the polishing process, as described in the previously cited report on a natural transparent pink diamond picked up by a magnet (Shen and Shigley, 2004).

The other magnetic natural diamond was a brownish yellow 0.61 ct round containing several large black inclusions (figure 6, right). The largest of them, 1.7 mm across and situated near the girdle, extended well into the interior of the diamond. Another large inclusion located just below the table did not extend to the surface. High-power magnification showed that some of the inclusions were fibrous, while most appeared in velvety black clumps.

This diamond did not respond to the direct method of magnetic testing, but the flotation method revealed a strong overall magnetic response. The largest inclusions were tested individually using an N52 pinpoint wand, and each showed a strong response. The composition of these inclusions has not been analyzed, but we can expect that sulfides are involved, with pyrrhotite as the likely magnetic component. This is the first reported case of a facetable natural diamond attracted to a magnet due to natural mineral inclusions.

Synthetic Diamonds. Like the transparent natural diamonds tested in this study, the 19 CVD-grown synthetic diamonds from Gemesis and Scio Diamond Technology showed no magnetic attraction. Black opaque inclusions were visible on the surface of several rough samples from Scio, but they were most likely composed of polycrystalline carbon, a diamagnetic material (A. Genis, pers. comm., 2012). No detectable metallic inclusions were present. These results indicate that magnetic testing cannot be used to distinguish CVD-grown synthetic diamonds from natural diamonds.

All the HPHT-grown synthetic samples in this study contained inclusions, but many were not detectably magnetic. HPHT synthetics that showed no magnetic attraction often contained clouds of pinpoint inclusions that were colorless, transparent, and visible only with high-power magnification. Yet some opaque inclusions in the HPHT-grown samples were not detectably magnetic either. The composition of these inclusions might involve materials such as silicon carbide and amorphous graphite, two opaque diamagnetic materials known to occur in HPHT products (Yin et al., 2000).

Most HPHT synthetic diamond samples that could be picked up or dragged by a magnet contained opaque magnetic inclusions large enough to be visible with the unaided eye or a 10× loupe. These inclusions appeared brown or black in transmitted light (as shown in figure 7, left). Reflected light would at times reveal a silver sheen indicative of synthetic metallic flux, but this sheen was not always apparent. Metallic inclusions occasionally appeared in layered or striated patterns conforming to crystal growth planes (figure 7, right). Tiny inclusions that appeared as dark pinpoints often elicited weak magnetic responses detectable only with flotation using the strongest wands: a ½ in. neodymium wand or a pinpoint wand. In some instances, these inclusions were visible only with high-power magnification.

Results for magnetic testing of HPHT-grown synthetic diamonds are presented in table 2 according to manufacturing source. These results do not accurately portray the amount of metallic flux content in HPHT-grown synthetic diamonds currently being produced by any particular manufacturer, as the number of samples was not representative of an individual manufacturer's overall production, and approximately half of the samples were not from recent production runs.

Table 2 shows that of the 85 HPHT-grown synthetic diamonds tested, 58% exhibited magnetic attraction to an N52-grade neodymium magnet. No difference in rate of detection was found between the HPHT synthetic diamonds supplied in 2012 by various manufacturers and the HPHT synthetics acquired in previous years by the GIA Museum. Direct contact with a magnet elicited either a pickup response or drag response in 45% of all samples. An additional 13% exhibited either a weak or strong magnetic response when the more sensitive flotation and pinpoint methods were applied. Alnico and ferrite magnets were adequate for detecting magnetic attraction in 38% of all samples, while another 20% required stronger neodymium magnets.

Of the samples that showed direct magnetic responses (pickup or drag), 76% could be detected with ferrite and alnico magnets, while the remaining 24% required neodymium magnets to produce a response. The three neodymium wands (½ in. N52, 1/16 in. N52, and ⅛ in. Hanneman wand) were equally effective in eliciting direct responses (without flotation) in synthetic diamonds.

Of the 11 samples that required the flotation method to reveal magnetic attraction, eight required pinpoint testing with a 1/16 in. diameter neodymium wand. The Hanneman wand, which is larger and weaker than the 1/16 in. N52 wand, detected magnetic responses in only two of these eight samples and was therefore significantly less effective for pinpoint testing. These comparisons of magnet strength prove that N52-grade neodymium magnets achieve the highest rate of magnetic detection when distinguishing natural and synthetic diamonds.

Yellow was the most prevalent color in the HPHT-

Figure 7. HPHT-grown synthetic diamonds that contain large flux inclusions typically show a pickup response. The inclusion in the partially faceted 0.58 ct yellow sample on the left is dark brown in transmitted light. In the photomicrograph on right (magnified 60×), a striated inclusion that formed along crystal growth planes in a 0.22 ct blue sample displays a silvery metallic sheen in reflected light. Photo and photomicrograph by K. Feral.

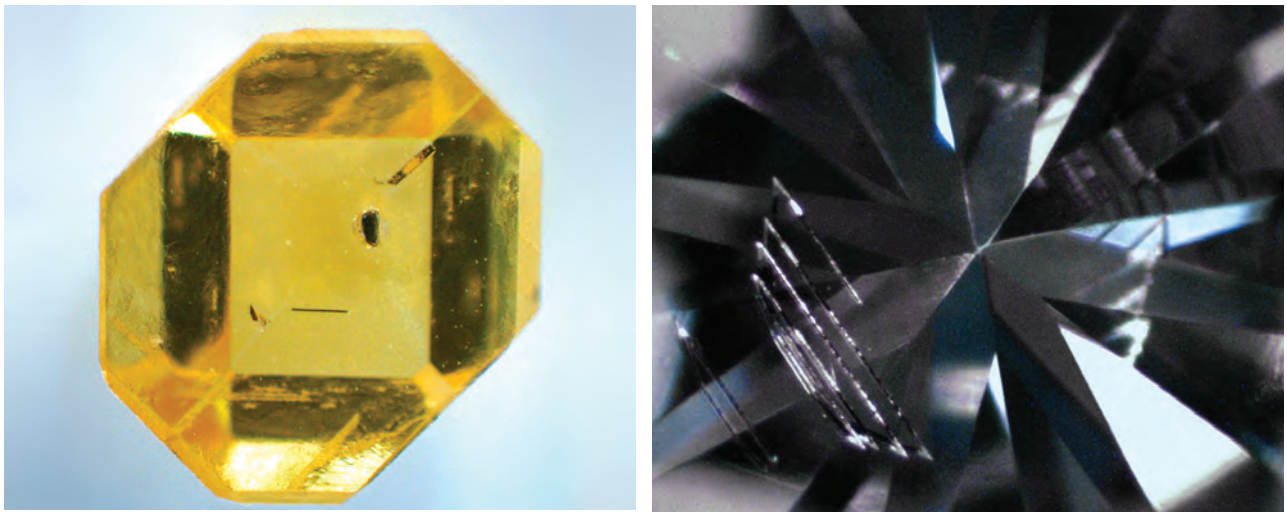

TABLE 2. Magnetic responses of HPHT-grown synthetic diamonds, by manufacturer.

Manufacturer	DeB	TCG	GTL	Sum	Chat	GDC	AOTC	NAD	UIM	Total no.	Percentage detected[a]
Sample quantity	1	3	3	8	10	5	7	21	27	85	
Total magnetic responses	0	2	3	2	3	1	3	19	16	49	58%
Direct responses (pickup or drag)	0	1	3	1	2	0	3	18	10	38	45%
Direct responses requiring a neodymium magnet	0	0	0	1	1	0	1	4	2	9	11%
Flotation required	0	1	0	1	1	1	0	1	6	11	13%
Flotation responses requiring a pinpoint magnet	0	1	0	1	1	1	0	0	4	8	9%

[a] *Percentage of all HPHT-grown samples*

grown samples. The distribution by color was: yellow and brown (51 samples), blue (15), pink and red (13), and colorless (6). No black synthetic diamonds were tested in this study. The blue synthetic diamonds showed the highest rate of detection at 73%. Magnetic detection of yellow and brown synthetics was at 63%, while pink and red samples were at 23%. Of the colorless samples, 33% were attracted to a magnet. These results are consistent with earlier findings that linked the concentration of doping elements such as nitrogen (yellow color) and boron (blue) with the number of inclusions in an HPHT synthetic diamond, and consequently on a sample's magnetic susceptibility (Lysenko et al., 2008).

Coloring agents alone do not induce magnetic attraction in synthetic diamonds. Nitrogen and boron are both diamagnetic elements. Radiation, which may have been used to induce the pink and red colors in the HPHT synthetic samples in this study, does not affect magnetic susceptibility.

Nearly half of the HPHT-grown synthetic diamonds in this study were faceted, and the rest were rough or partially cut. Of the faceted samples, 44% were detectable with a handheld magnet, while the rough or partially cut goods had a higher detection rate of 70%. Though not conclusive, this finding suggests that flux inclusions may be more concentrated near the surface of rough gems, disproportionately reducing the magnetic inclusions during the cutting process.

In HPHT-grown synthetic diamonds, larger size correlated with higher rates of magnetic detection. Approximately half of the HPHT-grown samples in this study were melee-size (0.02–0.20 ct), and 45% of these were detectable with a magnet. Mid-size samples ranging from 0.21 to 0.50 ct (29% of the HPHT-grown test group) had a somewhat higher detection rate of 56%. Large samples ranging from 0.51 to 3.81 ct (24% of the HPHT-grown set) showed a detection rate of 85%. All samples larger than 1 ct were detectable with a magnet.

Test results indicated that lower clarity in HPHT-grown synthetics correlates with higher rates of magnetic detection. Of the HPHT synthetic samples with VS_1 or higher clarity grades, none showed detectable magnetism. Twelve of the HPHT-grown samples had been assigned clarity grades by the manufacturer, and eight of these were diamagnetic. Seven of these eight graded synthetics that showed no magnetic attraction were graded VS_1 (very slightly included) to IF (internally flawless), and one was graded SI_1 (slightly included). The four graded specimens that exhibited detectable magnetism had clarity grades of SI_1 to I_1 (included).

CONCLUSIONS

Inclusions of flux materials such as iron, nickel, and cobalt are commonly found in synthetic diamonds grown under conditions of high pressure and high temperature. Detection of these ferromagnetic particles using a handheld magnet separates HPHT-grown synthetics from natural diamonds, which are typically diamagnetic. In this study, an N52-grade neodymium magnet detected 58% of the HPHT-grown samples. The detection rate varied from 20% to 100%, depending on the manufacturer and the sample's clarity, color, and size, and whether it was cut or in rough form. Synthetic diamond samples grown by the CVD process are free of flux impurities, and consequently cannot be distinguished from natural diamonds by magnetic response.

To maximize the detection rate of HPHT-grown synthetics, magnetic testing must be standardized to the strongest permanent magnet available: the N52-grade neodymium magnet. Sensitive flotation and pin-

point testing methods can also be used to detect a significantly higher percentage of synthetic diamonds than direct testing alone. Pinpoint testing with flotation is also useful for individually testing small diamonds and melee mounted in jewelry for synthetic origin.

Natural diamonds often contain microscopic mineral inclusions with small magnetic susceptibilities that are ferromagnetic and paramagnetic. Faceted natural diamonds may also contain minute amounts of ferromagnetic impurities due to contamination during polishing and handling. Regardless, such particles in natural diamond are rarely detectable with a magnet.

Two rare cases of natural diamond with detectable magnetism were found in this study: one likely due to surface contamination during polishing, and the other due to natural magnetic mineral inclusions of anomalous size. Although the percentage of natural diamond samples that showed magnetic attraction was slightly above 1%, a general sampling of gem diamonds in the marketplace would be expected to yield a far smaller figure.

As growth methods are refined, many gem-quality HPHT-grown synthetic diamonds being manufactured do not contain flux particles in sufficient sizes or concentrations to be detected with a magnet. CVD-grown synthetic gems, which are non-magnetic and often colorless, have also assumed a more prominent role in the marketplace. A lack of magnetic attraction therefore does not rule out that a diamond may be synthetic. But any visible magnetic attraction indicates that it is almost certainly synthetic. A high-grade neodymium magnet remains an important supplemental tool for those who buy, sell, or work with diamonds, particularly yellow gems. As a low-cost instrument that is simple to use, the magnetic wand is effective in detecting a significant percentage of synthetic diamonds.

ABOUT THE AUTHOR

Mr. Feral (San Diego, California) is a gemologist by avocation, with a particular interest in research. His educational website gemstonemagnetism.com presents comprehensive instruction on gem identification through magnetic testing.

ACKNOWLEDGMENTS

The author thanks GIA's Terri Ottaway and James Shigley for access to natural and synthetic diamond samples. For making their products available for testing, the author is grateful to Tom Chatham (Chatham Created Gems), Eric Franklin (D.NEA and AOTC Created Diamonds), Mike McMahon and Amy Nicholls (Scio Diamond Technology Corp.), Alex Grizenko (Lucent Diamonds), Sonny Pope and Robert Lee (Suncrest Diamonds), Mary Siemens and Scott Shaffer (New Age Diamonds), Stephen Lux (Gemesis Corp.), and Uriah Prichard (Morion Company). Norman Leitman provided access to natural diamonds mounted in jewelry. Alex Grizenko, Sonny Pope, Al Genis (Scio), and Jeff Harris (University of Glasgow) offered helpful insights and comments. And thanks to Don Hoover for reviewing the results of this study.

REFERENCES

Barnard A.S. (2000) *The Diamond Formula: Diamond Synthesis: A Gemmological Perspective*. Butterworth-Heinemann, Woburn, MA, 166 pp.

Bibby D.M. (1982) Impurities in natural diamond. *Chemistry and Physics of Carbon*, Vol. 18, pp. 3–81.

Boyd F.R., Meyer H.O.A. (1979) *Kimberlites, Diatremes, and Diamonds: Their Geology, Petrology, and Geochemistry*. American Geophysical Union, Washington DC, pp. 16–26.

Clement B.M., Haggerty S., Harris J.W. (2008) Magnetic inclusions in diamonds. *Earth and Planet Science Letters*, Vol. 267, No. 1–2, pp. 333–340, http://dx.doi.org/10.1016/j.epsl.2007.11.052.

Gumpesberger S. (2006) Magnetic separation of gemstones. *Canadian Gemmologist*, Vol. 27, No. 4, pp. 120–124.

Hoover D.B, Williams B. (2007) Magnetic susceptibility for gemstone discrimination. *The Australian Gemmologist*, Vol. 23, pp. 146–159.

Kitawaki H., Abduriyim A., Okano M. (2008) Identification of melee-size synthetic yellow diamonds in jewelry. *G&G*, Vol. 44, No. 3, pp. 202–213, http://dx.doi.org/10.5741/GEMS.44.3.202.

Kitawaki H., Abduriyim A., Kawano J., Okano M. (2010) Identification of CVD-grown synthetic melee pink diamond. *Journal of Gemmology*, Vol. 32, No. 1–4, pp. 23–30.

Koivula J.I., Fryer C. (1984) Identifying gem-quality synthetic diamonds: An update. *G&G*, Vol. 20, No. 3, pp. 146–158, http://dx.doi.org/10.5741/GEMS.20.3.146.

Koivula J.I. (2000) *The Microworld of Diamonds*. Gemworld International, Northbrook, IL, 157 pp.

Lysenko O., Novikov N., Grushko V., Shcherbakov A., Katrusha A., Ivakhnenko S. (2008) High-density data storage using diamond probe technique. *Journal of Physics: Conference Series 100*. Part 5, pp. 1–4, http://dx.doi.org/10.1088/1742-6596/100/5/052032.

Matlins A., Bonanno A.C. (2008) *Gem Identification Made Easy*, 4th ed., GemStone Press, Woodstock, VT, 354 pp.

Rossman G., Kirschvink J.L. (1984) Magnetic properties of gem-quality synthetic diamonds. *G&G*, Vol. 20, No. 3, pp. 163–166, http://dx.doi.org/10.5741/GEMS.20.3.163.

Shen A.H., Shigley J.E. (2004) Lab Notes: "Magnetic" natural pink diamond. *G&G*, Vol. 40, No. 4, pp. 324–325.

Webster R. (1970) *Gems: Their Sources, Descriptions, and Identification*, 2nd ed., Butterworths, London, 931 pp.

Yelisseyev A.P., Afansiev V.P., Ikorsky V.N. (2008) Magnetic susceptibility of natural diamonds. *Doklady Earth Sciences*, Vol. 425, No. 2, pp. 330–333.

Yin L.W., Zou Z.D., Li M.S., Liu Y.X., Cui J.J., Hao Z.Y. (2000) Characteristics of some inclusions contained in synthetic diamond single crystals. *Materials Science and Engineering: A*, Vol. 293, No. 1-2, pp. 107–111. http://dx.doi.org/10.1016/S0921-5093(00)01051-0.

Color Origin of Lavender Jadeite: An Alternative Approach

Ren Lu

The market value of jadeite has risen dramatically in recent decades, often rivaling that of fine ruby and sapphire. Understanding the color origin of jadeite and reliably determining treatments have become increasingly important in the trade. This study uses single-crystalline analogs in conjunction with polycrystalline jadeite to examine the color origin of lavender jadeite through quantitative spectroscopy and modern trace-element analytical techniques. Several previously proposed chromophores are assessed for their possible contribution to jadeite coloration. Quantitative analysis confirms that green and lavender colorations are caused by chromium and manganese, respectively. The relative significance of these two chromophores is compared to determine their impact on observable coloration. The findings on color origin are applied to the identification of treated material on the current market.

Jadeite is a highly regarded gemstone, particularly in Asian markets. Some of the finest pieces command premium values, often surpassing those for top-quality ruby, sapphire, and emerald, as evidenced by recent auctions (Leblanc, 2012). At Christie's Hong Kong sale on May 29, 2012, a lavender jadeite bangle fetched US$453,003.

The value of a gem material largely depends on whether it is of natural, treated, or synthetic origin (figure 1). Gemological testing and detection of color enhancement rely on a clear understanding of color origin. The detection of chromophore(s) appropriate for the observed color is required for a natural color determination.

Trivalent chromium (Cr^{3+}) and iron (Fe^{3+}) have long been known as the source of "emerald" and "grassy" green colors in jadeite, respectively (Harlow and Olds, 1987; Rossman, 1977). Yet the origin of lavender color has been a subject of debate among various studies over the past 30 years. Various chromophores—including single transition metal ions Mn^{3+}, Mn^{2+}, Ti^{3+}, Fe^{3+}, and V^{3+}, and paired charge-transfer ions Fe^{2+}-Fe^{3+}, and Ti^{4+}-Fe^{2+}—have been proposed based on UV-visible spectroscopic data, chemical analyses, and comparisons to similarly colored minerals (Rossman, 1974; Shinno and Oba, 1993; Chen et al., 1999; Ouyang, 2001; Harlow and Shi, 2011).

Quantitative analysis relies on the precise determination of chromophore concentration and the op-

Figure 1. Most intense lavender-color jadeite has been treated to achieve that saturation of color but this cabochon is natural color. Photo by Tino Hammid/GIA.

See end of article for About the Author and Acknowledgments.
Gems & Gemology, Vol. 48, No. 4, pp. 273–283,
http://dx.doi.org/10.5741/GEMS.48.4.273.

tical path length that light travels through a region of particular absorption characteristics. Such direct and quantitative correlation between proposed chromophores and observed lavender jadeite color has been lacking, however. Three main challenges intrinsic to jadeite have hindered our understanding of the gem's chromophores:

1. The polycrystalline and sometimes near crypto-crystalline nature of the finest jadeite poses fundamental difficulties. In polycrystalline materials, light does not follow a direct path. The path length is not simply the thickness of the material, but rather an indirect and complicated path through all the irregularities of crystal grains.
2. Chromophore characterization has traditionally relied on electron microprobe analysis, which is best suited for major elements but insufficient for detecting trace elements. Yet chromophores are often trace elements at parts-per-million (ppm) levels, rather than main elements at percent (parts-per-hundred) levels. For instance, a trace amount of chromium at only a few hundred ppm can produce appreciable colors in ruby (McClure 1962; Eigenmann et al., 1972; and the author's recent analysis of hundreds of ruby samples) or green jadeite (analysis presented below). Similarly, a few tens of ppm of beryllium will readily alter the color of sapphire (Emmett et al., 2003). Thus the true chromophore(s) responsible for the observed color may not be correctly identified due to limited sensitivity of analytical techniques.
3. Multiple transition metal ions or pairs are known to produce broad absorption bands in the same general region (near 550–650 nm) responsible for a lavender color.

This study takes a completely different approach to addressing color origin in lavender jadeite by quantitatively analyzing high-quality single-crystals of closely matched materials.

Spodumene and jadeite share closely matched crystallographic structures and optical and spectroscopic properties. Similar to jadeite, spodumene is available in both green (hiddenite) and pink/lavender (kunzite) color. Unlike jadeite, which is polycrystalline and rarely exhibits large crystals, high-quality single crystals of spodumene are widely available, which facilitates quantitative spectroscopic and trace-element (chromophore) analysis. The quantitative results are consequently instructive to the analysis of color origin and to determining enhancement of lavender jadeite

In terms of technical approach, two key components of this study are quantitative absorption spectroscopy and trace-element analysis at the parts-per-million level (Box A). This is achieved through laser ablation–inductively coupled plasma–mass spectrometry (LA-ICP-MS), a technique that has become practical only in recent years. These mass spectrometers provide point-by-point chemical analysis with micrometer-size spatial resolution and concentrations better than parts-per-million, which can be fully correlated to quantitative absorption spectroscopy in color analysis.

MATERIALS AND METHODS

Nine natural jadeite slabs ranging from ~16 to 88 ct with well-known provenance (Nant Maw mine 109, Myanmar; Kotaki-Gawa Itoigawa, Japan; and near Saltan and La Ensenada, Guatemala) were provided by Dr. George Harlow of the American Museum of Natural History in New York. These materials were mostly whitish, with zones of pinkish lavender (Burmese) and bluish lavender (Japanese and Guatemalan) colors. Sixteen faceted pieces of known impregnated and/or color-enhanced lavender and purplish jadeite materials were provided by Chinese dealers. To test the alternative approach to establishing color origin, three centimeter-size gem-quality natural crystals of spodumene (hiddenite and kunzite varieties) from Afghanistan were obtained from GIA collections.

UV-Visible Spectroscopy. Jadeite and spodumene samples were prepared as wafers with parallel polished surfaces and various thicknesses. For single crystals of spodumene, three sets of parallel polished surfaces with maximum pleochroic colors were prepared using a custom-built optical orientation device. UV-visible spectra were collected with a Perkin-Elmer PE950 spectrometer equipped with mercury and tungsten light sources, and photomultiplier tube/PbS detectors that were built into an integrating sphere. A custom-made sample holder specially developed for quantitative analysis was used to ensure the precise positioning of the sampling area in a 3 mm diameter window. The same sampled area was further analyzed by LA-ICP-MS, particularly for trace-element composition to correlate spectral features with potential chromophores. Polarized spectra

BOX A: QUANTITATIVE CHROMOPHORE ANALYSIS FROM SPECTROSCOPY AND TRACE-ELEMENT CHEMISTRY

The combination of UV-visible absorption spectroscopy and chemical analysis allows us to determine the chromophore(s) that cause the observed color. Figure A-1 illustrates how this is accomplished. Absorption is proportional to the concentration of absorbers through which light passes (known as the Beer-Lambert law). A few relatively simple mathematical steps will lead to the following:

Equation 1 $$\sigma = \frac{A}{Nd} * \ln 10$$

Equation 2 $$A = A_0 \frac{Nd}{N_0 d_0}$$

where:
A is absorbance
σ is the absorption cross section
N is the concentration of absorbers
d is the thickness the light path length
and symbols with the subscript "0" are sets of known values of these parameters.

Absorption cross section is a constant for a particular chromophore. Consequently, absorption for any chromophore concentration and sample thickness can be predicted from the relationships above. For instance, more saturated color (and correlating absorbance A) can be achieved by either increasing chromophore concentration (N) or thickness of sample (d).

In this sample for ruby (personal data), a known set of values A_0, N_0, and d_0 are established from the UV-visible absorption spectrum, LA-ICP-MS analysis, and measurement of thickness, respectively. Color coordinates (CIE L*a*b*) can be calculated from absorbance/transmittance, and the color of the sample is quantitatively reproduced using software such as Adobe Photoshop.

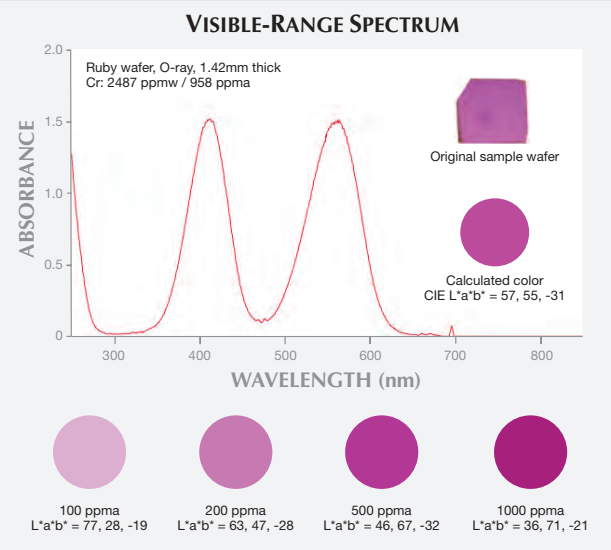

Figure A-1. This visible-range spectrum depicts the determination of chromophore (Cr) in a ruby sample. The color circles (below the spectrum) demonstrate coloration for rubies with various Cr concentrations for a 5 mm path length. Rubies with twice the Cr concentration and half the path length appear the same as 200 ppma and 2.5 mm path length.

were collected in the 200–1400 nm range with a 0.65 nm spectral resolution at a scan speed of 96 nm/min.

Quantitative UV-visible spectroscopic measurement for colors relies on correctly identifying the spectral baseline. Internal scatter in polycrystalline aggregates offsets and distorts the baseline, particularly in the UV spectral region. The spectral baseline was corrected by subtracting spectral offset at or beyond 1000 nm, where the chromophore's features were insignificant or nonexistent.

LA-ICP-MS Analysis. Detailed chemical compositions were obtained in the same region characterized by spectroscopy. A ThermoFisher X-series II mass spectrometer from Electro Scientific Industries, Inc. coupled with a deep UV laser at 213 nm excitation was used in the trace-element analysis. NIST (National Institute of Science and Technology) glass standards SRM 610 and 612 were used for internal calibration (http://www.nist.gov/srm/). Ablation conditions were 7 Hz repetition rate, 7 J/cm^2 fluence, and a laser spot size of 40 µm.

RESULTS AND DISCUSSION

Gemological Observation. Gemological properties of natural, treated, and synthetic jadeite have been extensively documented (e.g., Koivula, 1982; Nassau and Shigley, 1987). Details and additional references can be found therein and are not discussed here.

Within the gem trade, lavender jadeite loosely refers to a broad range of colors from pinkish, purplish, violetish, to bluish hues. Of the samples col-

lected for this study, the Japanese and Guatemalan jadeite displayed only bluish to bluish green coloration, with virtually no lavender color. The Burmese material showed more pinkish and purple hues with a whitish matrix. Furthermore, lavender regions exhibited a more granular texture, sometimes with large and transparent elongated or orthogonal crystals in concentrated colors (figure 2).

The warmer-toned, more pinkish Burmese samples were inert or showed a very weak reddish reaction under long-wave (~365 nm) and short-wave (~254 nm) UV radiation. The more bluish Japanese and Guatemalan samples exhibited no visible reaction under long- and short-wave UV.

Jadeite and Spodumene as Close Analogs. Jadeite ($NaAlSi_2O_6$) and spodumene ($LiAlSi_2O_6$) share closely matched mineralogical and gemological properties. These properties include Mohs hardness (6.5–7), RI (1.66 vs. 1.66–1.68), and SG (3.34 vs. 3.18). Pure jadeite and spodumene with this ideal chemical composition are colorless.

As members of the pyroxene mineral group, both jadeite and spodumene share the monoclinic *C*2/*c* symmetry and have similar structures (Cameron et al., 1973; see figure 3). The largely distorted octahedral M2 site is occupied by Na (jadeite) or Li (spodumene). The SiO_4 tetrahedral site is likely not involved in producing colors through substitution by trace elements such as transition metals. The slightly distorted M1 octahedral site is occupied by Al or substituted by chromophores such as Cr (which causes green color) supported by the color origin in chromium end-member kosmochlor ($NaCrAl_2O_6$) (White et al., 1971) and by the current data comparing green jadeite and hiddenite (discussed below). These octahedra are edge-shared, facilitating possible paired substitutions by chromophore ions in neighboring octahedra. Furthermore, there is only a ~1% difference in the average <Al–O> distance in the aluminum octahedral site between jadeite and spodumene. Consequently, chromophores substituted into the Al site are expected to present similar UV-visible absorption features.

The following analysis of chromophore chemistry and absorption spectroscopy indicates the chromophore similarities between green jadeite and hiddenite, and between lavender jadeite and kunzite.

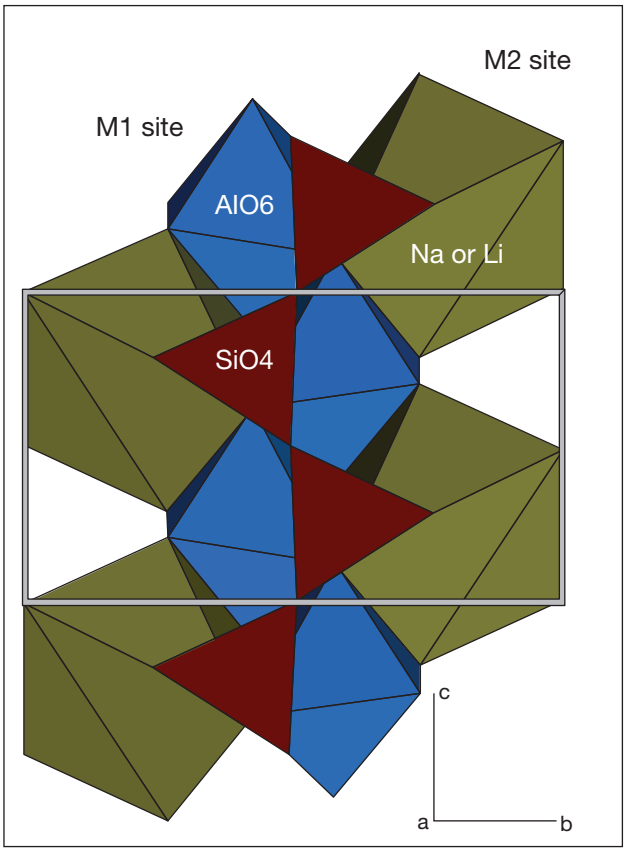

Figure 3. This view of the crystal structure of jadeite and spodumene illustrates the basic building blocks: AlO_6 octahedra and SiO_4 tedrahedra, and their geometric relationships (based on structural refinement data of Cameron et al., 1973). The crystallographic orientation is shown in the lower right corner projected down the a-axis.

Figure 2. Saturated lavender colors are often associated with a granular texture, sometimes with orthogonal crystals, as in this Burmese lavender jadeite. The color of these crystals varies noticeably from purplish to bluish when illuminated by directional lighting at various angles. The matrix is mostly whitish. Photo by R. Lu; image width ~12 mm.

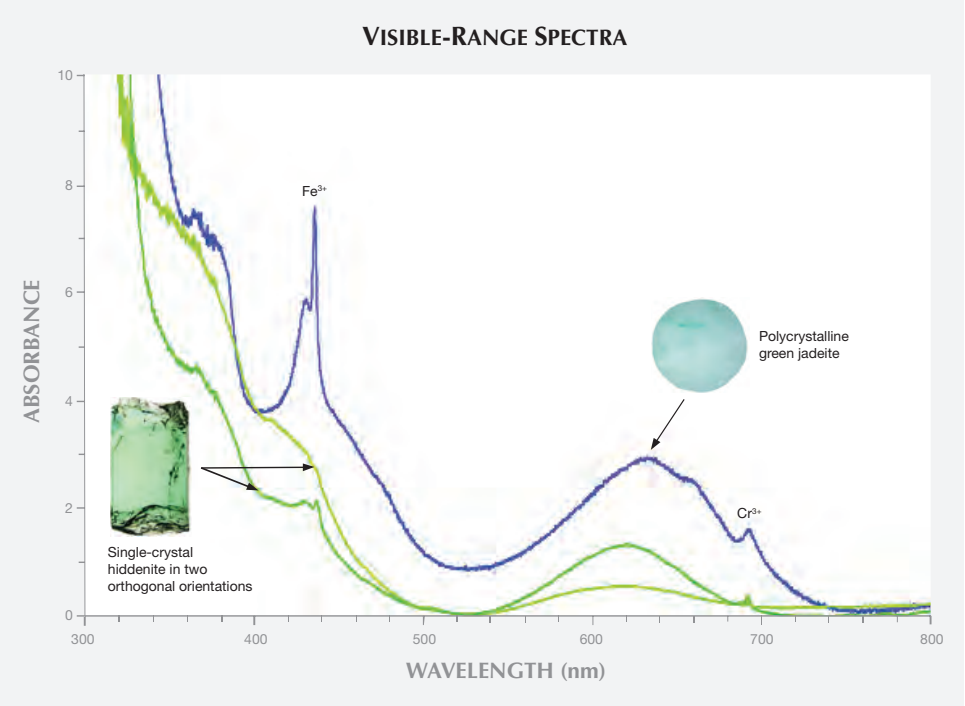

Figure 4. The UV-visible spectra of green jadeite and green spodumene (hiddenite) exhibit closely matched absorption features. Hiddenite spectra were collected from two orthogonal orientations, with polarized light demonstrating noticeable pleochroism in single crystals. The visible difference in green saturation is mostly due to the disparity in sample thickness (~0.94 mm for jadeite and ~2.7 mm for hiddenite) rather than a difference in chromium concentration (see table 1). The spectra are for element concentrations listed on table 1.

UV-Visible Spectroscopy. Correlating an observed color to a specific chromophore requires precise measurement of absorption features through a known optical path in the UV-visible spectrum as well as chemical analysis of the chromophore's concentration. High-quality single-crystal spodumene presents an ideal opportunity for quantitative understanding of color origin in polycrystalline jadeite, which is complicated by textural and chemical variations.

The UV-visible spectra of hiddenite show features corresponding with those of chromium-bearing green jadeite (figure 4). The characteristic 437 nm absorption band of Fe^{3+}, commonly present in natural jadeite with various green hues, is about 1 nm higher in hiddenite. The narrow 691 nm absorption band of Cr^{3+} is virtually the same in both minerals.

Pleochroic colors from yellowish green to bluish green, visually observable with a handheld dichroscope, were quantitatively reproduced in single-crystal spectra of hiddenite. Figure 4 shows the variation in green saturation and hue observed approximately along two principal optical orientations with the maximum contrast in hue and saturation. The crystal orientation device used in this current study is being redesigned to allow analysis of fully oriented crystals in all three principal optical orientations of biaxial crystals such as spodumene.

In general, pleochroism is not observed among randomly oriented polycrystalline jadeite, particularly fine-grained, high-quality specimens.

UV-visible spectra of kunzite (figure 5) showed strong pleochroism ranging from variously saturated pink to a bluish hue dominated by broad bands above ~500 nm in the three orthogonal directions.

An aggregate of randomly oriented crystals of lavender jadeite showed a combination of pink and blue (purplish) hues. A large variation in both saturation and hue is commonly observed with directional illumination (such as a fiber-optic light) at different angles. The variation is more pronounced in single-crystal kunzite and in polycrystalline lavender jadeite with coarse grains (figure 2).

In Brief

- The color origin (natural or otherwise) of lavender jadeite is an essential aspect of its commercial value.
- While detecting the color-causing elements of polycrystalline jadeite is difficult, the single-crystal analog spodumene has very similar properties and lends itself to quantitative analysis.
- LA-ICP-MS analysis mapped to quantitative spectroscopy confirms that manganese and chromium are responsible for lavender and green colorations in jadeite, respectively.
- A reddish fluorescence reaction to deep UV radiation is a likely indication of the presence of manganese, and of natural color in lavender jadeite.

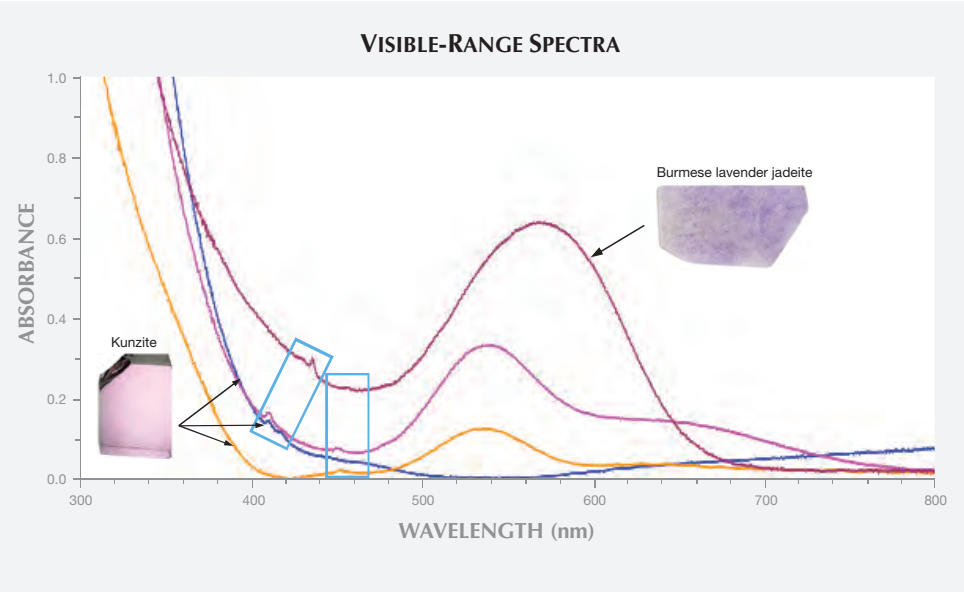

Figure 5. As these UV-visible absorption spectra demonstrate, polycrystalline Burmese lavender jadeite and single-crystalline pink spodumene (kunzite) share similar weak narrow bands (blue boxes) between 400 and 460 nm and similar broad bands above 500. The single-crystal kunzite spectra were collected from the three orthogonal orientations that displayed the most pleochroism, ranging from pink (pink line) to light pink (orange line) and very light blue-green (blue line).

A larger difference was observed in the iron-related narrow bands between kunzite and lavender jadeite (blue boxes in figure 5) than between hiddenite and green jadeite. The source of this large difference is unknown and requires further study. One possible source might be the interaction between neighboring Mn and Fe replacing Al.

Chromophore Analysis. Trace elements were thoroughly analyzed for the chromophores that cause lavender and other hues in jadeite. These included the transition-metal ions proposed by previous studies, listed in table 1. The polycrystalline jadeite samples showed variation in chromophore concentration that correlated to visible differences in color saturation. The chromophore concentration was averaged over 30 laser ablation spots across a 3 mm circular area through which spectroscopic characterization was performed.

Element concentration was measured by LA-ICP-MS analysis of jadeite and spodumene samples (transition metals V and Co were below detection limits and not listed). Concentrations for polycrystalline jadeite samples with various lavender saturations were averaged over 30 analysis spots. For Burmese lavender jadeite, Mn concentrations ranged from as low as 4 ppma for whitish matrix to as high as 195 ppma in more saturated lavender areas (further evidenced by the fluorescence image in figure 10b).

For kunzite, manganese is clearly the only available chromophore for the pink/lavender coloration. For Burmese lavender jadeite, similarly, iron below 100 ppma is insignificant in producing any color, and consequently the only chromophore is manganese.

Consideration of Ionic Structure. Valence and size of ions play a critical role in their incorporation as possible chromophores. Isovalent ions Mn^{3+}, Cr^{3+}, Fe^{3+}, Co^{3+}, and V^{3+} are charge-balanced, and their ionic radii fall closely to that of Al^{3+} in six-fold coordinated octahedral sites, facilitating substitution into the Al octahedral site (figure 6). Cobalt and vanadium are not shown or discussed further because they are absent in lavender jadeite (table 1).

Manganese is virtually the only chromophore in pink spodumene and clearly responsible for its coloration. Both Mn^{2+} and Mn^{3+} can occur in six-fold octahedral coordination, and they are known to cause pink or red colors in minerals (e.g., rhodonite, andalusite, grossular, morganite, red and pink tourmaline, and kunzite).

For consideration of ionic radii, isovalent Mn^{3+} is the preferred chromophore because its ionic charge and size match those of Al^{3+}. Aliovalent Mn^{2+} has a noticeably larger ionic size than Al^{3+} and requires additional charge compensation to fit into the Al^{3+} octahedral site. It is thus a less likely candidate for the lavender or pink hue in jadeite and spodumene.

Unlike Mn^{3+}, Mn^{2+} tends to produce relatively weak absorption bands, attributed in the technical literature to weak oscillator strength or low cross-section involving spin-forbidden transitions, when coordinated to oxygen ligands (Mn^{2+}-O^{2-}) (Burns, 1993, p. 217). Consequently, the divalent Mn^{2+} pro-

TABLE 1. Elemental concentrations in ppma.

Name	^{55}Mn	^{53}Cr	^{57}Fe	^{47}Ti
Lavender jadeite (Burmese)	99	0	76	0
Green jadeite (avg)	41	268	1528	48
Bluish jadeite Japan	10	0	1011	586
Bluish jadeite Guatemala	1	0	73	356
Kunzite	127	0	0	5
Hiddenite	374	21	1676	27
Treated materials				
Lavender jadeite B+C type (sample A)	5	0	404	13
Lavender jadeite B+C type (sample B)	15	0	465	12
Lavender jadeite dyed bicolored ring	15	0	451	11
Detection limit	0.3	1	16	1

duces near-colorless or weak coloration, as opposed to the more effective trivalent Mn^{3+} chromophore. At the low Mn level of 100 ppma (table 1), the pink and lavender coloration in kunzite and lavender jadeite should correlate to their Mn^{3+} concentration.

For the same reason, trivalent Fe^{3+}, which shares the same electronic structure as Mn^{2+}, is a weak chromophore and only produces noticeable color at high concentrations. For instance, a saturated yellow color in sapphire requires at least ~1000 ppma Fe^{3+} (author's personal data). This is important in understanding the relatively weak contribution of Fe^{3+} to coloration.

The kunzite and Burmese lavender samples showed pink/lavender colors owing to their desirable combination of appreciable Mn and the absence of Fe. By comparison, the lack of appreciable Mn in bluish Japanese and Guatemalan materials explains their lack of a pinkish color component.

Other Candidate Chromophores. Three other transition metal ions—titanium (Ti), vanadium (V), and cobalt (Co)—are effective chromophores and may produce broadband absorption features that overlap with those from Mn in the 600 nm region (Wood and Nassau, 1968; Shigley and Stockton, 1984). But in Burmese samples with a warm pinkish lavender color, the concentrations of Ti, V, and Co are too low to cause any noticeable color.

Furthermore, incorporation of chromophores in minerals depends on their availability in nature and the physical and chemical compatibility of the substituting ion (e.g., Al^{3+} in jadeite). A mechanism for chromium incorporation in green jadeite has been proposed based on petrological and chemical analysis (e.g., Shi et al., 2005; Harlow et al., 2007). Information about the petrological source and incorporation of Mn in lavender jadeite is still lacking, however.

Comparison of Chromophore Effectiveness. To better understand jadeite coloration, it is worthwhile to compare the effectiveness of chromophores Cr (green) and Mn (lavender). As shown in table 1, hiddenite contains an appreciable amount of Mn in addition to Cr. Yet chromium features dominate hiddenite's absorption spectrum.

For a given sample thickness, absorbance in the UV-visible spectrum is proportional to the concentration of the absorbing element in the part of the stone where light passes through according to the Beer-Lambert law. For a 5 mm thickness, UV-visible spectra were calculated for various chromophore concentrations based on experimentally collected hiddenite and kunzite absorption spectra. Figure 7 compares the effectiveness of Cr and Mn as chromophores.

Figure 6. Ionic radii of trivalent ions such as Mn, Fe, and Cr (isovalent to Al^{3+}, in solid circles) closely match those of Al^{3+} and can readily replace Al^{3+} as chromophore ions. Divalent ions (aliovalent to Al^{3+}, in solid triangles) are less suited in terms of size and charge balance. The label "HS" represents high-spin configuration. Data for ionic radii of six coordinated ions are based on Shannon (1976).

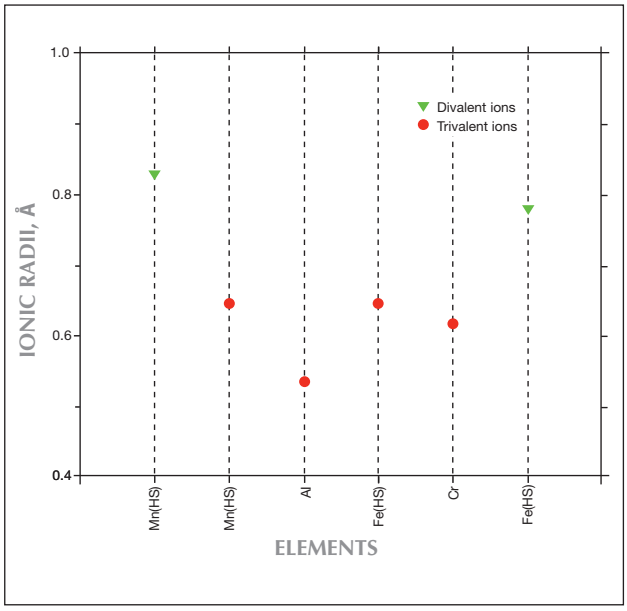

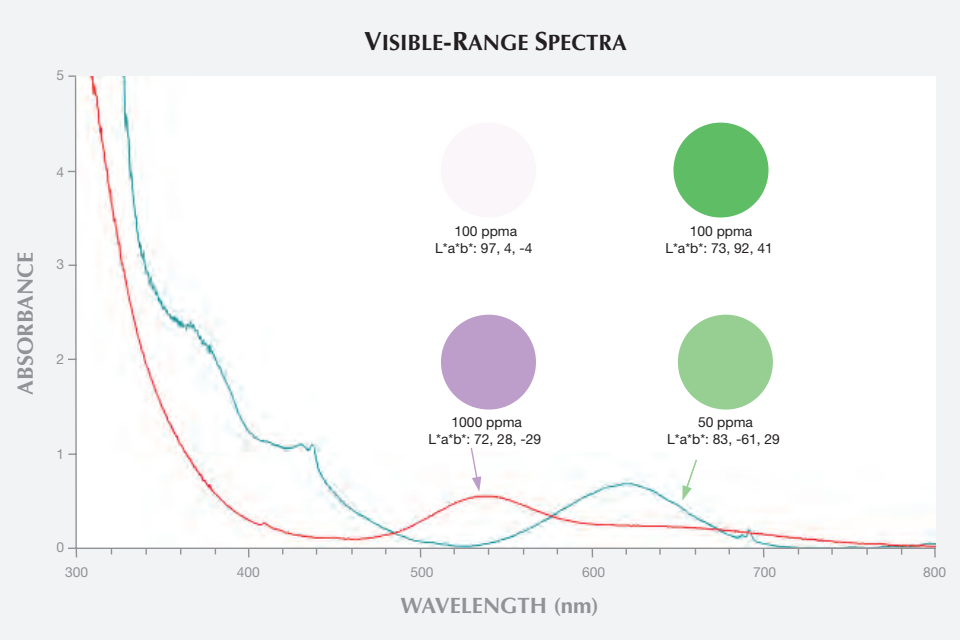

*Figure 7. Absorption spectra and their corresponding color circles compare the chromophore effectiveness of Mn and Cr (5 mm path length). The lower circles represent similar color saturations for lavender and green jadeite. The upper circles demonstrate the color saturations (and absorbance) for matching chromophore concentrations of 100 ppma. A relatively low Mn concentration (e.g., < 100 ppma) would be virtually colorless. The CIE L*a*b* color coordinates are presented with specification of CIE Adobe RGB1998 and D55.*

The implication of figure 7 is that pink/purple color from manganese only becomes noticeable at very high concentrations and in the absence of the much more effective chromophore chromium. This result is expected to be at least qualitatively true for Cr-bearing green jadeite and Mn-bearing lavender jadeite. Hatipoglu et al. (2012) recently reported Mn levels as high as 1540 ppmw (565 ppma) in deep lavender/purple jade from Turkey, in general agreement with this study.

Detecting Dyed Lavender Jadeite. Earlier dyed jadeite tended to show obvious color concentrations and an orangy color reaction under long-wave UV radiation (Koivula, 1982). These characteristics are often much less pronounced in the dyed material currently on the market, particularly fine-textured specimens (figure 8).

UV-visible spectra of dyed lavender/purple jadeite generally show broad absorption bands near 530 nm, but multiple broad bands are possible, presumably due to variations in the dyes (figure 9). These dye materials

Figure 8. This dyed bicolored ring shows easily identifiable color concentrations in grain boundaries (left) but exhibits no reaction to long-wave UV radiation (right). The width on the left image is ~5.5 mm, and the outer diameter of the ring is 11 mm. Photos by Jian Xin (Jae) Liao.

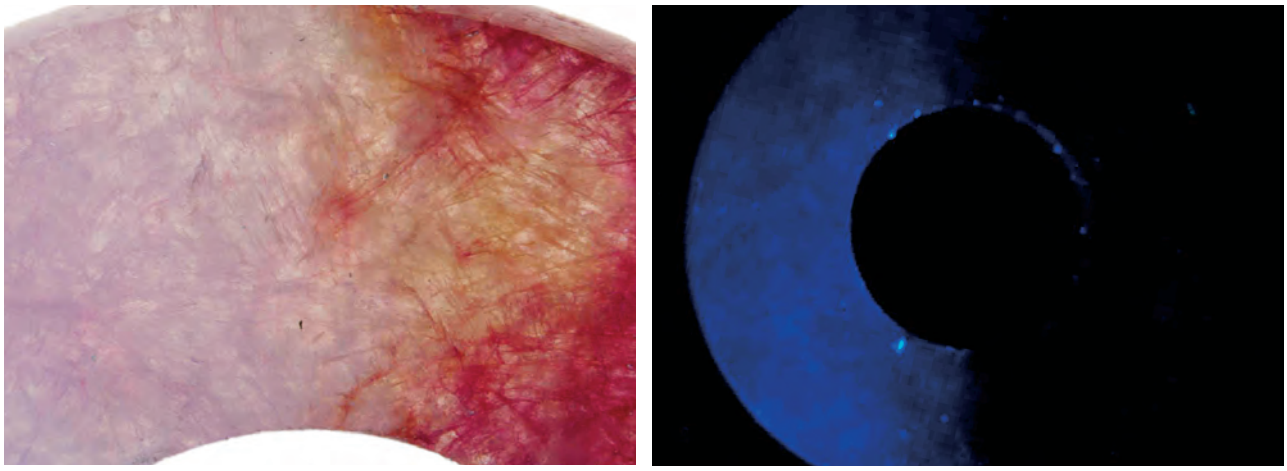

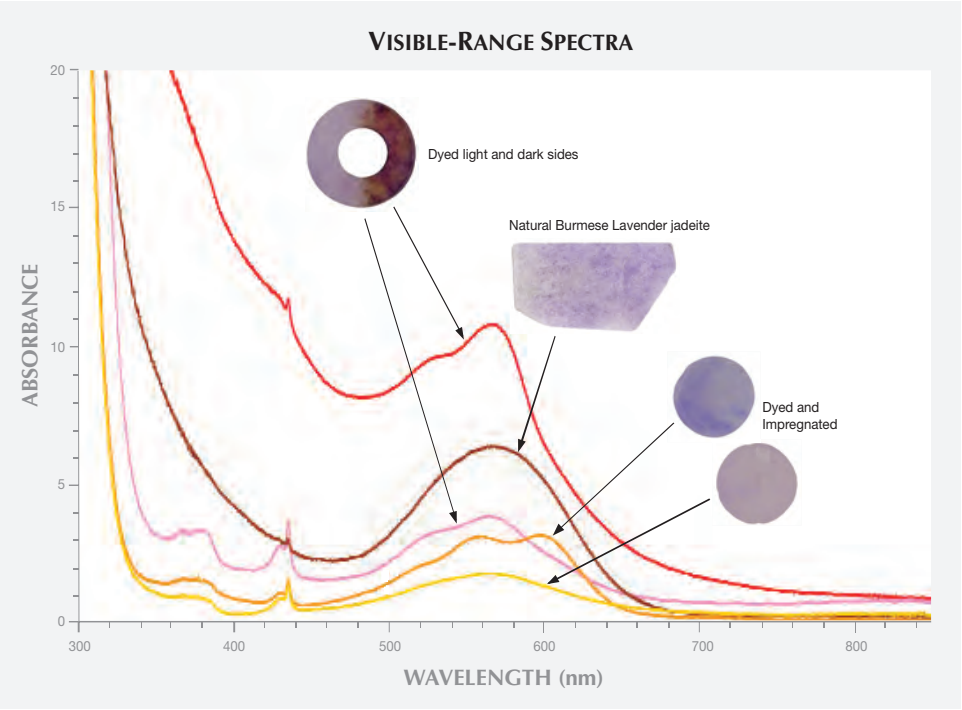

Figure 9. The UV-visible spectra of dyed jadeite show single or multiple broad bands between 500 and 650 nm that generally overlap with the broad band from Mn near 570 nm observed in untreated Burmese material. The narrow Fe^{3+} features near 437 nm in the treated material are more pronounced due to higher iron concentration.

are likely of organic origin and are not detected by LA-ICP-MS trace element analysis. When the concentration of natural Mn is too low to produce a saturated lavender color, a dye is introduced. Dye-related broad bands are superimposed with the Mn broad band near 570 nm to produce multiple bands.

A pronounced Fe^{3+} absorption in the blue spectral region near 437 nm indicates a relatively high iron concentration, which typically produces an undesired yellow-brown overtone. A combination of strong Fe^{3+} bands and multiple broad bands in the 550–650 nm region would be unlikely to yield a lavender color.

Additional tests were performed with a DTC DiamondView to explore potential techniques for identifying color origin and treatment. Under the strong short-wave UV radiation of the DiamondView (at wavelength shorter than ~230 nm), the Burmese samples showed an intense reddish reaction correlating to higher Mn concentrations, up to 195 ppma (figure 10B, also refer to table 1). The kunzite crystal exhibited a pinkish color (figure 10A) due to a relatively lower Mn concentration (127 ppma). Dyed lavender jadeite with various pinkish or purplish colors did not show the reddish reaction observed in Burmese samples under the DiamondView (figure

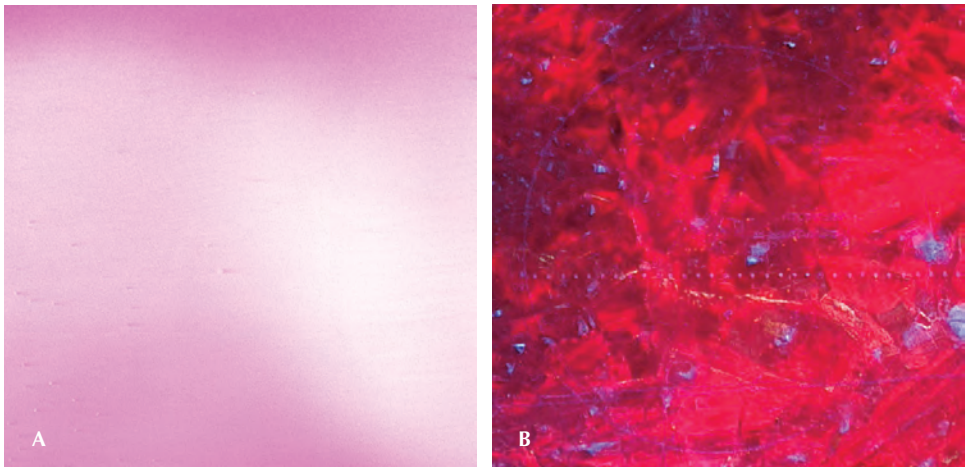

Figure 10. DiamondView images show reactions in Mn-bearing single-crystal kunzite (A) and polycrystalline Burmese lavender jadeite (B). The row of tiny dots (0.1 mm apart) in the center of image B is from LA-ICP-MS analysis, and the bluish speckles are due to reflection. Image widths ~5 mm. More saturated reddish colors (B) correlate to higher Mn concentrations in jadeite. Photos by R. Lu.

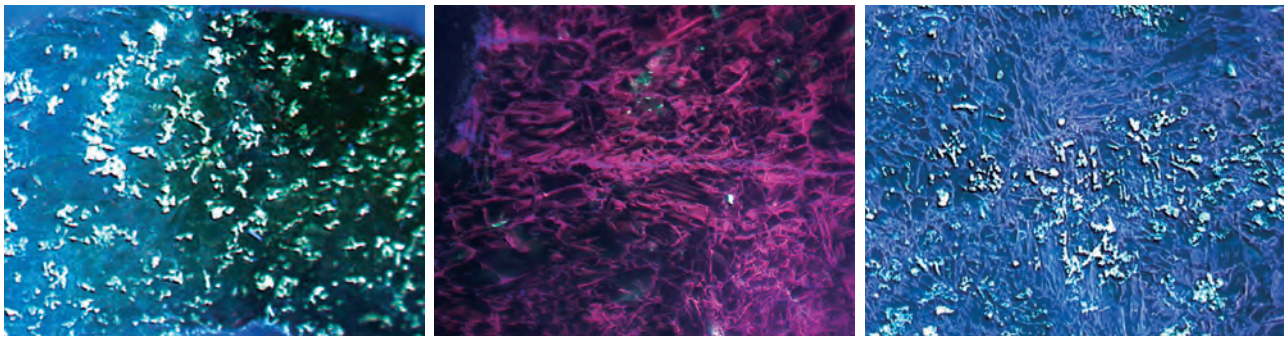

Figure 11. DiamondView images of a dyed bicolored ring (left) and two dyed and impregnated purplish lavender samples (center and right) show no reaction or a weak purplish and bluish reaction. The reddish reaction seen in natural Mn-bearing Burmese samples and the well-known orangy "dye reaction" were not observed in the dyed materials currently on the market. Image widths ~5.5 mm. Photo by R. Lu.

11). The same observation was performed on bluish natural jadeite materials from Japan and Guatemala. Due to the absence of Mn in these samples, only bluish or greenish reactions were observed.

CONCLUSIONS

Nature provides high-quality single-crystal spodumene in both green and pink varieties. Their properties closely match those of jadeite, providing a framework for an alternative approach to the quantitative study of chromophore species in polycrystalline jadeite.

The current quantitative chromophore analysis is achieved by employing the unique high spatial resolution of LA-ICP-MS analysis of trace elements which is precisely mapped to quantitative spectroscopy. This technique is applicable to studies of a wide range of gemological materials.

This study confirms that manganese and chromium are responsible for lavender and green colorations in jadeite, respectively. Furthermore, chromium is at least two orders of magnitude more effective in producing green coloration than manganese for lavender of similar saturation. The sharp difference in chromophore effectiveness between chromium and manganese dictates that green coloration is more readily observable than lavender. Consequently, a natural lavender color is not expected to be associated with a high chromium concentration within the same sample area.

Reddish (or blue/green) fluorescence reaction from deep UV radiation is a likely indication of the presence (or absence) of manganese, and of natural color in lavender jadeite. Further validation of this result will benefit color origin determination in jadeite testing. In combination with this fluorescence reaction, the detailed structure of absorption bands near 570 nm in UV-visible spectra is helpful in detecting dye treatment.

ABOUT THE AUTHOR

Dr. Lu is a senior scientist at GIA's New York laboratory.

ACKNOWLEDGMENTS

Dr. George Harlow (American Museum of Natural History, New York) graciously provided natural lavender jadeite materials mostly collected from his personal trips to Myanmar, Japan, and Guatemala. Terri Ottaway (GIA, Carlsbad) kindly selected gem-quality natural single crystals of hiddenite and kunzite spodumene. Sincere thanks go to Dr. Wuyi Wang (GIA, New York) for obtaining known treated samples from dealers in the Hong Kong and mainland Chinese markets. The author would like to sincerely thank the manuscript's three reviewers for their constructive comments.

REFERENCES

Burns R.G. (1993) *Mineralogical Applications of Crystal Field Theory*, 2nd ed. Cambridge University Press, New York, p. 523.

Cameron M., Sueno S., Prewitt C.T., Papike J.J. (1973) High-temperature crystal chemistry of acmite, diopside, hedenbergite, jadeite, spodumene, and ureyite. *American Mineralogist*, Vol. 58, pp. 594–618.

Chen B. Qiu Z. Zhang X. (1999) Preliminary study on the mineralogical characters of lavender jadeite jade. *Journal of Gems and Gemmology*, Vol. 3, No. 1, pp. 35–39 (in Chinese).
Eigenmann K., Kurtz K., Günthard H.H. (1972) The optical spectrum of α-Al_2O_3:Fe^{3+}. *Chemical Physics Letters*, Vol. 13, No. 1, pp. 54–57.
Emmett J.L., Scarratt K., McClure S.F., Moses T., Douthit T.R., Hughes R., Novak S., Shigley J.E., Wang W., Bordelon O., Kane R.E. (2003) Beryllium diffusion of ruby and sapphire. *G&G*, Vol. 39, No. 2, pp. 84–134, http://dx.doi.org/10.5741/GEMS.39.2.84.
Harlow G.E., Olds E.P. (1987) Observations on terrestrial ureyite and ureyitic pyroxene. *American Mineralogist*, Vol. 72, pp. 126–136.
Harlow G.E., Shi G.H. (2011) An LA-ICP-MS study of lavender jadeite from Myanmar, Guatemala, and Japan. *G&G*, Vol. 47, No. 2, pp. 116–117.
Harlow G.E., Sorensen S.S., Sisson V.B. (2007) Chapter 7. Jade, In L.A. Groat, ed., *The Geology of Gem Deposits*, Short Course Handbook Series, Vol. 37, pp. 207–254.
Hatipoglu M., Basevirgen Y., Chamberlain S.C. (2012) Gem-quality Turkish purple jade: Geological and mineralogical characteristics. *Journal of African Earth Sciences*, Vol. 63, pp. 48–61.
Koivula J.I. (1982) Some observations on the treatment of lavender jadeite. *G&G*, Vol. 18, No. 1, pp. 32–35, http://dx.doi.org/10.5741/GEMS.18.1.32.
Leblanc D. (2012) Color stays high at spring and summer auctions. *InColor*, No. 20, pp. 62–67.
McClure D.S. (1962) Optical spectra of transition-metal ions in corundum. *Journal of Chemical Physics*, Vol. 36, No. 10, pp. 2757–2779.
Nassau K., Shigley J.E. (1987) A study of the General Electric synthetic jadeite. *G&G*, Vol. 23, No. 1, pp. 27–35, http://dx.doi.org/10.5741/GEMS.23.1.27.
Ouyang Q. (2001) Characteristics of violet jadeite jade and its coloration mechanism. *Journal of Gems and Gemmology*, Vol. 3, No. 1, pp. 1–6 (in Chinese).
Rossman G.R. (1974) Lavender jade. The optical spectrum of Fe^{3+} and Fe^{2+}→Fe^{3+} intervalence charge transfer in jadeite from Burma. *American Mineralogist*, Vol. 59, pp. 868–870.
Shannon R.D. (1976) Revised effective ionic radii and systematic studies of interatomie distances in halides and chaleogenides, *Acta Crystallographica Section A*, Vol. 32, Part 5, pp. 751–767, http://dx.doi.org/10.1107/S0567739476001551.
Shi G.H., Stöckhert B., Cui W.Y. (2006) Texture and composition of kosmochlor and chromian jadeite aggregates from Myanmar: Implications for the formation of green jadeite. *G&G*, Vol. 42, No. 3, pp. 150–151.
Shigley J.E., Stockton C.M. (1984) "Cobalt-blue" gem spinels. *G&G*, Vol. 20, No. 1, pp. 34–41, http://dx.doi.org/10.5741/GEMS.20.1.34.
Shinno I., Oba T. (1993) Absorption and photo-luminescence spectra of Ti^{3+} and Fe^{3+} in jadeites. *Mineralogical Journal*, Vol. 16, No. 7, pp. 378–386, http://dx.doi.org/10.2465/minerj.16.378.
White W.B., McCarthy G.J., Scheetz G. E. (1971) Optical spectra of chromium, nickel and cobalt-containing pyroxenes, *American Mineralogist*, Vol. 56, pp. 72–89.
Wood D.L., Nassau K. (1968) The characterization of beryl and emerald by visible and infrared absorption spectroscopy. *American Mineralogist*, Vol. 53, pp. 777–800.

Update on the Identification of Dye Treatment In Yellow or "Golden" Cultured Pearls

Chunhui Zhou, Artitaya Homkrajae, Joyce Wing Yan Ho, Akira Hyatt, and Nicholas Sturman

Dye treatments in yellow or "golden" cultured pearls have improved to the point that some samples show little surface evidence. In addition to routine gemological observations, analytical techniques such as UV-Vis reflectance and Raman photoluminescence (PL) spectroscopy are critical to identifying the treatment. This study demonstrated three indications of dye treatment: broad reflectance features between 410 and 450 nm, the lack of a reflectance feature at 350 nm in the UV-Vis spectra, and intense fluorescence in the visible spectrum under 514 nm wavelength laser excitation. These diagnostic features may be used independently, even when no visual evidence of a dye exists.

Most dyed yellow or "golden" cultured pearls can be identified with routine microscopic observations. Dye residues usually accumulate within drill holes and surface blemishes, making them easy to detect with magnification. In some cases, long-wave UV fluorescence and UV-Vis reflectance spectrophotometry have been used to provide further evidence of dyeing (Elen, 2002; Qi et al., 2008; Chen et al., 2009). In recent years, though, GIA has begun receiving more "golden" cultured pearls with atypical UV fluorescence or UV-Vis reflectance characteristics but no evidence of dye residue. As processing techniques continue to improve, the authors believe it is important to update the trade on the situation to make sure that current identification methods are up to par with the treatments.

See end of article for About the Authors and Acknowledgments.
Gems & Gemology, Vol. 48, No. 4, pp. 284–291,
http://dx.doi.org/10.5741/GEMS.48.4.284.

The term "golden" is used to describe mid- to light-tone cultured pearls with a strong saturation in the yellow and orangy yellow hues (Gemological Institute of America, 2000). These cultured pearls are formed within *Pinctada maxima* (gold-lipped) oysters and have gained popularity over the years with the help of extensive marketing efforts by the industry (Shor, 2007; "The fabulous golden pearls of the Philippines…," 2010). In the meantime, increasing amounts of dyed "golden" South Sea and freshwater cultured pearls ("Supplier warns trade against dyed golden," 1998; Roskin, 2005) and, to a lesser extent, heat-treated "golden" products have also appeared on the market (Elen, 2001 and 2002). Detecting the treatment remains an important consideration in pearl identification, and an ongoing research investigation at GIA aims to provide solutions to the issue.

The present study focuses on the identification of eight sample groups of yellow or "golden" cultured pearl using routine gemological testing methods and advanced analytical techniques (figure 1). The known

Figure 1. These cultured pearls represent each of the eight sample groups. Top row: NSSP, NSSM, DSS, and DSS2. Bottom row: DSS3, DAK, DAK2, and DFW. Photo by Sood Oil (Judy) Chia.

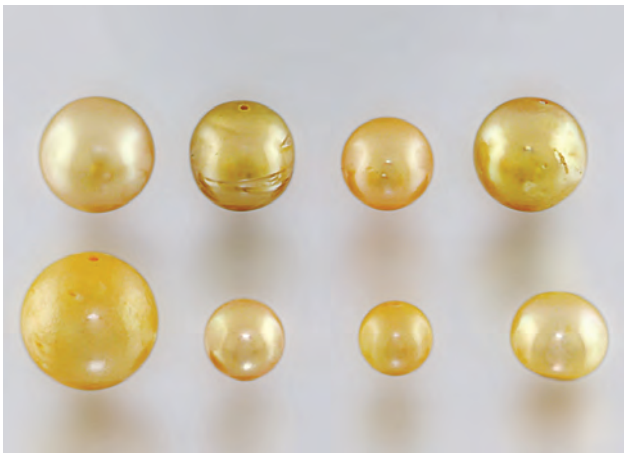

TABLE 1. Cultured pearl sample groups and advanced testing techniques used in this study.

Group	Quantity	Geographic Source	UV-Vis	IR	Raman	PL
NSSP	10	Philippines	Tested all	Tested one	Tested one	Tested one
NSSM	8	Myanmar	Tested all	Tested one	Tested one	Tested one
DSS	7	Various[a]	Tested all	Tested one	Tested one	Tested one
DSS2	7	Various[b]	Tested all	Tested one	Tested one	Tested one
DSS3	7	Various[b]	Tested all	Tested one	Tested one	Tested one
DAK	10	Various[a]	Tested all	Tested one	Tested one	Tested one
DAK2	10	Various[b]	Tested all	Tested one	Tested one	Tested one
DFW	10	Various[a]	Tested all	Tested one	Tested one	Tested one
Heat-treated	3	Various[a]	Tested all	N/A	N/A	Tested all
Additional natural-color	>100	Philippines[c]	Tested all	N/A	N/A	Tested >50

[a]*Provided by Wuyi Wang*
[b]*Provided by Ahmadjan Abduriyim*
[c]*Provided by Jewelmer*

dyed samples exhibiting no traces of surface dye concentrations were singled out for analytical testing. The results suggest that advanced techniques such as UV-Vis reflectance and PL spectroscopy can detect the dye even when surface concentrations are absent. More than 100 naturally colored yellow cultured pearls were tested with the UV-Vis reflectance technique to provide additional reference datasets. Some of the latter were also tested with PL for the same purpose. Lastly, three heat-treated yellow cultured pearls were tested; their results are discussed briefly, since the sample size is minimal.

MATERIALS AND METHODS

A total of 69 yellow and "golden" cultured pearls ranging from 6.5 to 14 mm were studied. The eight sample groups consisted of:

- 10 naturally colored South Sea cultured pearls from the Philippines (NSSP)
- 8 naturally colored South Sea cultured pearls from Myanmar (NSSM)
- 21 dyed South Sea cultured pearls, in three separate groups (DSS, DSS2, and DSS3)
- 20 dyed akoya cultured pearls, in two separate groups (DAK and DAK2)
- 10 dyed freshwater nonbead-cultured pearls (DFW)

These samples were obtained from reliable sources who provided information on the samples' provenance. Real-time micro-radiography examination with a Faxitron CS-100-AC confirmed they were all cultured pearl products.

Each sample was examined with a standard gemological microscope, and photomicrographs were taken using a Nikon SMZ 1500 stereomicroscope. Fluorescence reactions were observed in a darkened room using a conventional 5-watt long-wave (366 nm) UV lamp. UV-Vis reflectance spectra were obtained using a PerkinElmer Lambda 950 UV-Vis spectrophotometer with an integrated sphere accessory. Selected samples from each group were also tested with a Thermo Nicolet Nexus 670 FTIR spectrometer and a Renishaw inVia Raman microscope.

The three heat-treated cultured pearls were obtained from a reliable source. In addition, more than 100 naturally colored yellow or "golden" South Sea cultured pearls (from Jewelmer) were tested using an Ocean Optics USB 2000+ UV-Vis spectrometer. This unit takes less than one minute to run a pearl sample, making it ideal for rapidly examining bulk quantities. Some of these cultured pearls were also tested with PL spectroscopy. A summary of the various sample groups and advanced testing techniques is provided in table 1.

RESULTS

Gemological Observations and UV Fluorescence. All 69 cultured pearls exhibited light yellow, orangy yellow, yellow, or strong yellow bodycolors of uniform color distribution except the dyed samples from

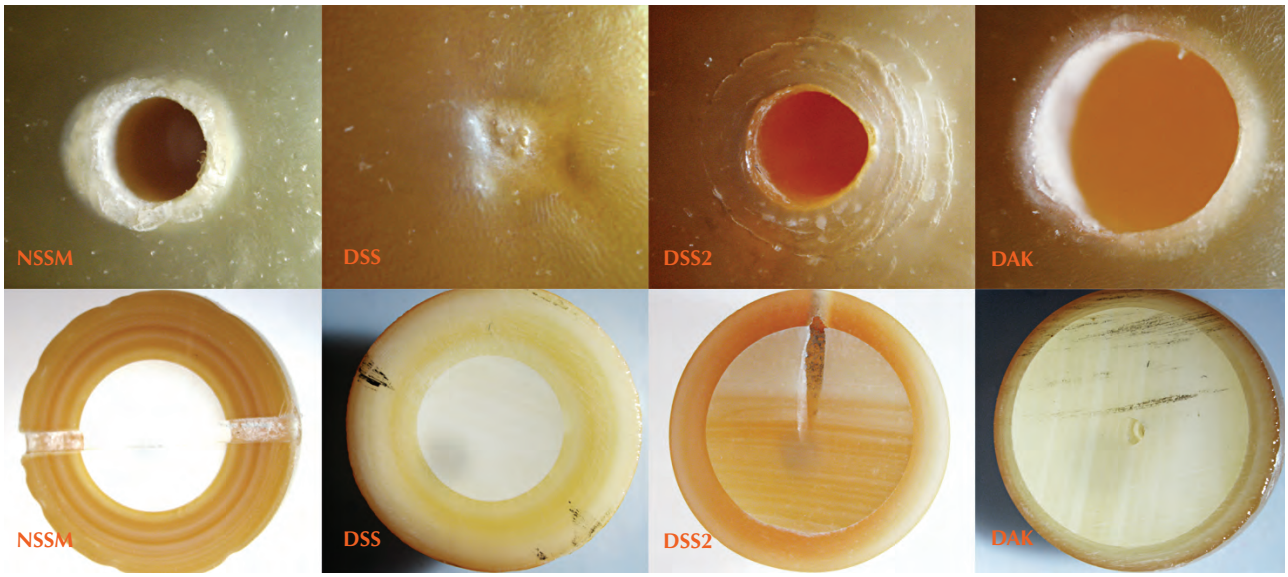

Figure 2. These microscopic images show the surfaces and cross-sections of representative samples from groups NSSM, DSS (high-quality dyed), DSS2 (low-quality dyed), and DAK (high-quality dyed). Photos by Chunhui Zhou; magnified 10×–70×.

group DSS3, which showed distinctly uneven color distribution. Under magnification, concentrated dye features were observed in three additional dyed groups (DSS2, DAK2, and DFW), while the other two dyed groups (DSS and DAK) showed no evidence of surface treatment (figure 2). To make matters even more challenging, cultured pearls from the DSS group did not possess drill holes, which serve to enhance the diffusion of the dye material, suggesting that a different dyeing technique was applied to them. Representative samples from groups NSSM, DSS, DSS2, and DAK were cut in half to observe the color distribution throughout their cross-sections. Typical concentric growth rings were noted on the nacre of the naturally colored sample, while the growth structures in the dyed cultured pearls were largely masked by the infiltration of dyes. The presence of a drill hole in the samples from DSS2 and DAK had caused the dye materials to diffuse into the bead used to culture the pearls.

In Brief

- The dyeing of yellow or "golden" cultured pearls from *Pinctada maxima* has been common for many years.
- While most dyed yellow or "golden" cultured pearls are readily identified by microscopic observation of dye concentrations, some have very clean surfaces lacking any evidence of treatment.
- These higher-quality dyed samples can be detected by broad reflectance troughs between 410 and 450 nm, a lack of a reflectance feature at 350 nm, or intense fluorescence in the visible spectrum under 514 nm wavelength laser excitation.

UV fluorescence generally followed the bodycolor of the sample. Naturally colored orangy yellow to strong yellow cultured pearls usually exhibited weak yellow fluorescence, while lighter yellow samples exhibited moderate to strong yellow fluorescence. It is a challenging task, however, to accurately and consistently describe fluorescence color, since there is no reference for comparison. In this study, dyed samples also showed varying degrees of yellow or orangy yellow fluorescence, but not distinctive enough to consistently separate them from the naturally colored variety. Samples from DSS3 and DFW showed uneven color distribution due to dye concentrations on their surfaces. General observations and measurements are shown in table 2.

UV-Vis Reflectance Spectra. Within each group, UV-Vis reflectance properties were generally consistent. Naturally colored samples (NSSP and NSSM) showed

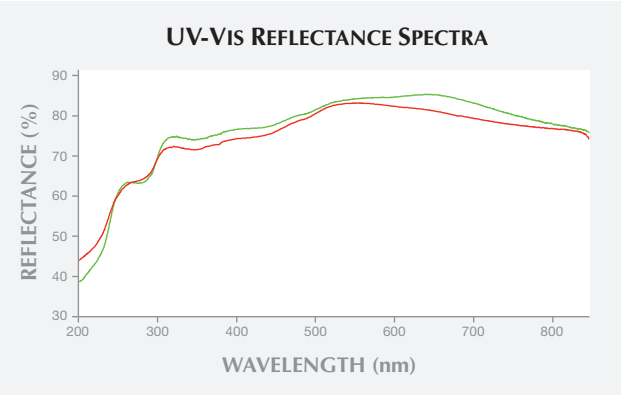

Figure 3. The UV-Vis reflectance spectra of representative samples from two naturally colored groups, NSSP (green) and NSSM (red), are compared.

decreasing reflectance toward the lower visible and long-wave UV range, with subtle local reflectance troughs at about 350 and 440 nm (figure 3). These reflectance troughs may be due to (but not equal to) absorptions at specific wavelengths. Cultured pearls from five of the dyed groups (DSS, DSS2, DSS3, DAK, and DAK2) all showed distinct reflectance characteristics within the same range, but with broader, more prominent, and sometimes shifted reflectance features between 410 and 450 nm, consistent with previous findings (Elen, 2002; Qi et al., 2008; Chen et al., 2009). Some of the dyed cultured pearls (DSS, DAK, and DAK2) also lacked the 350 nm reflectance feature, while others (DSS2 and DSS3) showed a steeper slope between 430 and 480 nm than that of naturally colored samples (figure 4), also consistent with previous findings. Dyed freshwater cultured pearls showed reflectance patterns similar to those of the naturally colored samples within the lower visible range, but lacked the 350 nm reflectance feature.

Figure 4. These UV-Vis reflectance spectra are of representative cultured pearls from six dyed sample groups: DFW (black), DAK (violet), DAK2 (yellow), DSS (purple), DSS2 (greenish blue), and DSS3 (blue).

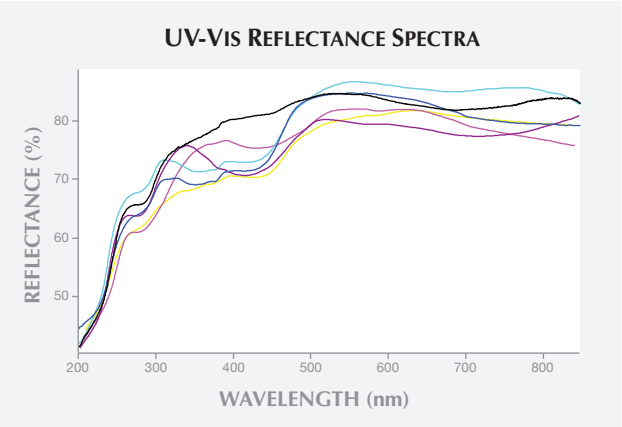

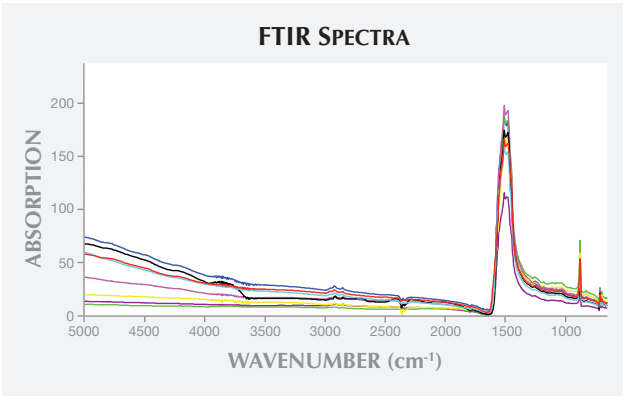

Figure 5. FTIR spectra of representative pearls from each of the eight groups are compared. All showed the same peaks related to the aragonite crystal structures of nacreous pearls.

FTIR, Raman, and PL Spectroscopy Results. We performed infrared and Raman spectroscopy on representative samples from each of the eight groups. The FTIR spectra only showed the vibrational modes of aragonite, the major component of all pearls, dyed or naturally colored (figure 5). Raman spectroscopy was performed with both 514 and 830 nm lasers. The 830 nm laser gave much better peak resolution (figure 6),

Figure 6. Raman spectra of representative samples from each of the eight groups are shown. All displayed the same peaks related to the aragonite crystal structures of nacreous pearls. The higher spectral intensity toward the lower wavenumber in some samples is due to their higher fluorescence.

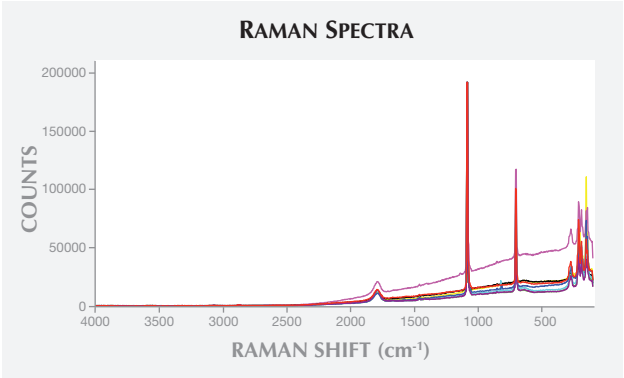

TABLE 2. General observations and measurements of the cultured pearls examined in this study.

Type	Measurements (range)	Color	Drilling	UV fluorescence
NSSP	12–14 mm	oY/Y/Strong Y	N	Weak/Very Weak Y
NSSM	12 x 11 mm–10.5 mm	Light Y/Y/Strong Y	In some cases	Strong/Moderate/Weak Y
DSS	8–10 mm	oY/Y/Strong Y	N	Moderate/Weak/Weak Y
DSS2	10–13 mm	oY/Y	Y	Weak/Very Weak Y
DSS3	10–14 mm	oY/Y	Y	Moderate/Weak Y/Moderate oY (uneven)
DAK	7.85–8 mm	oY/Y	Y	Strong/Moderate Y
DAK2	6.5–7.5 mm	oY/Y	Y	Weak Y
DFW	9.5 x 8 mm–9 x 7.5 mm	Light Y/Y	Y	Strong Y/Weak oY (uneven)

Color abbreviations: Y (yellow), oY (orangy yellow).

while the 514 nm laser (data not shown) registered significantly higher background fluorescence in the dyed and naturally colored samples.

To clearly visualize the fluorescence characteristics of these samples upon laser excitation, we performed PL measurements. These confirmed that most of the dyed cultured pearls fluoresced at much higher levels than naturally colored pearls—in a few cases, reduced power had to be used to prevent peak oversaturation—making it a useful tool in identifying some cases of dye treatment (figure 7). A more useful way to look at the data, though, is to compare the ratio between overall fluorescence intensity (600–700 nm) and the height of the main aragonite peak at 545 nm (i.e., the F/A ratio; figure 8). Dominant or significant aragonite peak intensities were observed in the spectra of naturally colored samples, with the F/A ratio consistently below 5. For dyed samples, the ratio varied more due to the different dye materials used, but they were more likely to have F/A ratios of at least 10.

Figure 7. PL spectra of representative samples from each of the eight groups are shown: NSSP (green), NSSM (red), DFW (black), DAK (violet, 5% laser power), DAK2 (yellow, 50% laser power), DSS (purple), DSS2 (greenish blue), and DSS3 (blue). Naturally colored cultured pearls generally gave lower fluorescence upon laser excitation, while most dyed samples fluoresced at much higher intensity.

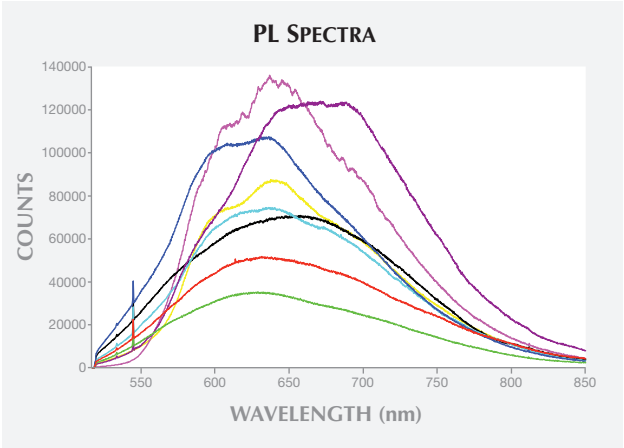

Additional Reference Collection Data Results. In addition to the 18 reportedly naturally colored yellow samples, we examined more than 100 reportedly naturally colored yellow to orangy yellow cultured pearls of various saturations using UV-Vis reflectance

Figure 8. In this representative PL spectrum, comparing the ratio between the total fluorescence (F) and intensity of the aragonite main peak (A) helps separate naturally colored from dyed cultured pearls.

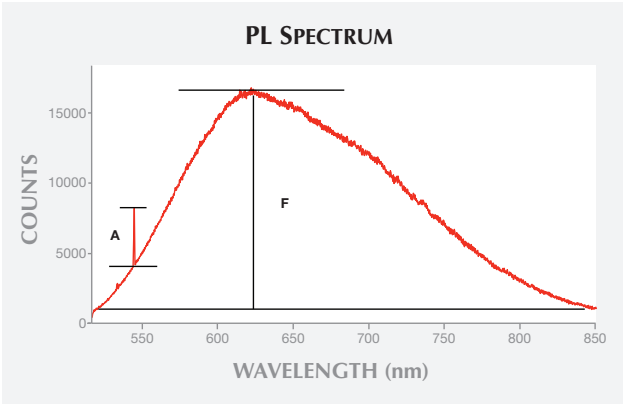

Figure 9. Naturally colored cultured pearls generally show consistent UV-Vis reflectance characteristics and less-intense PL features, which may be useful in identifying unknown samples. Photo by Adirote Sripradist.

and PL methods. These provided useful baselines for comparing unknown samples. The UV-Vis reflectance results of these naturally colored yellow samples showed consistent spectroscopic characteristics, similar to those observed in groups NSSP and NSSM (again, see figure 3). Low PL fluorescence signals (and F/A ratio) were also observed in all of the cultured pearls. Building and maintaining a spectral database from naturally colored yellow samples of various saturations (figure 9) is important for comparative analysis and identification of dye treatment.

Heat-Treated Yellow Cultured Pearls. In addition to dye treatment, heat-treated yellow cultured pearls have been reported (Elen, 2001). The exact mechanism of color alteration is still unclear. One theory suggests that heating changes the amino acid compositions of conchiolin proteins, altering their physical and chemical properties (Akiyama, 1978). Another possibility is that heating proteins and sugars (found in conchiolin) at high temperature under intermediate moisture levels and alkaline conditions will promote Maillard reaction, resulting in a color change similar to the browning effect caused by heating many kinds of food. The three reportedly heat-treated cultured pearls were tested using UV-Vis reflectance and PL spectroscopy. The UV-Vis spectra lacked the obvious broad reflectance pattern found in dyed samples, consistent with an earlier report (Elen, 2001) that their heat treatment did not involve any addition of dye materials. Yet the PL spectra showed extremely intense fluorescence, which could be useful in separating them from naturally colored samples. A brief summary of these results appears in box A.

DISCUSSION

The dyeing of cultured pearls has been a common practice for many years (Alexander, 1960; Liddicoat, 1962; Johnson and Koivula, 1999), and it can usually be detected through careful examination of the surface. In our study, four of the six groups of dyed yellow or "golden" samples could be detected through conventional microscopic observation. Concentrated dye residues and uneven color distribution provided definitive evidence. These products are usually treated after drilling, which was confirmed by the dye residue within and around the drill holes. The other two groups (DSS and DAK) had relatively clean surfaces, and even a trained gemologist would have difficulty in separating them from naturally colored samples. Cultured pearls from the DSS group were treated without the aid of drill holes, while samples from the DAK group were dyed either before or after drilling. If they were dyed after drilling, further treatment such as bleaching may have been used to lighten any color concentrations that accumulated near the drill holes.

All the yellow or "golden" cultured pearls showed decreasing reflectance in the violet/blue region of the visible spectrum, which corresponds with the color reflected, in accordance with complementary color theory and human color perception. But naturally colored samples displayed a gradual decrease in reflectance, with subtle local reflectance troughs at

BOX A: CHARACTERISTICS OF HEAT-TREATED SAMPLES

The three reportedly heat-treated cultured pearls ranged from light yellow to yellow, with various surface characteristics (figure A-1). In one of them, we observed color concentrations similar to those expected in dyed samples.

While their UV-Vis spectra differed from those of dyed cultured pearls in this study (figure A-2), they showed significantly higher PL properties than naturally colored samples tested under the same conditions (figure A-3).

Figure A-1. These three reportedly heat-treated cultured pearls (top left) show various surface characteristics: even light yellow color with no obvious color concentration (top right), patchy yellow color with obvious orangy concentrations observed at blemishes (bottom left), and even yellow color with no obvious concentration (bottom right).

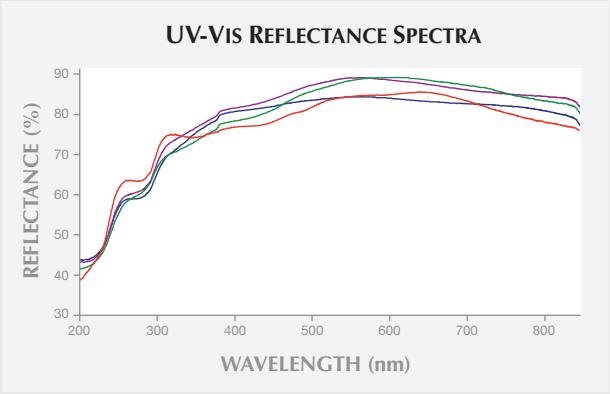

Figure A-2. The UV-Vis reflectance spectra of one naturally colored sample (red) differed from that of three heat-treated yellow cultured pearls.

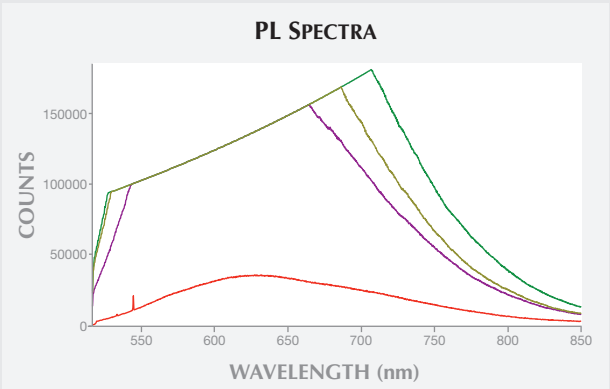

Figure A-3. The PL spectra of the three heat-treated samples show more complete saturation (no Raman signal) than the naturally colored sample (red) under the same conditions, due to their excessive fluorescence signal.

350 and 440 nm, while five of the six dyed groups showed significant reflectance troughs between 410 and 450 nm. These distinct reflectance characteristics can be explained by the different reflectance properties of natural pigments and the predominantly single-component artificial dyes applied to the treated products, as well as the variable concentrations of either. Interestingly, the origin of the golden color found in South Sea cultured pearls may also be derived from nano-composite structures of the nacre, as reported by Snow (2004), which helps further explain the different reflectance features between naturally colored and dyed cultured pearls. For the DFW group, no significant differences were found in the violet/blue region of the visible spectrum, in part because they contained less dye than the other groups. Some of the dyed groups also lacked the local reflectance trough at 350 nm, which occurs almost exclusively in cultured pearls with yellowish hues and may be attributed to a particular pigment.

Although some previous studies have reported the presence of natural pigments in naturally colored freshwater, Tahitian, and *Pteria* species samples (Karampelas et al., 2007; Bersani and Lottici, 2010), our study found no obvious differences using either infrared or Raman spectroscopy. Low pigment or dye concentrations, the location of these materials inside

nacre platelets, and strong signal interference by aragonite crystal structure of the pearls could all make it difficult to detect any pigment or dyes using Raman spectroscopy. Yet dyed cultured pearls generally show higher PL under 514 nm laser excitation, likely a consequence of the fluorescence characteristics of the particular dye(s) applied. The result agrees with earlier studies (Liu and Li, 2007; Chen et al., 2009).

CONCLUSIONS

While most dyed yellow or "golden" cultured pearls can still be detected with relative ease using magnification, some show very clean surfaces lacking any evidence of dye. We have demonstrated that these can be identified by nondestructive, advanced instrumental techniques such as UV-Vis reflectance and PL spectroscopy. Our study suggests three indications of dyeing: broad reflectance troughs between 410 and 450 nm, a lack of a reflectance feature at 350 nm, or intense fluorescence in the visible spectrum under 514 nm wavelength laser excitation. When testing cultured pearls using advanced instrumentation, comparative analysis between naturally colored and dyed samples is an important part of the identification process in certain cases. GIA has collected sets of data from numerous naturally colored yellow or "golden" cultured pearls with varying degrees of saturation to use as references for comparison against the spectra of unknown samples. Further analysis of "golden" cultured pearls is needed due to the unlimited number of dye materials that can be used to treat off-color or low-grade goods.

ABOUT THE AUTHORS

Dr. Zhou is a research technician, Ms. Ho is a staff gemologist, and Ms. Hyatt is a staff gemologist at GIA in New York. Ms. Homkrajae is a staff gemologist, and Mr. Sturman is supervisor of pearl identification, at GIA in Bangkok.

ACKNOWLEDGMENTS

The authors thank several companies and individuals for providing samples used in this study. Jewelmer kindly provided the naturally colored cultured pearls from the Philippines. Drs. Ahmadjan Abduriyim and Wuyi Wang of GIA supplied the dyed samples from various sources. Thanks are also extended to Dr. Ren Lu of GIA for assisting with gemological and instrumental aspects of this study, and Sheryl Elen of the GIA's Richard T. Liddicoat Gemological Library and Information Center for obtaining reference articles.

REFERENCES

Akiyama M. (1978) Amino acid composition of heated scallop shells. *Journal of the Faculty of Science*, Hokkaido University, Series IV, Vol. 18, No. 1–2, pp. 117–121.

Alexander A.E. (1960) Several diagnostic tests for dyed pearls. *The Gemmologist*, Vol. 29, No. 343, pp. 28–29.

Bersani D., Lottici P.P. (2010) Applications of Raman spectroscopy to gemology. *Analytical & Bioanalytical Chemistry*, Vol. 397, No. 7, pp. 2631–2646, http://dx.doi.org/10.1007/s00216-010-3700-1.

Chen Y., Guo S.G., Shi L.Y. (2009) Non-destructive testing of golden saltwater pearls. *Journal of East China University of Science and Technology (Natural Science Edition)*, Vol. 35, No. 4, pp. 578–581.

Elen S. (2001) Spectral reflectance and fluorescence characteristic of natural-color and heat-treated "golden" South Sea cultured pearls. *G&G*, Vol. 37, No. 2, pp. 114–123, http://dx.doi.org/10.5741/GEMS.37.2.114.

——— (2002) Update on the identification of treated "golden" South Sea cultured pearls. *G&G*, Vol. 38, No. 2, pp. 156–159, http://dx.doi.org/10.5741/GEMS.38.2.156.

The fabulous golden pearls of the Philippines: A lustrous future. (2010) *Pearl World*, Vol. 19, No. 1, pp. 3, 10–12, 14–15.

Gemological Institute of America (2000) *GIA Pearl Grading Color Reference Charts*. Carlsbad, CA.

Johnson M.L., Koivula J.I., Eds. (1999) Gem News: "Blatant" dyed pearls. *G&G*, Vol. 35, No. 1, pp. 55–56.

Karampelas S., Fritsch E., Mevellec J.-Y., Gauthier J.-P., Sklavounos S., Soldatos T. (2007) Determination by Raman scattering of the nature of pigments in cultured freshwater pearls from the mollusk *Hyriopsis cumingi*. *Journal of Raman Spectroscopy*, Vol. 38, No. 2, pp. 217–230, http://dx.doi.org/10.1002/jrs.1626.

Liddicoat R.T. (1962) Dyed rosé cultured pearls. *G&G*, Vol. 10, No. 9, p. 279.

Liu W.W., Li L.P. (2007) Technology and identification of golden dyed pearls. *Journal of Gems and Gemmology*, Vol. 9, No. 4, pp. 33–36.

Qi L.J., Huang Y.L., Zeng C.G. (2008) Colouration attributes and UV-NIS reflection spectra of various golden seawater cultured pearls. *Journal of Gems and Gemmology*, Vol. 10, No. 4, pp. 1–8.

Roskin G. (2005) The mystery of the dyed gold pearls. *Jewelers' Circular-Keystone*, Vol. 176, No. 8, p. 46.

Shor R. (2007) From single source to global free market: The transformation of the cultured pearl industry. *G&G*, Vol. 43, No. 3, pp. 200–226, http://dx.doi.org/10.5741/GEMS.43.3.200.

Snow M.R., Pring A., Self P., Losic D., Shapter J. (2004) The origin of the color of pearls in iridescence from nano-composite structures of the nacre. *American Mineralogist*, Vol. 89, No. 10, pp. 1353–1358.

Supplier warns trade against dyed golden (1998) *Jewellery News Asia*, No. 164, pp. 58, 60.

IDENTIFICATION OF IRRADIATED SOUTH SEA CULTURED PEARLS USING ELECTRON SPIN RESONANCE SPECTROSCOPY

Youngchool Kim, Hyunmin Choi, Bohyun Lee, and Ahmadjan Abduriyim

Irradiated South Sea cultured pearls (SSCPs) from the *Pinctada maxima* mollusk typically show colors from light gray to silver. It is difficult to identify gamma-ray irradiation of SSCPs using standard gemological methods because of their thick nacre. Therefore, an advanced analytical technique such as electron spin resonance (ESR) spectroscopy is needed to detect the treatment. ESR measurements of minute amounts of SSCP powders revealed the formation of CO_2^- radicals, and the parameter known as the *g*-factor was measured at 2.0015 ± 0.0005. Higher levels of CO_2^- radicals were detected in the pearl nacre than in the nucleus. Therefore, the existence of CO_2^- radicals is an indicator of irradiated SSCPs.

Irradiation, dyeing, bleaching, and heat treatment are widely used methods to alter pearl color. Although most artificial colors are easily recognized, some resemble attractive colors that occur in nature (Elen, 2001; Li and Chen, 2001; Zachovay, 2005; Wang et al., 2006; "Better techniques improve brown pearls," 2006; McClure et al., 2010).

Lower-quality freshwater and saltwater cultured pearls are regularly exposed to ^{60}Co gamma-ray radiation in an attempt to simulate black pearls or enhance orient (Crowningshield, 1988; Li and Chen, 2002; O'Donoghue, 2006). In recent years, the irradiation process has been applied to not only Akoya cultured pearls and freshwater cultured pearls (FWCPs), but also to South Sea cultured pearls (SSCPs) (Choi et al., 2012). The irradiation-induced color change results from the darkening of the nucleus, caused by $MnCO_3$ oxidation, as well as denatured damage to the pearl's conchiolin (Matsuda and Miyoshi, 1988). FWCPs have a higher abundance of proteinous components and manganese than saltwater pearls (Hatano and Ganno, 1962).

Gamma-ray irradiated SSCPs (figure 1) were first discovered in the Korean market in April 2011. At the March 2011 Hong Kong Jewelry Show, a Japanese trader reportedly sold a Korean counterpart irradiated SSCPs without disclosing the treatment. They were light gray or silver loose cultured pearls and beads 10–16 mm in size. While a cream, yellow, or black color is produced by a protein pigment in the nacre, a blue or silver color is caused by organic material between the nacre and nucleus (Komatsu, 1999; O'-

Figure 1. This necklace contains gamma-ray irradiated silver South Sea cultured pearls (12.0–14.0 mm). Electron spin resonance (ESR) spectroscopy proved effective in identifying the gamma irradiation. Photo by Jae Hak Ko.

See end of article for About the Authors and Acknowledgments.
GEMS & GEMOLOGY, Vol. 48, No. 4, pp. 292–299,
http://dx.doi.org/10.5741/GEMS.48.4.292.

Donoghue, 2006). Korean consumers typically prefer SSCPs with a silver color created by organic material.

According to the research of Choi et al. (2012), gamma-ray irradiated SSCPs with colors ranging from white to cream turned light gray to silver, with the depth of color correlating with increasing irradiation dose. A dose of 0.5–1 kGy caused a light gray color, while a dose above 5 kGy produced a silver color.

For Akoya cultured pearls, with a typical nacre thickness of 0.2–0.6 mm, irradiation can be identified through standard gemological tests (Komatsu, 1999; O'Donoghue, 2006). But for SSCPs, which have a nacre thickness of roughly 1.5–3.0 mm, detecting irradiation is difficult with methods such as transmitted light, magnification, fluorescence reaction, and UV-Vis spectrometry (Choi et al., 2012).

This study attempted to identify irradiated SSCPs using electron spin resonance (ESR) spectroscopy. This method, also known as electron paramagnetic resonance (EPR) spectroscopy, identifies the presence of unpaired electrons. Moreover, the study sought to minimize damage during examination by obtaining a minimal sample of powder from each cultured pearl.

MATERIALS AND METHODS

For the study, some 300 SSCPs weighing 6.55–18.05 ct (8.0–16.6 mm in diameter) with white to cream color were exposed to gamma-ray irradiation at room temperature. The irradiation was conducted at the ^{60}Co facility of the KAERI (Korea Atomic Energy Research Institute) in Jeongeup, South Korea. The absorbed doses were set at 0.2, 0.4, 0.6, 0.8, 1, 5, and 100 kGy.

Inductively Coupled Plasma-Atomic Emission Spectrometer. Chemical composition analyses of the SSCPs were performed with an inductively coupled plasma–atomic emission spectrometer (ICP-AES, Varian Vista-PRO). The nacre, nucleus (bead), and conchiolin were separated and powdered, and 0.2 g of each powder was dissolved in a solution of 37% HCl (6 ml) and 65% HNO_3 (2 ml). We tested the samples after 20 minutes at 200°C and after 10 minutes at the same temperature to obtain an average value.

Electron Spin Resonance Spectroscopy. This study relied on electron spin resonance analysis to observe radicals produced by the irradiation process. The ESR spectrometer gauges the absorbed dose corresponding to the splitting energy of unpaired electrons in a magnetic field. The technique can rapidly identify an irradiation-related signal from a small amount of sample in a few minutes. For this study, we collected at least 10 mg of SSCP powder from both the nacre and the nuclei of each cultured pearl. To determine if the ESR signals correlated with Mn^{2+}, solid samples of FWCP, which contain more manganese than SSCPs, were irradiated with a 100 kGy dose.

Figure 2. This JEOL FA-300 spectrometer with a manganese marker is the ESR instrument used in the study. Photo by Y. C. Kim.

Room-temperature ESR spectra were recorded using a JEOL FA-300 spectrometer with a manganese marker (MgO: Mn^{2+}), using 9.8 GHz microwave frequency, 1 mW microwave power, a 1–2 G modulation amplitude, a 2 min sweep time, and a 0.03 s response time (figure 2).

Mn marker for ESR analysis. The *g*-factors of free radicals created by irradiation are approximately 2.00. For comparison, the "free electron" *g*-factor is 2.0023. Standard reference samples can be used to correct for any systematic errors in the measured magnetic field values and to verify the sensitivity of the system. Standard samples include DPPH (2.2-diphenyl-1-picryl-hydrazyl), TCNQ-Li (tetracyanoquino-dimethane Li

BOX A: WHAT IS ESR?

Electron spin resonance (ESR), alternatively known as electron paramagnetic resonance (EPR), is a spectroscopic method for observing the resonance absorption of microwave power by paramagnetic molecules, defects or free radicals (characterized by at least one unpaired electron) which are simultaneously subjected to an applied magnetic field. For most materials the electrons are "paired," and are thus invisible to ESR. ESR can be used to detect paramagnetic defects or free radicals introduced by irradiation in some materials, and has been applied to the study of irradiated food (Chauhan et al., 2008). Oftentimes, its high sensitivity allows the detection of irradiation-related defects in small sample volumes in just a few minutes, making it an effective and minimally invasive technique.

In a typical ESR experiment the sample is subjected to microwaves of a fixed energy (i.e., fixed frequency ν), while the magnitude of the magnetic field is varied. A property called *electron spin* is attributed to each unpaired electron, where a single unpaired electron has only two allowed energy states. ESR is used to probe the energy differences between those states. In the absence of a magnetic field the two states have the same energy, yet when a magnetic field is applied the energy separation of the states will increase. The dominant interaction governing the splitting is known as the *Zeeman effect*, whereby the energy difference increases linearly with increasing magnetic field according to the equation $\Delta E = g\beta H$. Here ΔE denotes the energy difference, g is the spectroscopic splitting factor known as the *g-factor*, β is a constant called the Bohr magneton, and H is the magnetic field. The *g*-factor is influenced by the characteristic environment of the unpaired electron(s) of a free radical, providing a "fingerprint" to be used for identification. The *g*-factor values of known paramagnetic molecules, defects and free radicals are tabulated in the literature. There are additional interactions which can lead to more complicated spectra and a wealth of additional information, but those will not be discussed here.

Figure A-1 shows the energy diagram for the electron spins of two different radical species with differing *g*-factors, one given by g_1 and the other by g_2. As the magnetic field is increased it is apparent that the energy levels for the two radical species split at different rates. The ESR resonance condition is met when the energy separation is equal to the energy of the applied microwave radiation,

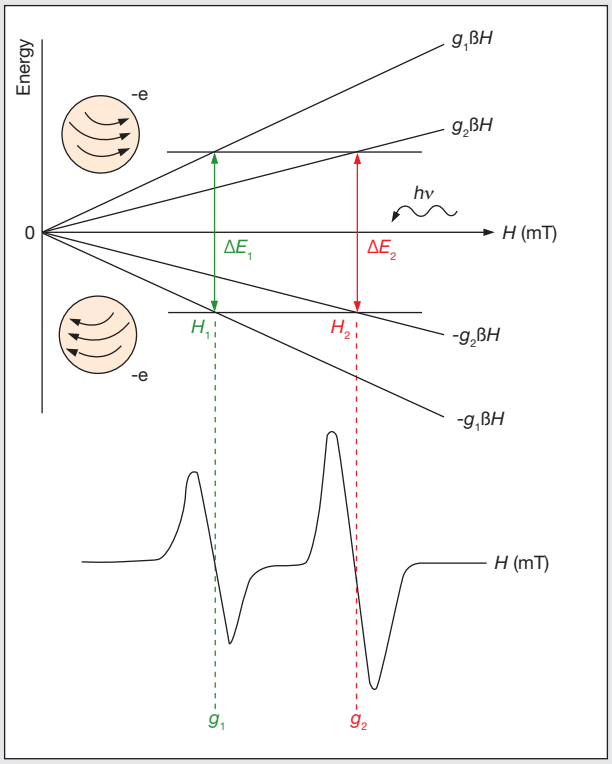

Figure A-1. Energy levels of two paramagnetic species with g-factors g_1 and g_2. As the magnetic field H is increased the energy levels for the two species split at different rates, according to the Zeeman effect. Resonance occurs, and signals with derivative lineshapes are detected, when the energy separations (ΔE_1 and ΔE_2) are equal to the energy of the applied microwaves ($h\nu$). From Ikeya (1993).

$\Delta E = g\beta H = h\nu$ (where h is Planck's constant), leading to an absorption of the microwaves and the detection of an ESR signal. Thus, the signals for the radical species with *g*-factors g_1 and g_2 will occur at H_1 and H_2, respectively. Hence, the identity of the radical(s) producing the ESR spectrum can be determined by careful analysis of the magnetic field values at which the resonance signals are detected. Furthermore, the intensity of the ESR signal is proportional to the number of radicals present, allowing quantitative analysis.

saly), CaO:Mn^{2+}, and MgO:Mn^{2+}. The choice of standard sample used depends on what the user wants to determine. For example, DPPH is used to calculate *g*-factors, to monitor the sensitivity of the equipment, and to quantify spin concentrations. TCNQ-Li is used to find the *g*-factor. CaO:Mn^{2+}, MgO:Mn^{2+}, and Mn^{2+} are used to measure the *g*-factor and to correct magnetic field variations.

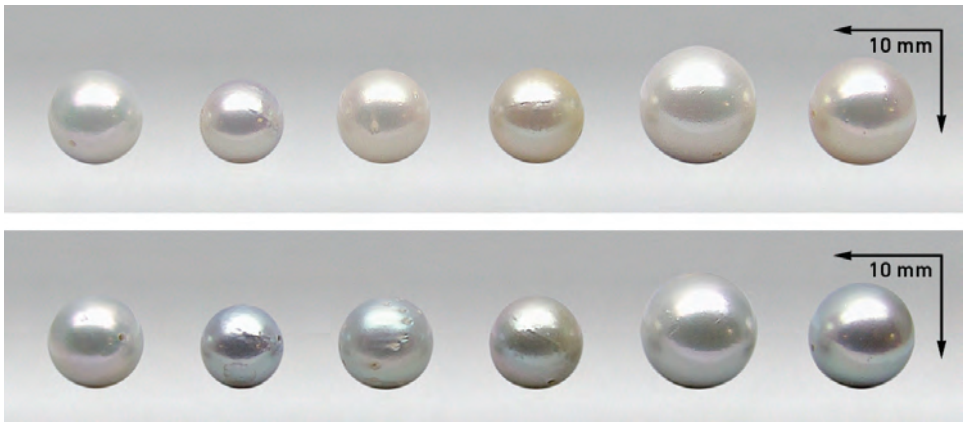

Figure 3. Before and after photos of SSCPs exposed to gamma irradiation at a dose of 5 kGy. The irradiated pearls turned gray to silver, slightly different from their original colors. Photos by H. M. Choi.

The *g*-factor of most standard samples is also located around 2.00. The Mn marker is shown with six Mn^{2+} signals; the third (2.034) and fourth (1.981) signals are used to correct magnetic field variations. Each signal has a regular interval from 2.00. From this property, the MgO:Mn^{2+} marker could be more suitable to measuring the *g*-factor than the alternative standard samples. The MgO:Mn^{2+} marker was supplied with the Jeol X-band spectrometer in the shape of a small rod that can be electromechanically inserted externally into the microwave cavity. When a sample and a Mn marker are measured simultaneously, the resulting ESR spectrum will contain signal contributions from both. It is easy to distinguish the ESR spectra of one from the other, since the Mn^{2+} signals have the opposite phase to that of the sample's signal (i.e., the signal's lineshape will appear to have been flipped across the baseline).

RESULTS AND DISCUSSION

The major element of a pearl is calcium. Chemical composition analysis of bead-cultured pearls using ICP-AES demonstrates that the nacre and the freshwater nucleus contain similar trace elements but vary in their composition. The nacre contains more Na, Mg, and Sr, while the nucleus has higher Mn and P contents (table 1).

After ^{60}Co gamma-ray irradiation at a dose of 5 kGy, the SSCPs exhibited gray to silver coloration (figure 3). The interior of one of the irradiated pearls revealed a grayish brown to dark gray nucleus, along with an altered nacre color (figure 4). The irradiation-induced color change is chiefly attributed to the darkening of the nucleus (bead), which in turn darkens the nacre—especially in the thinner-skinned Akoya cultured pearls (Komatsu, 1999). As shown in this experiment, color change took place in the nacre as well.

Figure 4. These photos show the interior (left) and exterior (right) of a light yellow South Sea cultured pearl before and after irradiation at a dose of 5 kGy. Left: The nucleus (bead) became grayish brown to dark gray, and the nacre color was similarly altered. Right: The pearl's surface turned a silver color. Photos by B. H. Lee.

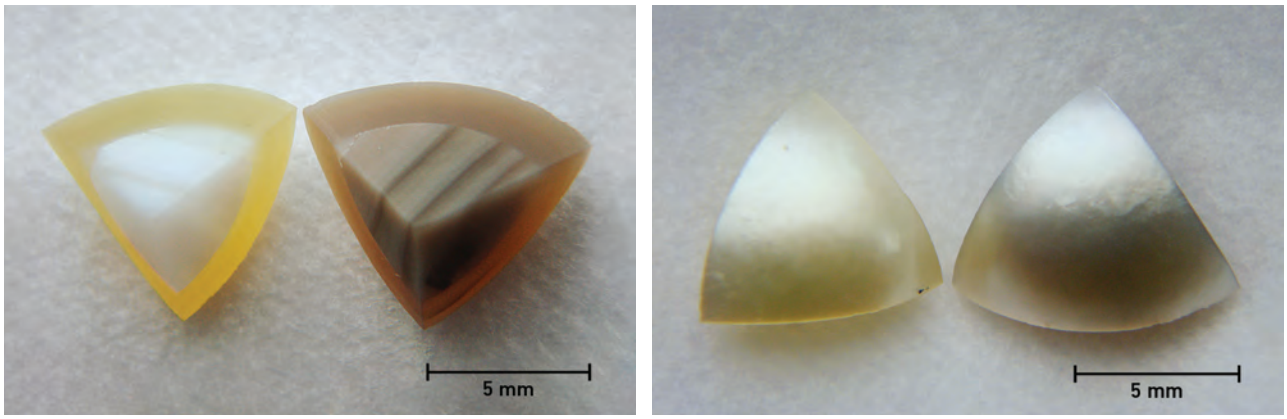

TABLE 1. Representative composition of the nacre and nucleus in South Sea cultured pearls in ppm (parts per million), determined by ICP-AES.

Sample	Ca	Na	Mg	P	Mn	Fe	Sr
Nacre	293099.06	4717.01	100.27	12.47	19.43	30.29	1086.80
Nucleus	287998.86	1704.52	26.24	94.42	431.43	26.80	249.21

Figure 5 shows that the concentration of radicals produced by irradiation exposure increases with the absorbed dose. Formerly undetected free radicals were observed after a low-dose radiation of 0.2 kGy. The *g*-factor was 2.0015 ± 0.0005, which agrees with that of CO_2^- radicals (Wieser et al., 1985; Ikeya, 1993; Seletchi and Duliu, 2007). With higher absorbed doses, the CO_2^- radical signal intensity further intensified. The identification of CO_2^- radicals through ESR analysis thus serves as a way to distinguish irradiated cultured pearls.

Matsuda and Miyoshi (1988) reported that the irradiation-induced change of color is caused by manganese (Mn). They noted that $MnCO_3$ in the nucleus (bead) turned into oxidations such as Mn_3O_4, Mn_2O_3, and Mn_2O after irradiation. Their results are still cited in literature related to color change in irradiated pearls (e.g., Komatsu, 1999; Wada, 1999; McClure, 2010).

Yet existing mechanisms are insufficient to explain the alteration of pearl color by irradiation (Li and Chen, 2002). Based on the results of gamma-ray irradiation tests in this study, the authors believe that post-irradiation color change cannot solely be attributed to $MnCO_3$ oxidation. Two factors support this hypothesis:

1. After irradiation, the pearl nacre blackened to a similar extent as the nucleus (bead), even though it contains approximately 20 times less Mn (see figure 4 and table 1).

Figure 6 is an ESR spectrum comparing untreated FWCP, irradiated (100 kGy) FWCP, and a Mn marker (MgO: Mn^{2+}) attached to the JEOL equipment. The Mn marker consists of Mn^{2+} and shows six sharp peaks in the ESR spectrum (figure 6b). Before (figure 6a) and after (figure 6c) irradiation spectra of FWCPs (typical in the carbonate spectrum) do not match the positions of the Mn^{2+} signals. Nevertheless, a change was observed in the spectra before and after irradiation: the formation of CO_2^- radicals between the third and fourth Mn^{2+} peaks (highlighted by the green circle in figure 6c). Because these results were the same

Figure 5. These ESR spectra show a South Sea cultured pearl's nacre (left) and nucleus (right) before and after irradiation up to 1 kGy. These spectra were obtained for a single cultured pearl irradiated with different doses. CO_2^- radicals appeared as irradiation doses increased in both the nacre (left) and nucleus (right). Nucleus spectra (right) show a large unassigned signal in the 333–337 mT range, both before and after irradiation.

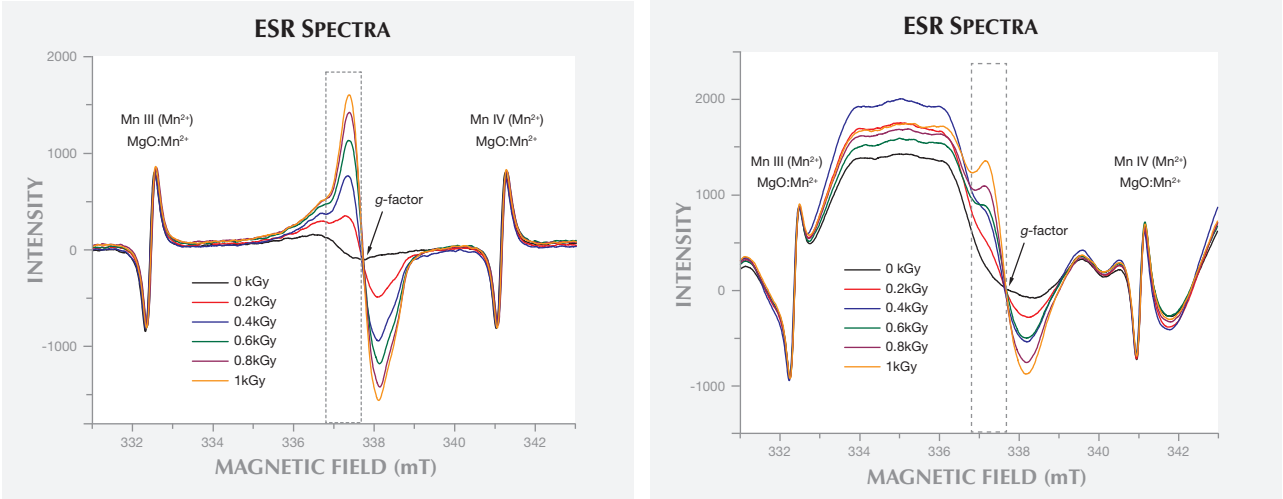

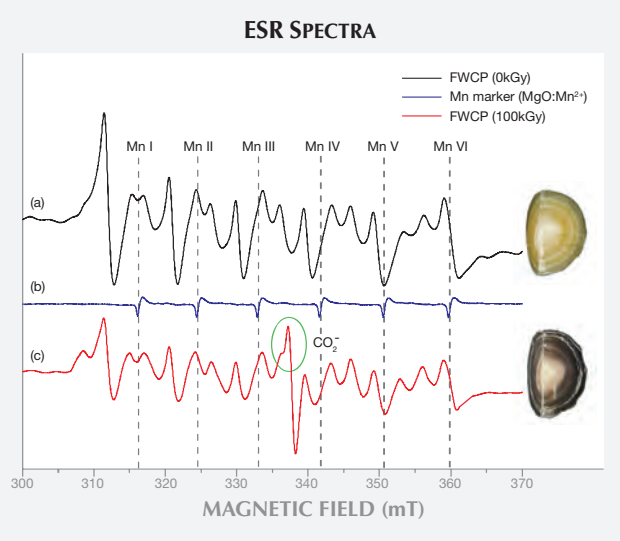

Figure 6. This graph demonstrates the spectra acquired for solid samples of FWCPs, which contain more Mn than saltwater cultured pearls. Shown are the spectra of untreated FWCPs (a), irradiated FWCPs (c), and a Mn marker (b). The Mn marker has six Mn^{2+} signals, and their positions are highlighted by the dotted vertical lines. After irradiation, CO_2^- radicals are observed only between the third and fourth Mn^{2+} resonance peaks. The signals before (a) and after (c) irradiation do not match the positions of the Mn^{2+} signals (b).

among all SSCPs investigated in this study, peaks in the ESR spectrum are unrelated to Mn.

2. CO_2^- radicals appeared as irradiation doses increased and multiplied in proportion to the dose (figure 7). The intensity of CO_2^- radicals was also proportional to the blackening of the pearl nucleus (bead). The CO_3^{2-} molecular ion in $CaCO_3$ is easily ionized by radiation. Elementary defects induced by ionizing radiation are an electron center (CO_3^{3-}) and a hole center (CO_3^-). While the CO_3^{3-} and CO_3^- centers are stable at low temperatures, the electron center CO_2^-, formed by irradiation, is an electron center similar but more stable than CO_3^{3-} (Ikeya, 1993). Additionally, we found that the color of nacre and nucleus had been bleached under incandescent light (approximately 50°C) for 30 days. The color changed by irradiation and heat (by light) is related to the color center. Therefore, the color change of the nacre and the blackening of the nucleus (bead) are believed to be related to color centers formed by CO_2^- radicals.

Choi et al. (2012) found that after irradiation, glutamic acid decreased 11.43% (from 3.5% to 3.1%), alanin 21.8% (from 22.5% to 21.8%), and histidine 43.75% (from 1.6% to 0.9%), according to amino acid analysis to examine the change of protein between aragonite platelets in pearl nacre. Hatano and Ganno (1962) found that gamma-ray irradiation destroyed 32% of the histidine, 16.6% of the methionine, 11% of the glutamic acid, and 9.3% of the proline in the protein of the FWCPs. The destruction of protein caused by irradiation can also alter the color of SSCPs.

In Brief

- Gamma-ray irradiation is routinely applied to South Sea cultured pearls (SSCPs), typically producing a light gray to silver color.
- For SSCPs, which have a particularly thick nacre, detecting irradiation is difficult using methods such as transmitted light, magnification, fluorescence reaction, and UV-Vis spectrometry.
- Electron spin resonance (ESR) spectroscopy rapidly identifies the presence of CO_2^- radicals, whose concentration is proportional to the absorbed irradiation dose.

CO_2^- radicals at the absorbed irradiation dose of 0.2 kGy are barely visible in the nucleus sample but far more intense at doses above 0.4 kGy (figure 5, right). In particular, CO_2^- radicals emerging after irradiation were better observed in the nacre than in the nucleus at the same absorbed dose (figure 5, left).

Figure 7. Normalizing the CO_2^- radical intensity of figure 5 shows that the radicals' intensity increases depending on irradiation dose, even though the CO_2^- radical of the nucleus (bead) decreased at 0.6 kGy.

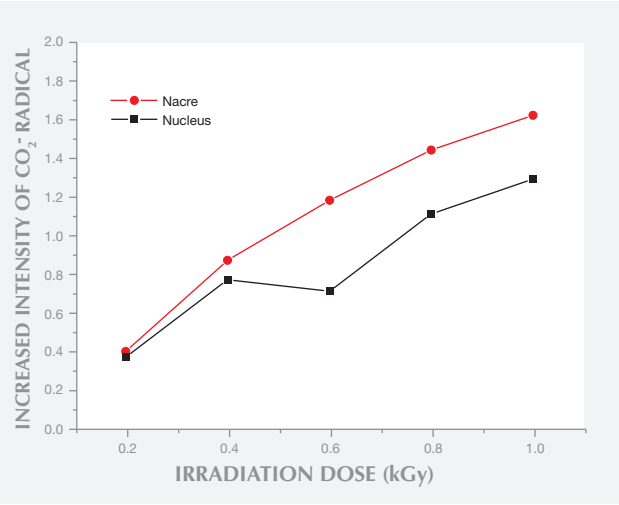

After normalizing the results of figure 5 to a nonirradiated spectrum (0 kGy, black line), the increased intensity of radicals was calculated by peak-to-peak height. The intensity of the CO_2^- radical is stronger in the nacre than in the nucleus when irradiated with a dose above 0.4 kGy (figure 7).

Ikeya (1993) reported that Mg^{2+} ions might be accompanied by H_2O molecules, leading to a rapid reduction in hydrated radicals. The saturation level of isotropic CO_2^- also increases with the Mg/Ca ratio. Barabas et al. (1989) studied synthetic carbonate crystals doped with Mg^{2+} and observed the following: (1) ESR spectra that displayed signals at the same spectroscopic properties as natural carbonates; and (2) an increase of the *g*-factor signal with Mg concentration in the carbonate crystals.

Mg also plays an important role in the formation of the crystal lattice of carbonates (Katz, 1973) and may enhance the formation of specific defects (Barabas et al., 1992). Lattice distortions caused by the incorporation of Mg^{2+} ions (Goldsmith and Graf, 1958) may lead to CO_2^- by creating larger interatomic distances (Barabas et al., 1992). In this context, the higher abundance of CO_2^- radicals in the nacre is thought to be related to the Mg/Ca ratio.

Considering the combined published observations on Mg^{2+} and CO_2^- (Ikeya, 1993; Barabas et al., 1989, 1992; and Katz, 1973) it is likely that the saturation level of CO_2^- rises proportionally with the Mg/Ca ratio in pearls of this study. As shown in table 1, the nacre and the nucleus (bead) contain 100 and 26 ppm of Mg, respectively. The nacre's Mg/Ca ratio is approximately four times greater than that of the nucleus (bead). Mg, which is more abundant in the nacre, therefore results in the preferential formation of CO_2^- in the nacre rather than in the nucleus when exposed to the same absorbed radiation dose. This is consistent with the higher CO_2^- ESR signal intensity observed in the nacre than in the nucleus (again, see figure 5). This suggests it is possible to identify an irradiated SSCP using ESR spectroscopy.

CONCLUSIONS

Identifying irradiated SSCPs through traditional gemological methods has been difficult, as their nacre is usually quite thick. But as this ESR study demonstrates, the separation of untreated pearls from irradiated pearls is possible. In doing so, an infinitesimal amount of sample was taken from the nacre in the form of powder. After irradiation, CO_2^- radicals were formed, and their presence was confirmed using ESR spectroscopy. The amount of CO_2^- radicals increased in proportion to the irradiation dose, and they were more observable in the nacre than in the nucleus (bead). Until now, irradiation-induced color changes in pearls were thought to be due to the change of the $MnCO_3$ oxidation number. But as this study notes, such color alteration is apparently related to an alteration caused by protein destruction rather than Mn, as well as color centers created by CO_2^- radicals.

ABOUT THE AUTHORS

Dr. Kim (hgi82@hanmail.net) is director, Dr. Choi is chief research scientist, and Dr. Lee is a research scientist at Hanmi Laboratory, in Seoul. Dr. Abduriyim is a senior research scientist and manager of color stone identification services at GIA's Tokyo laboratory.

ACKNOWLEDGMENTS

The authors are grateful to pearl dealers in Seoul for information and samples that made this study possible. Thanks to our technical staff members at Hanmi Laboratory for their assistance with this work. We are grateful to Hoon Choi and Byeongryong Park of Radiation Health Research Institute (KHNP), and the Korea Basic Science Institute (KBSI) for their help with ESR analysis. We also gratefully acknowledge the reviewers for significant improvements.

REFERENCES

Barabas M., Bach A., Mudelsee M., Mangini A. (1989) Influence of the Mg-content on ESR-signals in synthetic calcium carbonate. *Applied Radiation and Isotopes*, Vol. 40, No. 10–12, pp. 1105–1111.

——— (1992) General properties of the paramagnetic centre at g=2.0006 in carbonates. *Quaternary Science Reviews*, Vol. 11, No. 1–2, pp. 165–171, http://dx.doi.org/10.1016/0277-3791(92)90059-H.

Better techniques improve brown pearls (2006) *Jewellery News Asia*, No. 262, p. 60.

Chauhan S.K., Kumar R., Nadanasabapathy S., Bawa A.S. (2008) Detection methods for irradiated foods. *Comprehensive Reviews in Food Science and Food Safety*, Vol. 8, pp. 4–16.

Choi H.M., Lee B.H., Kim Y.C. (2012) Detection of gamma irradiated South Sea cultured pearls. *Journal of the Korean Crystal Growth and Crystal Technology*, Vol. 22, No. 1, pp. 36–41,

http://dx.doi.org/10.6111/JKCGCT.2012.22.1.036.
Crowningshield R. (1988) Gem Trade Lab Notes: Cultured pearls, irradiated. *G&G*, Vol. 24, No. 4, p. 244.
Elen S. (2001) Spectral reflectance and fluorescence characteristics of natural-color and heat-treated "golden" South Sea cultured pearls. *G&G*, Vol. 37, No. 2, pp. 114–123, http://dx.doi.org/10.5741/GEMS.37.2.114.
Goldsmith J.R., Graf D.L. (1958) Relation between lattice constants and composition of the Ca-Mg carbonates. *American Mineralogist*, Vol. 48, pp. 84–101.
Hatano H., Ganno S. (1963) Effects of radiations on colour of pearl and on amino acid composition of conchiolin in pearl. *Bulletin of the Institute for Chemical Research, Kyoto University*, Vol. 41, No. 1, pp. 83–88.
Ikeya M. (1993) *New Applications of Electron Spin Resonance: Dating, Dosimetry and Microscopy*. World Scientific, Singapore.
Katz A. (1973) The interaction of magnesium with calcite during crystal growth at 25–90°C and one atmosphere. *Geochimica et Cosmochimica Acta*, Vol. 37, No. 6, pp. 1563–1586, http://dx.doi.org/10.1016/0016-7037(73)90091-4.
Komatsu H. (1999) The identification of pearls in Japan—A status quo summary. *Journal of the Gemmological Society of Japan*, Vol. 20, No. 1–4, pp. 111–119.
Li L., Chen Z. (2001) Cultured pearls and colour-changed cultured pearls: Raman spectra. *Journal of Gemmology*, Vol. 27, No. 8, pp. 449–455.
——— (2002) Irradiation treatment of cultured pearls. *Journal of Gems & Gemology*, Vol. 4, No. 3, pp. 16–21.
Matsuda Y., Miyoshi T. (1988) Effects of r-ray irradiation on colour and fluorescence of pearls. *Japanese Journal of Applied Physics*, Vol. 27, No. 2, pp. 235–239, http://dx.doi.org/10.1143/JJAP.27.235.
McClure S.F., Kane R.E., Sturman N. (2010) Gemstone enhancement and its detection in the 2000s. *G&G*, Vol. 46, No. 3, pp. 218–240, http://dx.doi.org/10.5741/GEMS.46.3.218.
O'Donoghue M. (2006) *Gems*, 6th ed. Elsevier, Oxford, UK.
Seletchi E.D., Duliu O.G. (2007) Comparative study on ESR spectra of carbonates. *Romanian Journal of Physics*, Vol. 52, No. 5–7, pp. 657–666.
Symons M.C.R. (1992) ESR spectroscopy applied to the study of radiation mechanisms. *Applied Magnetic Resonance*, Vol. 3, No. 1, pp. 37–52, http://dx.doi.org/10.1007/BF03166779.
Wada K. (1999) *Science of Pearl.* Pearl Newspaper Company, Toyko.
Wang W., Scarratt K., Hyatt A., Shen H.T., Hall M. (2006) Identification of "chocolate pearls" treated by Ballerina Pearl Co. *G&G*, Vol. 42, No. 4, pp. 222–235, http://dx.doi.org/10.5741/GEMS.42.4.222.
Wieser A., Goksu H.Y., Regulla D.F. (1985) Characteristics of gamma-induced ESR spectra in various calcites. *Nuclear Tracks*, Vol. 10, No. 4–6, pp. 831–836, http://dx.doi.org/10.1016/0735-245X(85)90097-3.
Zachovay M. (2005) Gem News International: "Chocolate" Tahitian cultured pearls. *G&G*, Vol. 41, No. 2, pp. 183–184.

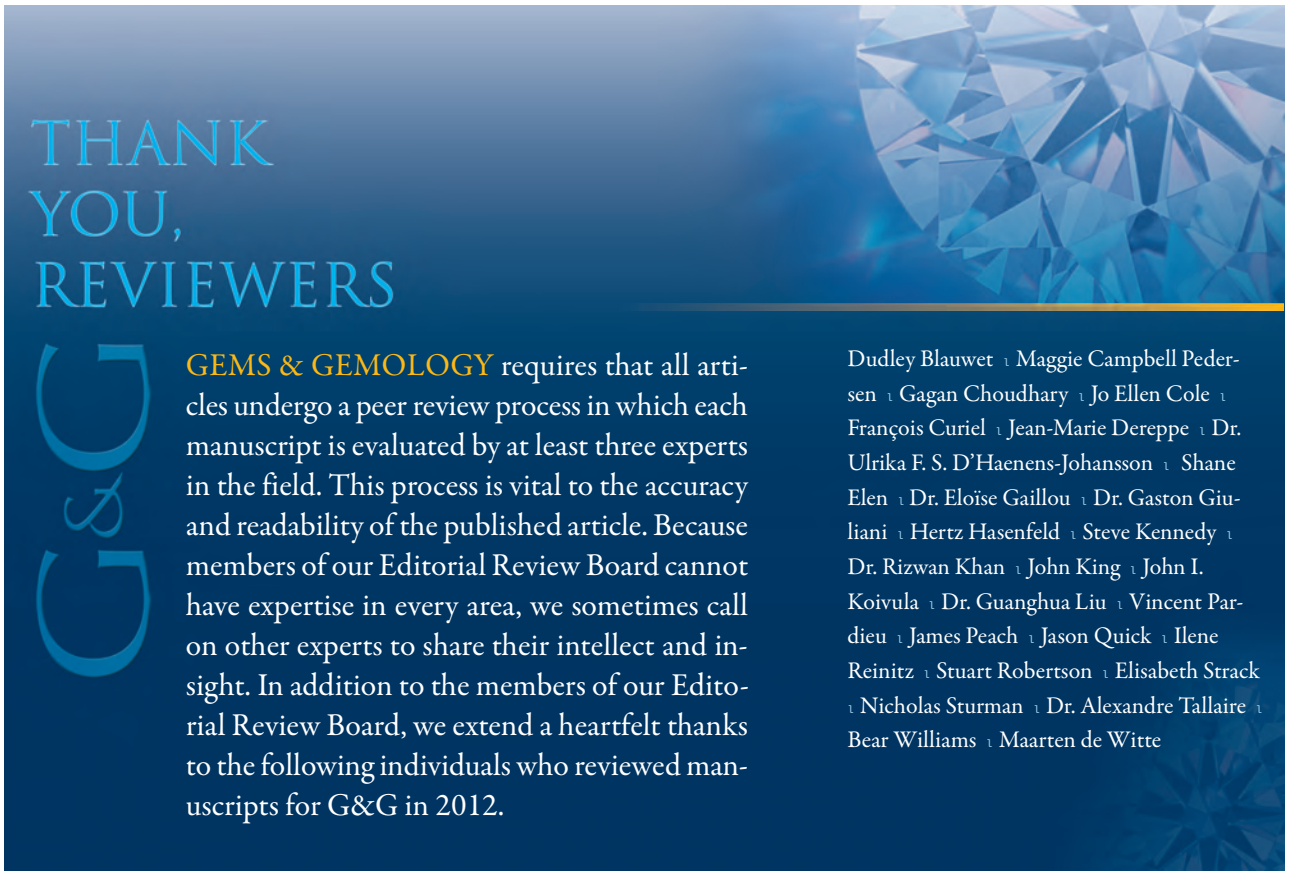

DIAMOND

Artificially Irradiated Brown

The combination of irradiation and annealing is commonly used to enhance a diamond's color appearance. Although green, blue, yellow, and pink are the main colors created through this process, brown hues are occasionally introduced. The New York lab recently tested one diamond with treated brown color whose spectral features were helpful for identification.

This 1.04 ct round brilliant (6.51 × 6.53 × 3.95 mm) was color graded as Fancy Reddish brown (figure 1). The color was distributed evenly throughout the whole stone. It fluoresced weak-moderate yellow to long-wave UV radiation and very weak yellow to short-wave UV. Infrared spectroscopy revealed it was a type Ia diamond with very high concentrations of aggregated nitrogen and a weak hydrogen-related absorption at 3107 cm^{-1}. Also revealed in its infrared absorption spectrum were strong absorptions from optical centers H1a (1450 cm^{-1}) and H1b (4935 cm^{-1}) and a moderate absorption from H1c (5165 cm^{-1}). Weak absorptions at 1355 and 1358 cm^{-1} were also recorded.

UV-Vis-NIR absorption spectroscopy collected at liquid-nitrogen temperature yielded interesting features (figure 2). In addition to very strong absorptions at 503 nm (H3 optical center), 594 nm, and 986 nm (H2), weak absorptions at 526, 534, 551, 578, 681, 724, 774, 805, and 871 nm were observed. Assignment for many of these weak peaks remains unclear. These features are not common in irradiated diamonds with more popular colorations.

The color of this diamond is obviously attributed to artificial irradiation. It is very likely that this diamond was heavily irradiated and then annealed at moderate temperatures. While the color looks natural, its spectral features are very distinct and easily separated from natural features.

Wuyi Wang

Figure 1. This 1.04 ct diamond was color graded as Fancy Reddish brown and identified as artificially irradiated.

Figure 2. In the UV-Vis-NIR region, in addition to very strong absorptions at 503 nm (H3 optical center), 594 nm, and 986 nm (H2), nine weak absorptions were observed. The assignment for many of these weak peaks is not yet clear.

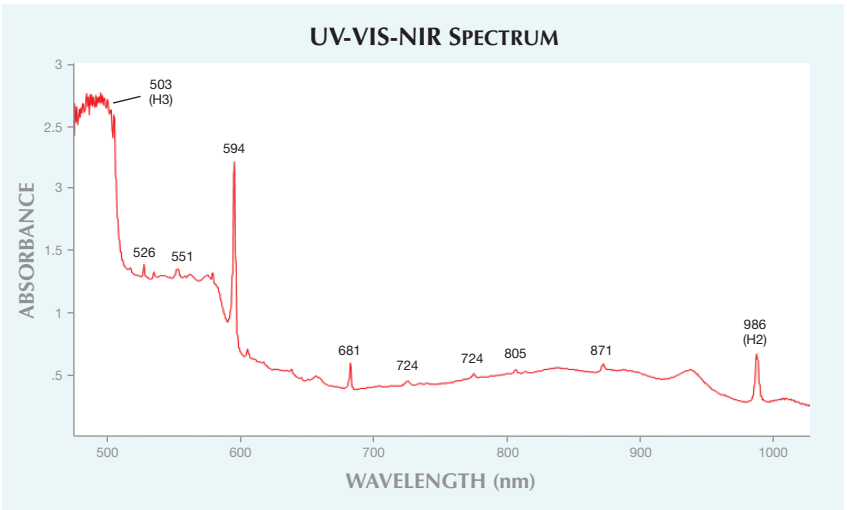

Editors' note: All items were written by staff members of GIA laboratories.

Gems & Gemology, Vol. 48, No. 4, pp. 300–305, http://dx.doi.org/10.5741/GEMS.48.4.300.

Figure 3. This 2.34 ct Fancy yellow diamond contained a rare contact inclusion pair of diopside and pyrope.

Figure 5. A few isolated prismatic, reddish pink pyrope crystals, the largest reaching the surface, were also visible through the pavilion (left, magnified 75×). The DiamondView image showed that the crystal inclusions formed in different growth zonations (right).

Diopside-Pyrope Contact Inclusion Pair

While isolated crystal inclusions are common in natural diamonds, it is rare to see two crystals in contact with one another. The New York laboratory recently examined a 2.34 ct Fancy yellow modified brilliant square (figure 3) that contained a pair of contact inclusions.

The inclusion pair showed red and green colors and a reflective interface in the face-up view (figure 4, left). When viewed through the pavilion, it clearly showed two inclusions: a small, green crystal atop a larger, reddish pink crystal (figure 4, right). Raman analysis identified the green crystal as diopside and the reddish pink inclusion as pyrope. A few isolated prismatic, reddish pink pyrope crystals were also observed (figure 5, left). The DiamondView image revealed that the crystal inclusions formed in different growth zonations with different orientations (figure 5, right). This suggests the inclusions had a syngenetic origin, meaning they formed during the diamond's growth.

The host was a typical cape diamond with natural color. The diopside-pyrope mineral assemblage indicates the diamond formed in a peridotitic geological environment. Syngenetic inclusions, connecting or otherwise, are useful in calculating the equilibrium pressure and temperature (EPT) of diamond formation. Such estimates can be found in the literature. The EPT for individual garnet-clinopyroxene inclusions is estimated at 5 GPa and 1138–1179°C (C.M. Appleyard et al., "A study of eclogitic diamonds and their inclusions from the Finsch kimberlite pipe, South Africa," *Lithos*, Vol. 77, 2004, pp. 317–332). The EPT for contact garnet-clinopyroxene inclusion pairs is estimated at 5 GPa and 1066–1072°C (see D. Phillips et al., "Mineral chemistry and thermobarometry of inclusions from De Beers pool diamonds, Kimberley, South Africa," *Lithos*, Vol. 77, 2004, pp. 155–179).

Still, the interpretation of these inclusions should be considered preliminary, since the EPT of solitary inclusions is subject to a changing geological environment during the prolonged growth period. Previous studies have also found that adjoining inclusions may represent the EPT of post-growth events, such as subsequent cooling of the earth's mantle or a temperature increase caused by kimberlite transportation, due to re-equilibration. Therefore, the diopside and pyrope inclusions in this sample may not represent the EPT at the time of diamond formation, though the aforementioned values fall within the diamond stability field.

Kyaw Soe Moe and Jason Darley

Figure 4. Red and green colors and a reflective interface were observed in the face-up view of the crystal inclusion (left, magnified 75×). Viewing the diamond through the pavilion revealed a small green crystal atop a larger reddish pink crystal (right, magnified 100×). The green crystal was identified as diopside and the reddish pink inclusion as pyrope.

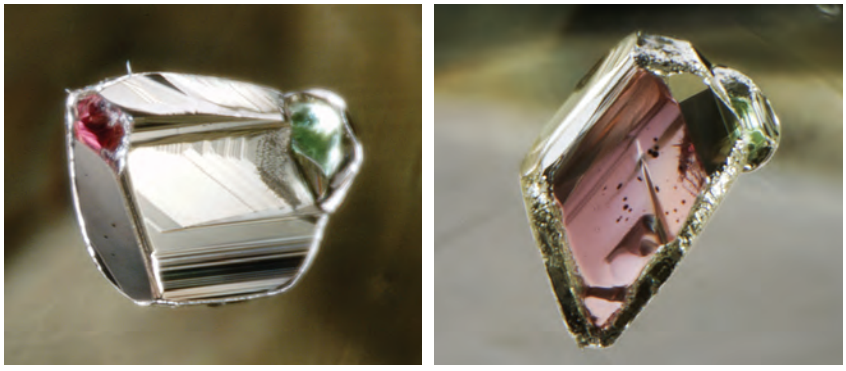

Figure 6. This 15.01 ct cushion-cut diamond (15.39 × 12.84 × 8.32 mm) was color graded as Fancy Intense yellow. Its color was found to have been treated from the original Fancy Light yellow.

Treated Yellow with Unusual Spectroscopic Features

It is well known that some "off"-color diamonds can be irradiated by a high-energy electron or neutron beam and then annealed at moderate temperatures to introduce fancy yellow, orange, or even "champagne" colors by adding optical centers H3 and H4. This treatment was recognized as early as the 1950s (G. R. Crowningshield, "Spectroscopic recognition of yellow bombarded diamonds and bibliography of diamond treatment," Winter 1957-58 G&G, pp. 99–104). Along with gemological features such as color distribution, the occurrence of irradiation-related optical centers such as 595 nm absorption in the visible-light region and H1b and/or H1c in the infrared region is a very important indication of irradiation and annealing. Recently, we encountered a diamond with a treated yellow color that lacked these identifying features. Crowningshield mentioned this type of treated yellow diamond, mainly in larger sizes.

This 15.01 ct cushion-cut diamond (15.39 × 12.84 × 8.32 mm) was color graded as Fancy Intense yellow (figure 6). Color was evenly distributed throughout the stone. It had a small black inclusion close to the edge in the table face. These measurements and internal features matched very well with a previously examined diamond in our database. Surprisingly, the earlier match was color graded as Fancy Light yellow. The significant difference in color appearance suggested that the diamond had been artificially treated after the initial examination.

Infrared absorption spectroscopy showed virtually identical features in both cases, such as very high concentrations of aggregated nitrogen and a very weak hydrogen-related absorption peak. In addition, weak absorptions at 1522 and 1546 cm^{-1} matched very well. Neither showed any irradiation- or treatment-related absorption features such as H1a, H1b, or H1c. The Fancy Light yellow diamond's absorption spectra at liquid-nitrogen temperature simply showed a "cape" line with absorption peaks at 478 and 415 nm (N3) only. In contrast, absorptions of optical centers H3 (503 nm) and H4 (496 nm) with moderate concentrations were observed in the Fancy Intense yellow diamond (figure 7). No GR1 (741 nm) or 595 nm centers were observed in either instance. The occurrence of H3 and H4 was obviously responsible for the color change and must have been introduced after the initial examination.

Separating artificially irradiated from naturally irradiated diamonds is often a challenge. Improvements in this treatment technology, leaving no detectable 595 nm absorption in the visible region or H1b/H1c in the near-infrared region, could make the identification even more difficult.

Wuyi Wang

Figure 7. Absorption spectra collected at liquid-nitrogen temperature revealed that H3 and H4 centers were introduced in the Fancy Intense yellow diamond. No 595 nm center was detected, however.

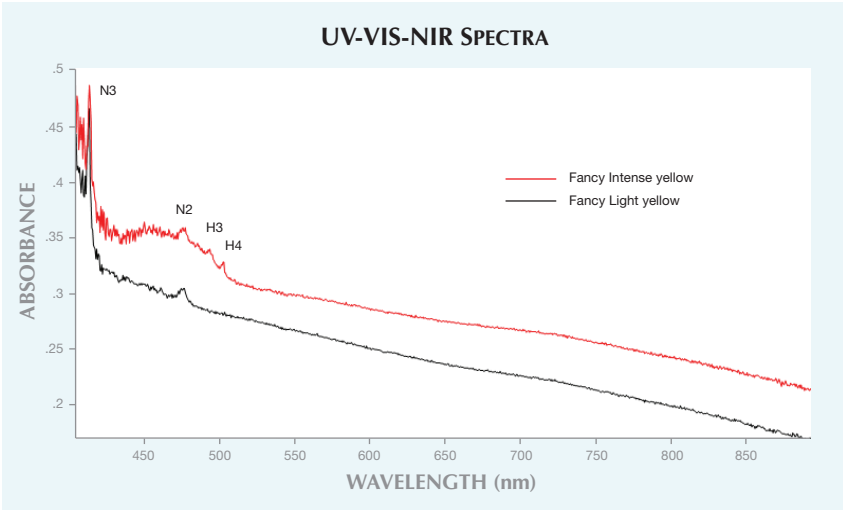

Unusual Omphacite and Pyrope-Almandine Garnet Inclusion

Recently examined in the Carlsbad laboratory was a 2.03 ct Fancy yellow-green diamond containing an inclusion of omphacite, a grayish blue pyroxene, in contact with an orange garnet inclusion of the pyrope-almandine species (figure 8). Both were identified by optical and visual observations.

Although omphacite and garnet sometimes occur as solitary crystals in diamonds that form in an eclogitic environment, the color contrast between these two inclusions in contact offers a more striking scene. Other bimineralic inclusions in diamond have been previously reported, such as chromium pyrope and pyroxene (e.g., E.J. Gübelin and J.I. Koivula, *Photoatlas of Inclusions in Gemstones*, ABC Edition, Zurich, 1986, p. 95), but this

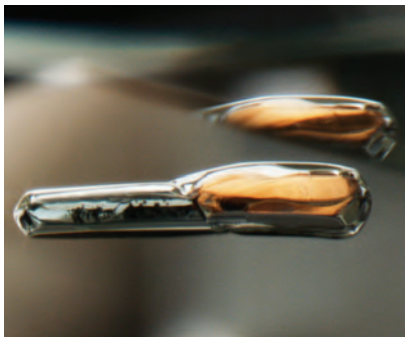

Figure 8. Contact inclusions of grayish blue omphacite and orange pyrope-almandine garnet confirmed the eclogitic origin of this 2.03 ct Fancy yellow-green diamond. Also observed was graphite along the interface between the inclusions and diamond host. Image width: 1.22 mm.

is the first example of an omphacite and pyrope-almandine contact inclusion seen in the Carlsbad laboratory. We also observed graphitization between the contact inclusion and the diamond host, and around one other solitary omphacite crystal.

Examined under polarized light, the diamond showed low-order dark gray strain around both the bi-mineralic inclusion and the solitary omphacite crystal with the graphitized interface, as in figure 9. However, other solitary omphacite inclusions in the diamond that did not show graphitization displayed high-order colored strain halos. While we do not know the exact cause of the high- and low-order strain variation, it could be related to graphitization, since the inclusions with graphite along their interface seemed to show less strain.

Figure 9. Examined in polarized light, the area around the omphacite/pyrope-almandine contact inclusion displayed low-order strain. Image width: 1.22 mm.

Figure 10. In this 9.96 × 9.56 × 7.32 mm polymer-beryl assemblage (left), an inclusion-free region with increasing thickness from the girdle to the culet was easily visible under darkfield illumination at 20× magnification (right).

This contact inclusion is a noteworthy example of how microscopic observations can provide clues to geologic origin while also raising unanswered questions, such as the potential relationship between graphitization and the degree of strain.

Troy Ardon and Tara Allen

Polymer-BERYL Assemblage

Recently, two transparent green octagonal step-cut samples (see figure 10, left) were submitted to the New York laboratory for emerald origin reports. Initial gemological testing revealed some characteristics typical of natural, clarity-enhanced emeralds with a fracture-filling polymer. The refractive indices measured 1.570–1.578 and 1.572–1.580 on the table facets, and infrared spectra collected through both girdles showed features typical of natural beryl, as well as polymer-related features in the 3100–2800 cm^{-1} region. Microscopic examination revealed jagged and irregular two-phase inclusions through the table and crown.

Still, some unusual features raised suspicion about the nature of the treatment. The samples had a hydrostatic SG of 2.43 and 2.37, unusually low for emerald (which usually measures around 2.7). No chromium-related lines were observed with the handheld spectroscope. Furthermore, both displayed strong, even whitish blue fluorescence under long-wave UV light, with a similar but weaker reaction under short-wave UV. The fluorescence appeared to originate in the pavilion and reflect through the stone.

Closer microscopic examination revealed that the natural two-phase inclusions were present only in the crown and in a confined, domed region extending into the pavilion (figure 10, right). The pavilion showed no inclusions within several millimeters of the surface, which was heavily scratched and yielded easily to a pointer probe. The unknown layer on the pavilion tapered toward the girdle, where a boundary between the pavilion and crown material was visible (figure 11). Under immersion in isopropyl alcohol, the beryl portion ap-

Figure 11. The polymer base thinned from the culet to the girdle, where a border separated it from the natural beryl top. Reflected light; magnified 50×.

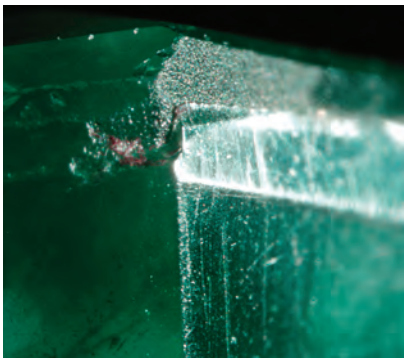

peared to have little or no green color, while the outer layer on the pavilion showed distinct green coloration. We determined that the beryl portion lacked sufficient color to be considered emerald.

To confirm the identity of the top and the base, we turned to Raman spectroscopy. Raman spectra taken from the table facets of each stone were consistent with beryl, while spectra from the pavilion corresponded with the polymer (figure 12). Notably, none of the spectral features from the table and pavilion overlapped, clearly demonstrating that the top and base were composed of different materials. We concluded that these specimens consisted of a natural beryl top and "core," with a thick, faceted polymer layer on the pavilion. Because a large portion of each sample was composed of polymer, we considered this case analogous to the case of heavily treated, lead glass–filled rubies, which receive a conclusion of "manufactured product". Identification reports with this conclusion were issued for the two green assemblages, with an additional description of them as a "manufactured product consisting of colored polymer and beryl."

Emily V. Dubinsky and Donna Beaton

Figure 12. Raman spectra collected from the table facet of both samples were consistent with beryl, whereas spectra from the pavilion facets were consistent with a polymer. Raman spectroscopy was performed with 514 nm excitation laser. The spectrum of the pavilion is offset 10,000 counts for clarity.

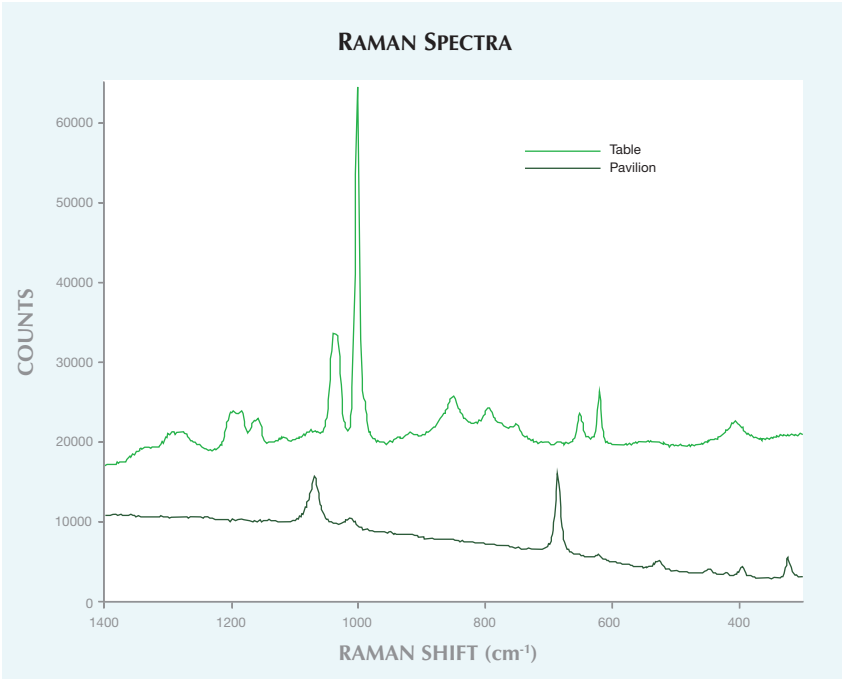

Bicolored SPINEL

The Bangkok laboratory occasionally sees bicolored stones submitted for identification, but a blue and red sample weighing 14.60 ct and measuring 22.06 × 12.39 × 6.29 mm (figure 13) recently caught our attention. Standard gemological testing gave an RI of 1.718 and a hydrostatic SG of 3.60, confirming the stone was a spinel. The red portion fluoresced a medium red in long-wave ultraviolet light and was inert in short-wave UV, whereas the blue region was inert in both long- and short-wave. Microscopic examination of the inclusions revealed small octahedral crystals and growth tubes. Investigation of the photoluminescence using Raman spectroscopy at liquid-nitrogen temperature indicated that the stone had not been heated to alter its color.

Figure 13. This 14.60 ct gem was identified as a bicolored spinel. Its blue and red zones were caused by the presence of iron and chromium, respectively.

Because of the unusual color zoning, we took advantage of the opportunity to collect the UV-visible spectrum on both the blue and red areas of the stone. As expected, the blue area exhibited a prominent feature at 458 nm and a broad absorption in the 550–680 nm region, caused by the presence of iron. The red area had strong absorption bands at 387 and 540 nm, indicating chromium.

While spinels are routinely submitted to the Bangkok laboratory for identification, a search of our databases found this was the first bicolored spinel.

Garry DuToit

SYNTHETIC DIAMOND

Silicon-Vacancy Defect in HPHT-Grown Type IIb Synthetic

The $[Si\text{-}V]^-$ optical center, which has zero-phonon lines at 736.6 and 736.9 nm and is active in absorption and luminescence, is common in CVD synthetic diamonds. Very few natural

Figure 14. The [Si-V]⁻ center was confirmed in these two HPHT-grown type IIb synthetic diamonds. The 0.51 ct round brilliant on the left was color graded as Fancy Light blue, and the 0.79 ct sample on the right had Fancy Deep blue color.

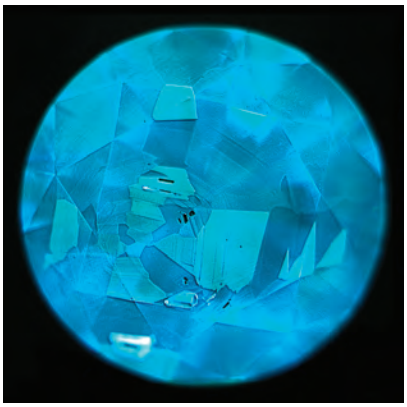

Figure 15. The fluorescence image of the 0.79 ct sample showed the typical growth pattern of an HPHT synthetic diamond. Strong blue phosphorescence was also observed.

diamonds contain this defect, and it has long been considered an important identification feature of CVD synthetic diamonds. The New York lab recently tested two type IIb HPHT synthetic diamonds that showed moderately intense emission of this defect.

One was a 0.51 ct round brilliant (5.19 × 51.6 × 3.07 mm), color graded as Fancy Light blue. The other was a 0.79 ct round brilliant (5.99 × 6.05 × 3.54 mm) with Fancy Deep blue color (figure 14). Absorption spectra in the mid-infrared region showed moderate boron-related absorption in the Fancy Light blue synthetic and very strong boron-related absorption in the Fancy Deep blue sample. Fluorescence images recorded with the DiamondView showed both octahedral and cubic growth sectors, typical patterns for HPHT synthetics (figure 15). Strong blue phosphorescence was also observed. But the most notable feature found in these two synthetic diamonds was the [Si-V]⁻ defect. Weak but distinct emissions at 736.6 and 736.9 nm were recorded in both with 633 nm laser excitation at liquid-nitrogen temperature (figure 16).

The [Si-V]⁻ defect reported earlier in an HPHT-grown synthetic diamond (also type IIb; see Winter 2010 Lab Notes, p. 302) was believed to be a very unusual feature. The discovery of two additional occurrences suggests that this defect may be more common in HPHT synthetic diamonds than previously expected. It is not fully understood why the feature has not been observed in type IIa HPHT synthetics. Because this optical center is a common feature of CVD synthetic diamonds, documenting it in HPHT-grown synthetics underscores the importance of testing with multiple technologies.

Wuyi Wang and Kyaw Soe Moe

Figure 16. Weak but distinct emissions at 736.6 and 736.9 nm were recorded in both HPHT synthetics with 633 nm laser excitation at liquid-nitrogen temperature. These emissions are attributed to the [Si-V]⁻ center, which is common in CVD synthetic diamonds.

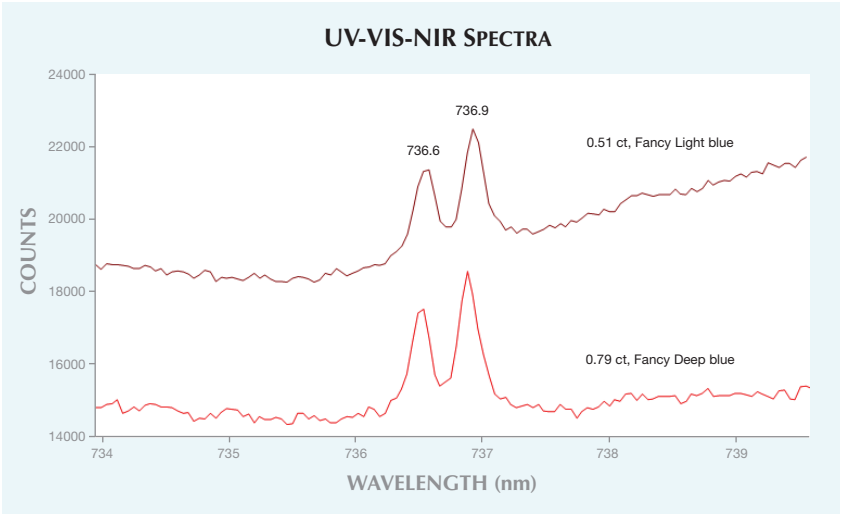

PHOTO CREDITS:
Josh Balduf—1; Sood Oil (Judy) Chia—3; Kyaw Soe Moe—4, 5, 15; Jian Xin (Jae) Liao—6, 14; Nathan Renfro—8, 9; Emily Dubinsky—10, 11; Nuttapol Kitdee—13.

G&G
Gem News International

Contributing Editors
Emmanuel Fritsch, *CNRS, Team 6502, Institut des Matériaux Jean Rouxel (IMN), University of Nantes, France* (fritsch@cnrs-imn.fr)
Michael S. Krzemnicki, *Swiss Gemmological Institute SSEF, Basel, Switzerland* (gemlab@ssef.ch)
Franck Notari, *GGTL GemLab–GemTechLab, Geneva, Switzerland* (franck.notari@gemtechlab.ch)
Kenneth Scarratt, *GIA, Bangkok, Thailand* (ken.scarratt@gia.edu)

COLORED STONES AND ORGANIC MATERIALS

Naturally healed fractures in Ethiopian opal. During the examination of opals from Shewa, Ethiopia, we encountered several samples showing fractures filled with a translucent material that appeared to be different from the opal. The fractures were about 50 µm wide and distributed over the whole stone. The stones looked as if they had been broken and then glued back together (figure 1). We investigated these samples to verify if this fracture filling was a natural phenomenon or the result of a treatment.

During polishing, we noted that the filling substance was harder than opal (figure 2). With magnification, we observed minute black, opaque octahedral inclusions in both the filling substance and the host opal (again, see figure 2). This suggested that both were opal. We measured the Raman spectrum of the host opal and the filling substance using a Bruker FT Raman equipped with a Nd:YAG laser emitting at 266 nm quadrupled to 1064 nm and coupled to an optical microscope, allowing the measurement of volumes smaller than 100 µm^3. We measured each material several times and obtained Raman spectra with nearly identical features in both zones. a major broad at about 320 cm^{-1}, weaker peaks at 780 and 1057 cm^{-1}, and a broad, intense band centered at about 2900 cm^{-1}. These spectral features are typical for opal. We observed no additional peak in the fracture's spectrum. The difference in visual appearance and hardness between the host and the filler opal may be explained by their different porosity and water contents, for example.

Figure 1. This 29.68 ct play-of-color opal from Shewa, Ethiopia, shows thin fractures filled with a colorless substance. Photo by B. Rondeau.

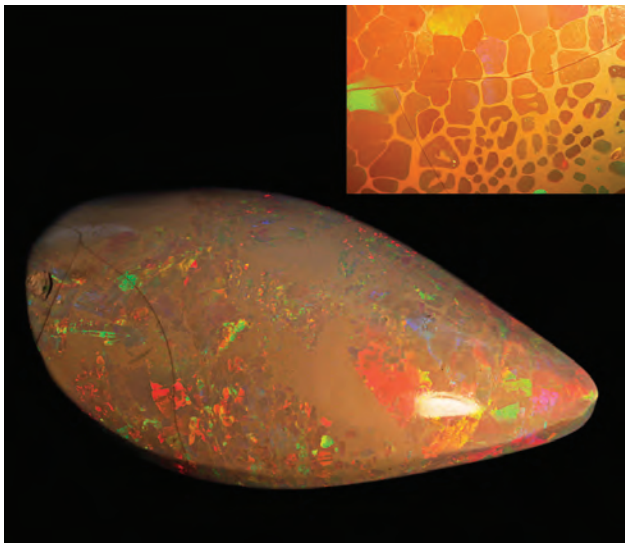

Figure 2. Reflected light on the surface shows that the filling substance is slightly harder than the host opal. The shiny dots are opaque inclusions observed in both the host opal and the filling substance. Photo by Jean-Pierre Gauthier.

Editor's note: Interested contributors should send information and illustrations to Justin Hunter at justin.hunter@gia.edu or GIA, The Robert Mouawad Campus, 5345 Armada Drive, Carlsbad, CA 92008.

Gems & Gemology, Vol. 48, No. 4, pp. 306–311,
http://dx.doi.org/10.5741/GEMS.48.4.306.

Figure 3. Black common opal from Brittany, France, also shows fractures that developed after the opal formation. They were naturally healed by gray common opal. Photo by B. Rondeau; image width 6 cm.

From these observations, we deduce that the filling of these fractures is a natural phenomenon: The fractures first developed in a well-formed opal, and then a second stage of opal precipitation naturally healed them. From our experience, the fracturing does not hinder the toughness of these opals.

We have encountered such a fracture filling in other opals, such as black common opal (without play-of-color) from Brittany, France. In this case, a network of fractures developed and was naturally healed by a later stage of gray common opal (figure 3). The resulting opal is homogeneous, as shown by the regular propagation of the conchoidal fracture that developed when the stone was extracted.

Gemological labs should note that correct identification requires careful examination to differentiate between naturally healed opals, as described here, and opals with fractures filled with an artificial substance. To our knowledge, this last case has not been documented in the gemological literature, though it is possible in theory.

Benjamin Rondeau
Laboratoire de Planétologie et Géodynamique
CNRS, Team 6112, University of Nantes, France
Jean-Pierre Gauthier
Centre de Recherches Gemmologiques, Nantes, France
Emmanuel Fritsch

New supplier of Montana sapphires. In March 2012, Lisa Brooks-Pike and Margo Bedman formed Sapphires of Montana, a new wholesale and retail outlet for heat-only sapphires originating from the United States. The company's focus is calibrated stones ranging from 2 to 6 mm, with the majority in the 4–4.5 mm range. Stones larger than 6 mm are occasionally offered. Colors available are primarily blue and greenish blue, as well as limited quantities of yellow, orange, and pink stones (figure 4).

Brooks-Pike and Bedman initially acquired about 65 kg of rough from existing stock mined at the Rock Creek deposit in Montana. The rough was then heat treated by Crystal Chemistry (Brush Prairie, Washington) without the addition of color-modifying chemicals (see J. L. Emmett and T. R. Douthit, "Heat treating the sapphires of Rock Creek, Montana," Winter 1993 *G&G*, pp. 250–272). Pike and Bedman have also collaborated with Colombia Gem House (Portland, Oregon) to oversee cutting operations, with the emphasis on optical performance rather than yield. This carefully controlled production is capable of manufacturing high-quality, well-matched suites of sapphire suitable for a number of jewelry designs.

While Montana sapphires have been available for some time, new sources of quality material are always a welcome addition to the trade.

Nathan Renfro
GIA, Carlsbad

Figure 4. Sapphires of Montana offers heat-only material in a variety of colors. The faceted stones pictured here range from 3 to 7 mm in diameter. Courtesy of Sapphires of Montana; photo by Sherman Pike.

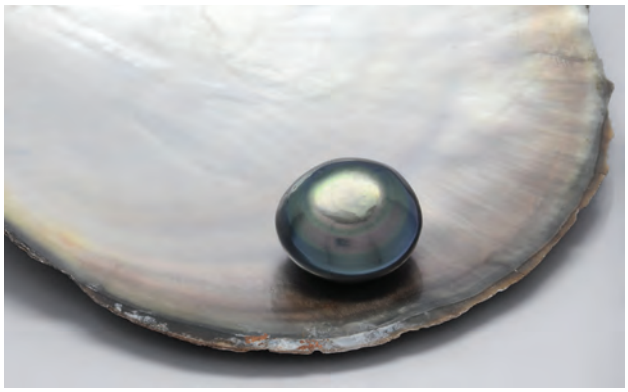

Figure 5. This was one of the large Tahitian black cultured pearls with a baroque-shaped nucleus. Photo by O. Segura.

Figure 6. The cultured pearl shown in figure 5 was cut in half, revealing a white, baroque-shaped nucleus. Photo by O. Segura.

***Pinctada margaritifera* cultured pearl with baroque-shaped nucleus.** The French Gemological Laboratory (Laboratoire Français de Gemmologie, or LFG) recently analyzed 110 Tahitian black cultured pearls presented as keshi (cultured pearls without a nucleus). They were large, up to 25.5 mm in the longest dimension, and slightly baroque, with a very good nacre quality (figure 5). Overtones ranged from green ("peacock") to purple ("aubergine").

Their UV-Vis-NIR spectrometry features were consistent with cultured pearls from *Pinctada margaritifera*, particularly the presence of the 700 nm band (S. Karampelas, "UV-Vis-NIR reflectance spectroscopy of natural-color saltwater cultured pearls from *Pinctada margaritifera*," Spring 2011 *G&G*, pp. 31–35). But microradiography did not reveal the expected structures of keshi (N. Sturman, "The microradiographic structures of non-bead cultured pearls," August 20, 2009, http://www.giathai.net/lab.php). A strong, easily visible delineation ran roughly parallel to the external shape, 0.8–2.8 mm below the surface. That line was similar to the structure encountered in cultured pearls at the boundary between nacre and nucleus, but here it had a "baroque" shape. The shape of the cultured pearl generally followed the shape of the nucleus. In many cases there were one or more cavities related to this structure. In several instances, this delineation opened into cavities, with a very similar appearance to that seen in keshis. X-ray opacity, which appeared as shades of gray in radiography, was very similar between the nucleus and the periphery, which is usually the case for cultured pearls.

We obtained permission to cut one of the submitted pieces in half to directly observe the type of core used for nucleation (figure 6). The material forming the nucleus is similar to that normally seen in cultured pearls, but the shape was different. Raman analysis indicated that the nucleus was indeed composed of calcium carbonate (aragonite). The yellow X-ray luminescence and the Sr/Mn ratio determined by EDXRF chemical analysis (Rigaku NexCG) confirmed that it was produced by a freshwater mollusk, not *Pinctada margaritifera*. When one of the two halves was cut again, the core and black nacre separated immediately, revealing another human intervention: a polished surface on the nucleus.

This appears to be a new type of core carved from a piece of shell from a freshwater mussel (e.g., *Megalonaias sp.*, *Fusconaia sp.*, or *Quadrula sp.*) conventionally used to create spherical nuclei but here carved with a baroque shape. The quality of the nacre used for the baroque nuclei seems lower than that used for spherical beads, however. Indeed, this lower quality induces many structures such as cracks, fissures, and areas of variable X-ray opacity that are visible in radiographs. These structures may lead one to believe that this is not a nucleus, as it looks more natural (figure 7).

Cultured pearls with spherical pieces of shell as nuclei have been long known, and nucleation with freshwater cultured pearls has appeared more recently. But this new baroque variety of nucleus may be difficult to properly identify using X-radiography because the features produced sometimes resemble those observed in keshis or baroque-shaped natural pearls.

Olivier Segura (o.segura@bjop.fr)
Laboratoire Français de Gemmologie (LFG), Paris
Emmanuel Fritsch

Figure 7. The sawed parts of the specimen are shown next to a classic round nucleus (far right). Both nuclei are similar except for their shape. Photo by O. Segura.

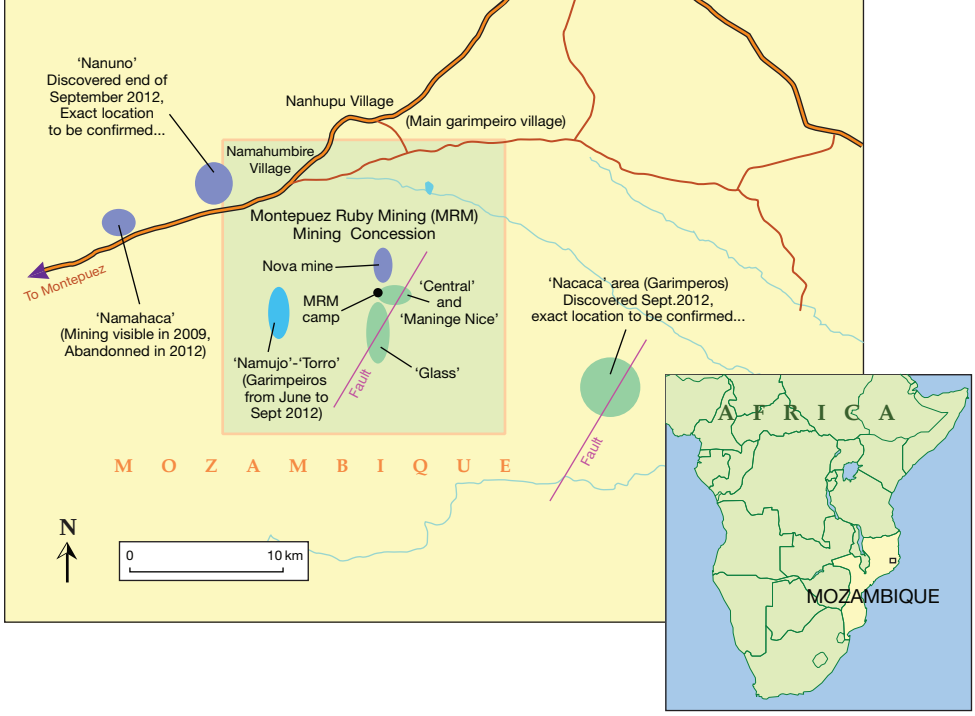

Figure 8. This map shows the different ruby mining areas around Montepuez, as of September 2012.

Update on ruby mining and trading in northern Mozambique. A few months after the gem rush in Winza, Tanzania, that brought many Thai and Sri Lankan ruby buyers to East Africa, two new ruby deposits were discovered in northern Mozambique in the Niassa and Cabo Delgado provinces (see Winter 2009 GNI, pp. 302–303).

In Niassa, the deposit was worked illegally by *garimpeiros* (the name used in Mozambique, a Portuguese-speaking country, for illegal miners) until the summer of 2009, when it was closed by law enforcement. But according to Niassa officials contacted in 2012, the *garimpeiros* have returned every year during the rainy season, when the area is too muddy for vehicles.

Near Montepuez, in the Cabo Delgado province, law enforcement was not as successful, and *garimpeiros* have been mining illegally the new deposit since its discovery in May 2009 (again, see Winter 2009 GNI). It is believed that they have mined most if not all of the stones currently in the market from that new deposit.

The new deposit is located on a private hunting reserve belonging to Mwiriti Ltd., a Mozambican company owned by a retired general. A few weeks after the discovery, the company was granted several mining licenses for an area that is approximately 20 km by 20 km. Mwiriti initially signed an agreement with a Thai company to mine the site.

More details on M'sawize, Montepuez rubies, and the GIA expedition in 2009 can be found on GIA's website at www.giathai.net/Mozambique_Ruby_Special_Issue.php.

The partnership did not last long, and in 2011 Mwiriti signed on with Gemfields, a British company involved in Zambian emerald and amethyst mining. The new company was called Montepuez Ruby Mining, or MRM. Like the previous partnership, MRM has had difficulty controlling the wide area. Since its discovery in 2009, the deposit has been worked by thousands of *garimpeiros* who have sold their stones to buyers from Africa, Thailand, and Sri Lanka. In 2010, Mozambique became the main source of rubies in the Bangkok and Chanthaburi markets. Since the site was not officially in production, the stones presumably were mined by *garimpeiros*.

During a visit to northern Mozambique in September 2012, we continued the work started by contributor VP during his previous three expeditions in 2009. After visiting the MRM ruby mine September 9–12, we stayed to visit the areas currently being mined by the *garimpeiros*.

Between March and June 2012, after the rainy season, MRM had been building infrastructure and securing the area. MRM security personnel said they spent a month trying to peacefully expel the *garimpeiros* from four areas inside the concession: "Central," "Maninge Nice" (meaning "very nice" in local languages and referring to the quality of the rubies), "Nova Mina," and "Glass" (because of the rubies' clarity). After a three-month battle, MRM finally regained control of the areas, apparently because the *garimpeiros* heard that good rubies could be found near Namujo village at a place called "Torro."

While MRM was securing the core of its concession, including Maninge Nice and Glass, the *garimpeiros* were busy at Namujo/Torro, which is also inside the concession (figure 8). According to an MRM manager and some independent miners we met, over 4,000 of them were at Namujo/Torro on a 5 km area along a stream. MRM first tried to persuade them to leave, with little success—in fact, the *garimpeiros* at Namujo/Torro threw stones at their cars. The situation was tense, but compared to the three-month guerilla-like conflict for control of the MRM core area, it represented a de facto cease-fire.

Between March and September 2012, MRM built a fortified camp near Maninge Nice and prepared for the arrival of a large washing plant, reportedly on its way by boat. Near Namahumbire village, a large camp is also being constructed to accommodate hundreds of employees. All over the middle of the concession, including Maninge Nice and Glass, there are prospecting pits, security posts, roads, and boreholes.

Figure 9. Rubies were found in situ with amphibole (dark green), mica (yellowish), and feldspar (white) on the wall of the test pit. Note the white feldspar rim surrounding most of the rubies. Photo by Vincent Pardieu.

Garimpeiros informed us that a few days earlier, there was a rumor in Namahumbire of fine rubies found by gold miners working on a stream at Nacaca, a new area in the southeast of the MRM concession. We also learned that the area near Namahaca village (about 5 km west of Namahumbire, outside the concession), where contributor VP found some ruby diggings and low-quality samples in December 2009, is now nearly abandoned, as the stones there were inferior.

At MRM, the authors were able to collect samples for the GIA reference collection from all the areas except Namujo/Torro. It soon became clear that visiting Namujo/Torro with MRM would not be possible due to their fierce struggle with the *garimpeiros* for control of Central, Maninge Nice, and Glass.

Contributor VP had in fact already visited Maninge Nice in December 2009 with the support of Mwiriti Ltd. This gave us an opportunity to complete the field study started in 2009. An extensive report with our recent findings, including a study of the samples collected, will be published in *Gems & Gemology* and on GIA's website. What we can confirm is that rubies around Maninge Nice and Central are found within two types of deposits: (1) an alluvial ruby-rich soil corresponding to the weathering of the *in situ* ruby deposit, and (2) a primary deposit where rubies are found in veins associated with amphibole, feldspar, and mica (figure 9).

Samples collected from Maninge Nice and Central ranged from pink to deep red and up to about 20 ct. Most were very included and fractured, but a few small clean, beautiful gems were also collected. The deposit seems incredibly rich: After carefully mining and documenting less than one cubic meter of ruby-rich rock, we were able to collect more than 20 grams of rubies. By comparison, the authors could not find any rubies in matrix in the Glass and Nova Mina areas, where the *garimpeiros* were mining a secondary deposit along a stream.

After leaving the MRM mine, we started negotiating with *garimpeiros* and village elders to find a way to visit Namujo/Torro. Nearly a week later, while discussions were still in progress, our hopes of witnessing the *garimpeiros* vanished. That day, the police launched a major security operation with the support of special forces from Maputo, the capital of Mozambique. Within a day, the government forces expelled thousands from Namujo/Torro. One Tanzanian miner died after falling into a pit. On our way back to Montepuez, we saw hundreds walking along the road toward Montepuez, having escaped from Namujo/Torro.

Following the security operation, our local *garimpeiro* contacts were on the run, waiting for the situation to ease. The more adventurous attempted to collect their belongings left behind in haste. During the nights, after the operation, there were reportedly problems in the nearby village of Namahumbire, where *garimpeiros* damaged a school building and the house of a local government official. But overall the situation quieted within about three days.

Upon meeting with *garimpeiros* again on September 22, we learned that many of them were moving to Nacaca (again, see figure 8), the new ruby mining area about 35 km south of Mesa village and about 10 km southeast of the MRM concession. That was confirmed by other sources.

On September 24, we finally spent a full day at Namujo/Torro, where we confirmed that it is indeed a secondary deposit. The *garimpeiro* workings covered an area approximately one kilometer wide and two kilometers long. Judging from the area and the number of pits, it is likely that more than 4,000 people had been working there. Throughout the day, while a bulldozer refilled thousands of pits, we witnessed the cat-and-mouse game between the police and the *garimpeiros* returning to collect the gravels left behind (figure 10). Finally, after washing some of these gravels, we could see what all the excitement was about: small rubies of very fine color and high quality, rounded in form, as expected from secondary deposits (figure 11). Looking at the stones that day, we understood why some in Bangkok have claimed that the quality of Mozambique rubies is improving.

It is still too early to know if MRM can bring its mining concession under control. The key might be Nacaca: If good stones are found, it will likely draw *garimpeiros* there, and MRM will have an easier time securing its concession.

The success of any gem mining operation depends on three factors: (1) understanding the geology, to know where the stones are located; (2) understanding the mining technology, to find the most cost-efficient way to mine the deposit; and (3) management and security. The ruby deposit near Montepuez seems very rich and technically easy to mine. The most pressing issue facing MRM is security—many gem

Figure 10. Garimpeiros *collect ruby-rich gravels in Namujo/Torro a few days after the security operation. Photo by Vincent Pardieu.*

mining operations would love to have this as their problem.

Looking ahead, the Montepuez area seems very likely to remain the world's main ruby producer. The question that many ponder—particularly in Thailand, the main market for these rubies—is how and where MRM will commercialize its production. Currently, Gemfields seems to favor the auction system they already have in Singapore for their Zambian emerald production. According to MRM and Gemfields officials, the first auction including rubies from Montepuez is expected to take place in 2013.

Vincent Pardieu
GIA, Bangkok

Boris Chauvire
Nantes, France

Figure 11. These small rubies, weighing up to 3 ct, were the result of washing a few bags of ruby-rich gravels left behind by the garimpeiros*. The stones show a very fine color, good clarity, and the weathering typical of rubies from secondary deposits. Photo by Vincent Pardieu.*

CONFERENCE REPORT

2012 NAG Institute of Registered Valuers Conference. The National Association of Goldsmiths 24th annual Institute of Registered Valuers Conference took place September 22–24 at Loughborough University in Leicestershire, UK. A record 198 delegates attended the various presentations and hands-on workshop sessions. This year the Institute marked its 25th anniversary, and silver was the theme of the event.

The history of silver penny and the use of silver coins were reviewed by former Senior Master of the Supreme Court and Queen's Remembrancer **Robert Turner**. Besides discussing his judicial functions at the Royal Courts of Justice, Prof. Turner explained some of the diverse duties of the Queen's Remembrancer, such as presiding over the ancient Pyx Trial, which ensures that newly minted coins conform to required standards. **David Evans** (a former assay master of the London Assay Office) explained how hallmarking began in the UK and focused mainly on silver.

Grant Macdonald (Grant Macdonald Silversmiths, London) described how he expanded his business into different markets. He also illustrated many of his silver masterpieces and explained the use of technology in silver craftsmanship. **Alastair Dickenson** (Alastair Dickenson Ltd., London) described the challenges of buying silverware from the Internet and what to consider when buying from eBay. He provided guidelines on how to assess the item, showing some of the silverware live on the website and reviewing the descriptions.

Eric Knowles described his journey to become an antiquarian and how he got into this business working as an expert in ceramics and porcelains. **Stephen Kennedy** (The Gem and Peal Laboratory Ltd., London) reviewed the use of technology in his lab and provided tips on how to identify treatments in corundum. He also explained the common treatments he is seeing in the market and the challenges to detecting some of them.

Mehdi Saadian (msaadian@gia.edu)
GIA, London

Symphony of Jewels: Anna Hu Opus 1

By Janet Zapata, Carol Woolton, and David Warren, 167 pp., illus., publ. by Vendome Press, New York, 2012. US$75.00

Anna Hu is a rising star in the world of jewelry. Her firm, Anna Hu Haute Joallierie, has boutiques in New York and Shanghai. Her Shanghai store is located next to mega-jewelers Graff and Harry Winston, and an exhibition of her work was recently held at the renowned Musee des Arts Decoratifs in Paris.

This luxurious hardcover book celebrates "Opus 1," as Hu calls the collection of her first 100—a feat the designer intends to repeat every five years until she has completed ten opuses. Hu's foreword details the Gnossienne brooch/necklace, a beautiful crane motif that marked the beginning of her symphony of jewels, embodies who she is: a Taiwanese artist trained in Western craftsmanship, and a musician with a deep understanding of the melodic harmony of gems. From Hu's single-minded dedication to becoming a virtuoso cellist, playing with masters such as Yo-Yo Ma at age thirteen, to her years spent studying under renowned jewelry designer Maurice Galli at Harry Winston, the reader is given insight into her passion. The section by jewelry historian Janet Zapata summarizes Hu's studies, which include the Walnut School for the Arts in Boston, Parsons School of Design, Columbia University, the Fashion Institute of Technology, and GIA. Apprenticing at Christie's and Van Cleef & Arpels added to her knowledge of the gem and art worlds. Zapata relates how Hu evolved as a designer of traditional jewelry design to forge her own elaborate and poetic style.

Carol Woolton, jewelry editor of British *Vogue*, describes how Hu's designs fit in the modern fashion world and follow the path of many great couturier designers before her. This section reveals how the jeweler's formative years in Taiwan provided a rich source of inspiration for later work. Her parents were gem dealers from Thailand, and this early influence produced a natural gravitation toward high-end colored stones and diamonds. When a shoulder injury ended her career as a cellist, she took a jewelry design course. For Hu, designing jewelry is like composing music. She transferred her passion for creating beautiful music to fashioning objects of beauty, each with an energy of its own.

David Warren's "Appreciating Rarity" chapter gives the art world perspective on her works. Very few designers show the vibrant originality that "gives you a rush of excitement" and moves the soul. Warren describes what it takes for jewelry to stand the test of time, comparing Hu's work to pieces from the Art Deco, Belle Epoque, and Art Noveau periods. There are designers who take their inspiration from the great brands such as Cartier, Bulgari, and Van Cleef & Arpels, but Hu's pieces represent a truly creative new age fusion of Asian and Western influences that moves the soul.

The "Opus 1" catalogue takes the reader on the journey Hu traveled with each work. The 99 pieces are beautifully photographed, many with original drawings and sketches. Informative captions give the title of the piece and describe the gemstones used and the artistic inspiration. The designs draw upon nature, gradation (the blending of colors), organic forms, butterflies, koi fish, birds, and snakes. The "Fantasy Garden" section showcases Hu's botanical repertoire. Time spent in Monet's garden in Giverney at age 20 is revealed in her Monet's Water Lilies necklace and Van Gogh's Iris bangle. The four seasons are another recurring theme in her works. Beautiful photos help the reader understand how Hu's pieces represent, in her own words, a "song in love of jewels."

For the gemologist, *Symphony of Jewels* shows how important gemstones are being used today. It features mouthwatering Burmese rubies, jade, Kashmir sapphires, Golconda diamonds, tsavorite garnets, moonstones, alexandrite, Paraíba tourmaline, sapphires of all colors, and pearls. For the modern jewelry designer, it offers a look at a contemporary Asian design aesthetic, and the direction of high-end jewelry in this decade.

MELINDA (LINDY) ADDUCCI
DuMouchelles Art Gallery
Detroit

Celebrating Jewellery: Exceptional Jewels of the Nineteenth and Twentieth Centuries

By David Bennett and Daniela Mascetti, 323 pp., illus., publ. by Antique Collector's Club, Woodbridge, UK, 2012. $US125.00

In this extraordinary tome, jewelry auctioneers Daniela Mascetti and David Bennett reunite to deliver a sequel to their classic *Understanding Jewellery* (first published in 1989). Some of the jewels presented here are among the finest ever created. One could almost think of their work as the catalogue of an extraordinary jewelry exhibition. This remarkably hefty volume highlights 125 jewelry

pieces auctioned by Sotheby's over the past 30 years. The selections, based solely on the authors' personal tastes, include creations by Belperron, Boivin, Boucheron, Bulgari, Castellani, Chaumet, Giuliano, JAR, Lalique, Lemonnier, Schlumberger, Van Cleef & Arpels, and Vever.

Celebrating Jewellery takes the reader on a historical journey in five chapters, from before the 19th century through the 20th century. The authors have carefully selected some of the most exceptional jewelry pieces of each period. For instance, the emerald and diamond tiara of Princess Henckel von Donnersmarck is one of the iconic pieces of the "Nineteenth Century and Earlier" chapter. "Revivalism" displays artful creations from 1850 to 1890, with references to jewelry inspirations from antiquity. One of the strongest visuals of this chapter is the micromosaic Gorgon brooch. The most outstanding examples from the Belle Époque chapter is the Mountbatten Kokoshnik tiara. One of the most magnificent Art Deco pieces is Daisy Fellowes's emerald bead and diamond necklace/bracelets. The book's final chapter, "The Twentieth Century—The Nineteen Thirties and Later," is well illustrated with an opulent multi-gem cabochon bib necklace by Bulgari.

After a short historical introduction to each era, the authors' selections are described in brief vignettes, as in an exhibition catalogue. Illustrations are clearly the strong suit of this volume. The renderings are consistent throughout. Some of the photos are so clinically precise that the reader can observe abrasions on diamonds, culet sizes, and colored stone inclusions. One can also sense the thinness of mountings, types of settings, metal finishes, and other details. Some pieces, particularly in the Art Deco section, are displayed to showcase their flexibility and articulation. Micromosaic, granulation, and filigree textures are perceptible in other photos.

Two chapters are particularly captivating from a historical viewpoint: "Nineteenth Century and Earlier" presents extremely rare jewelry that has seldom been displayed. The historical context provided is of great value in understanding the uniqueness of the pieces. And the Belle Époque chapter is noteworthy for the magnificence of the jewelry and the stylistic contrasts between the garland-style and Art Nouveau creations. One might wish to see the actual jewelry sizes, since these details were available to the authors. Similarly, no mention is made of the end of the photo magnifications, which differ from one page to the next.

Even so, this volume is a must-have for jewelers, collectors, and antique jewelry professionals. The outstanding quality of the photos is an exceptional asset to that end.

DELPHINE A. LEBLANC
Hoboken, New Jersey

OTHER BOOKS RECEIVED

Jewels of the Early Earth: Minerals and Fossils of the Precambrian. *By Bruce L. Stinchcomb, 160 pp., illus., publ. by Schiffer Publishing, Atglen, PA, 2012. US$29.99.* This book addresses the geology, mineralogy, and paleontology of the earth's first two billion years, the Precambrian era. Topics from the nine chapters include: the geology of the shield areas and their rocks and minerals; outcrops of rocks that contain fossil evidence of the earliest life on the planet; early limestone that converted to marble, yielding decorative rocks and gemstones for mankind; pegmatites and the gems and minerals contained within; ancient rock belts of greenstone and their association with the planet's gold deposits; and the curious banded iron formation strata, rock associated with the very atmosphere. These and other topics are contained within 160 pages and supplemented by over 650 color photographs.

MICHAEL T. EVANS
Gemological Institute of America
Carlsbad, California

The Queen's Diamonds. *By Hugh Roberts. 319 pp., illus., publ. by Royal Collection Publications, London, 2012. US$95.00.* Published to coincide with Queen Elizabeth II's Diamond Jubilee, this work documents the personal jewelry collections of the female monarchs of Great Britain, from Queen Adelaide in 1831 to the present. Roberts provides a wealth of information on the jewelry, the makers, and the queens themselves. Includes extensive photographs, both black-and-white and color.

GIA LIBRARY STAFF
Gemological Institute of America
Carlsbad, California

Amethyst: Uncommon Vintage. *By H. Albert Gilg, Suzanne Liebetrau, Gloria A. Staebler, and Tom Wilson, Eds., 124 pp., illus., publ. by Lithographie, Ltd., Denver, 2012. US$35.00.* This monograph is a collection of articles from several contributors on topics such as amethyst's origin, mineralogy, optical properties, localities, and lore. It is lavishly illustrated with color photos of mineral specimens, localities, and jewelry. Also included are a glossary of terms and a bibliography.

GIA LIBRARY STAFF

COLORED STONES AND ORGANIC MATERIALS

Ein Beitrag zum Thema Bernstein—Unterscheidung von Bernstein und Kopal sowie Erkennung von behandeltem grünen Bernstein [A contribution to the topic amber—differentiation between amber and copal as well as determination of treated green amber]. K. Schollenbruch, *Zeitschrift der Deutschen Gemmologischen Gesellschaft*, Vol. 61, No. 1–2, 2012, pp. 13–34 [in German].

Copal and amber are natural resins at different stages of fossilization containing different amounts of volatile elements. A number of tests used to distinguish them (microscopic observation, color comparison, scratching, burning, organic solvents, UV fluorescence, and FTIR spectroscopy) are discussed in this article.

While two different types of natural green amber have been known for a long time, artificially colored green amber has become popular in recent years. Its color is produced by an autoclave treatment. This raises the problem of distinguishing natural from artificial green amber, and determining whether the starting material was copal or amber. Here the traditional tests such as scratching do not work. Only FTIR spectroscopy can provide definitive results. *RT*

Exotic common opals. H. Serras-Herman, *Rock & Gem*, Vol. 42, No. 10, 2012, pp. 26–30.

"Precious" opal exhibits the fiery multicolored flashes known as play-of-color. But there are a wide range of opals without this optical phenomenon that have beautiful colors and patterns in their own right. This article surveys the often underappreciated "common" opal and its versatility as a lapidary gem material.

This section is designed to provide as complete a record as practical of the recent literature on gems and gemology. Articles are selected for abstracting solely at the discretion of the section editors and their abstractors, and space limitations may require that we include only those articles that we feel will be of greatest interest to our readership.

Requests for reprints of articles abstracted must be addressed to the author or publisher of the original material.

The abstractor of each article is identified by his or her initials at the end of each abstract. Guest abstractors are identified by their full names. Opinions expressed in an abstract belong to the abstractor and in no way reflect the position of Gems & Gemology *or GIA.*

Vivid blue opal from Peru and Oregon often contains scenic white banding patterns, and specimens can be fashioned into cabochons, carvings, or slabs. Peru is also the source of fine pink opal, which ranges from pastel to deep pink and often has veining or dendritic inclusions. Its compact structure makes it a superb lapidary material. Similar-looking opal has come from Arizona and Idaho. Tanzania, Kosovo, and Brazil have supplied much of the green opal on the market. The new Morado opal from Mexico displays a purple color with swirls of white. There are also honey-colored, lemon yellow, and white varieties.

Common opal is hard enough to take a polish, and many specimens reveal their interesting patterns after cutting. The gem's beauty is completely natural rather than the product of heating or irradiation, which adds to its appeal. (Fractured specimens may be given a stabilizing treatment.) While common opal is generally more affordable than its play-of-color counterpart, the price of certain varieties has risen dramatically in the past two decades. *Stuart Overlin*

Geographic origin of gems linked to their geological history. G. Giuliani, D. Ohnenstetter, A. E. Fallick, L. Groat, and J. Feneyrol, *InColor*, Spring 2012, pp. 16–27.

In today's gem market, the geographic origin of a gemstone is critical. Knowledge of gem deposit geology is very important to determining the geographic origin of gemstones. There are two main types of gem deposits: primary and secondary. Primary deposits can be divided into three types: magmatic, metamorphic, and sedimentary. The magmatic type can be subdivided into two subgroups—magmatic deposits, such as corundum in alkali basalts, and magmatic-metasomatic deposits, such as pegmatite in schist or marble. The metamorphic type can also be divided into two subgroups: metamorphic deposits (e.g., corundum in marble) and metamorphic-metasomatic deposits, which are usually found in metamorphosed shale. The sedimentary type includes emerald deposits formed in black shales, such as Colombian emerald deposits, and it is usually related to the hydrothermal fluid circulation in fault and shear zones High-value colored gem stones usually formed in rift, subduction, and collision tectonic regimes for the past 3 Ga.

Three main periods were identified for the formation of corundum: (1) the Pan-African orogeny (750–450 Ma), which formed ruby, sapphire, garnet, tourmaline, and tanzanite in the Gemstone Belt of East Africa; (2) the Himalayan orogeny (45–5 Ma), associated with ruby and spinel formation in marbles; and (3) the Cenozoic (65–1.65 Ma), associated with the extrusion of alkali basalts carrying xenocrysts of blue-green-yellow sapphires.

Emeralds were formed during several orogenies from the Archean (2.9 Ga) to the Cenozoic (8 Ma). The Colombian emerald deposits were produced by reaction between high-salinity brines and black shales. Pyrite precipitation occurred before emerald formation, causing poor iron content in these specimens. The jagged three-phase inclusions were caused by alteration during the cooling process. The Chivor deposits were formed at 65 Ma, followed by Coscuez and Muzo at 38–35 Ma. These deposits were formed as a result of basinal fluid circulation along the hanging-wall of the faults in the Eastern Cordillera basin. In the Kaduna plateau of Nigeria, emerald deposits were formed in pegmatitic pods in anorogenic granites. These emeralds typically contain halite-bearing fluid inclusions, and very low Na, Mg, and Cr contents. Emerald deposits in Santa Terezinha de Goiãs in Brazil and Swat in Pakistan are metamorphic-metasomatic type. They were formed in shear zones of phlogopite- or talc-carbonate host rocks. Their oxygen isotope values and higher Mg, Cr, Na, and Fe contents can be used to determine specific origin. The Panjshir Valley deposits are metamorphic-metasomatic type, hosted in schist. These emeralds' fluid inclusions contain halite and sylvite. Some emerald deposits were formed by regional metamorphism, such as Habachtal in Austria; Jebel Sikait, Jebel Sakara, and Umm Kabo in Egypt; and Gravelotte in South Africa.

The three types of ruby deposits are based on oxygen isotope: marble, desilicated pegmatite, and mafic-ultra mafic. Similar geologic environments can produce rubies with similar characteristics and quality across different geographic locations, such as the ruby deposits from Afghanistan to Vietnam. Rubies were formed in either CO_2-COS-H_2S-S_8 or Na-Ca-K-SO_4-CO_3 fluids, which can mobilize Al, Cr, and V from host marble. Yet they are different from marble-hosted deposits in Lukande, Greyson, and Kitwalo in the Mahenge district of Tanzania, where marble was injected by amphibolitized mafic dikes. Ruby was hosted in metamorphic-metasomatic rocks in the Winza deposits of Tanzania. Corundum from an alkali basalt environment can be categorized into three groups. The first group includes ruby of metamorphic origin, regardless of geographic location. They are usually Cr-rich and Ga-poor. The second group contains blue, green, and yellow sapphires of alkaline origin. They are Cr-poor and Fe-Ti-rich. The third group is composed of sapphires of metamorphic-metasomatic origin formed in granulite facies.

There are two types of spinel deposits: metamorphic, in which red to pink to red-orange spinels formed, and metamorphic-metasomatic, the source of blue, violet, green, and brown specimens. The former is rich in Cr, Fe, Zn, and V, the latter in Fe, Zn, and Co. Alexandrite was formed at 254 Ma during the collision of the Gondwana and Laurasia (e.g., in the Urals). Identification of geographic origin for tsavorite is still in the preliminary stage. The combined application of $\delta_{18}O$ values and V-Cr-Mn concentrations may be useful for this purpose.

Although our geological knowledge of gemstone for-

mation has been broadened and more advanced technologies have been developed, limitations on geographic origin determination do still exist. *KSM*

Knights in pearly armour. R. Gupta, *Solitaire*, No. 61, August/September 2012, pp. 68–73.

Pearl farms are, out of necessity, eco-friendly enterprises: High-quality cultured pearls cannot be grown in polluted, overcrowded waters. But three manufacturers have gone a step further, and this article profiles their efforts to make pearl farming more sustainable and environmentally conscious.

Jewelmer, which harvests golden South Sea pearls in the Philippines, strives to control the release of potentially harmful emissions. The company has also created fish sanctuaries and supported foundations committed to marine conservation and sustainability.

For Tahitian pearl producer Kamoka, environmental conscientiousness begins at the grafting stage, with the use of nuclei made of mother-of-pearl from their own farms rather than the endangered North American mussel. Their farms harness solar and wind power and use fish to nibble-clean the oysters instead of blasting them with high-pressure water hoses.

Mikimoto, the brand that originated the cultured pearl a century ago, has conducted major research to prevent the spread of "red tide" plankton, which have devastated akoya oyster populations in the past two decades. Like Jewelmer, it is committed to a zero-emissions policy. Every part of the mollusk finds a use, from compost to cosmetics.

These companies' environmental measures have improved the quality of their products and helped position the cultured pearl as a symbol of natural harmony and sustainability. *Stuart Overlin*

Kristalle aus dem Gletschereis [Crystals from the ice of glaciers]. M. Wachtler, *Lapis*, Vol. 37, No. 9, 2012, pp. 22–30 [in German].

The recession of the glaciers in the Alps constantly exposes new areas of rocks covered by ice and snow for thousands of years, including alpine fissures with rock crystals and smoky quartz. The Tomaschetts, a well-known family of rockhounds from Disentis, Switzerland, are searching these areas in Val Cristallina, Graubünden/Grisons, Switzerland, near the glacier on Péz Valatscha. In 2006, the family discovered a series of alpine fissures filled with hundreds of sensational rock crystal and smoky quartz specimens, many of them floaters, of up to 1 m. The crystals were often embedded in chlorite sands, and many of the fissures were filled with ice (which is why the ancient Greeks thought rock crystals were unmeltable ice).

Working only in the summer, the Tomaschetts needed several years to recover the crystals, and the exploitation of the fissures is still ongoing. The author vividly describes the difficulties such as the constant danger of rockfall) and illustrates the article with beautiful photos, including some of spectacular specimens. *RT*

DIAMONDS

Causes of colour in fancy white diamonds. C. Payne and R. Bauer [info@bauergemlabs.com.au], *Australian Gemmologist*, Vol. 24, No. 9, pp. 212–214.

This paper discusses the causes of color in four fancy white faceted diamonds ranging from 0.89 to 1.62 ct, concluding with a brief discussion of white diamond clarity grading.

Two of the diamonds were translucent. One was colored by fine, complex multi-level whitish graining observed under 20× magnification. The other translucent stone did not show any inclusions, even under 100× magnification; its white color is probably due to light scattering from submicroscopic particles. The third diamond's patchy white, uneven saturation is caused in part by small voids from fine veils of negative crystals and their surface imperfections, as well as a possible growth defect (suggested by the cloud-like structure). The uniform color and saturation of the fourth fancy is caused by extremely subtle opaque white features raised on the surface; these are either microscopic knots or microdiamonds within the stone, and their associated surface draglines.

White diamonds with an even color are clarity graded by ignoring their bodycolor and focusing on visible inclusions using established criteria. *ERB*

Infrared microspectroscopy of natural Argyle pink diamond. C. Byrne, [kbyrne@physics.uwa.edu.au], J. Anstie, J. Chapman, and A. Luiten, *Diamond and Related Materials*, Vol. 23, 2012, pp. 125–129, http://dx.doi.org/10.1016/j.diamond.2012.01.032.

The crystalline lattice defect responsible for the coloration in natural pink diamond (its "color center") has yet to be identified. One of the distinctive features of pink diamonds is their color-containing lamellae, or "graining," believed to be atomic dislocations from plastic deformation while the diamond was still in the earth's upper mantle. The pink coloration, which produces a pair of absorption bands at 550 and 390 nm, also exhibits photochromic behavior. When exposed to blue (435 nm) and ultraviolet (310 nm) light, the intensity of the pink coloration and its absorption bands can be changed in a controlled and reversible fashion.

This study considers whether the atomic defect associated with the coloration is related to variation within the colored graining and the transparent regions of a pink diamond, and if it may be explained by correlating common infrared absorption features of the diamond and corresponding visible-light outputs.

Optical and IR microspectroscopy were used to identify the degree of spatial correlation between the IR absorp-

tion peaks and the pink coloration of single-crystal Argyle natural pink diamond. A distinctive feature is noted in the ~1500–1000 cm^{-1} spectral region. The results from defect population mapping indicate a relative scarcity of the nitrogen B-center (N–V–N3) in the regions of strongest pink color. Further, no change is observed in any IR feature (including the B-center) in response to induced photochromic changes of the sample pink diamonds.

The authors propose a possible mechanism by which B-centers might have been destroyed during the creation of the pink lamellae graining: Diamond planes sheared during plastic deformation, generating daughter defects of various nitrogen/vacancy forms, such as H3, N3 (N_3–V), and N centers. It is also possible that the pink color center, like the H3 and N3 centers, has no specific absorption feature. *ERB*

GEM LOCALITIES

Li-bearing tourmalines in Variscan granitic pegmatites from the Moldanubian nappes, Lower Austria. A. Ertl (andreas.ertl@a1.net), R. Schuster, J. M. Hughes, T. Ludwig, H.-P. Meyer, F. Finger, M. D. Dyar, K. Ruschel, G. R. Rossman, U. Klötzli, F. Brandstätter, C. L. Lengauer, E. Tillmanns, *European Journal of Mineralogy*, Vol. 24, No. 4, 2012, pp. 695–715, http://dx.doi.org/10.1127/0935-1221/2012/0024-2203.

The authors examine the crystal structure, chemistry, and spectroscopy of colored tourmaline and chemical data of coexisting minerals from three granitic pegmatites from the Moldanubian nappes. They are located at Konigsalm, Maigen, and Blocherleitengraben in the area northwest of Krems an der Donau.

The authors also determine the time of crystallization of two of the pegmatites by Sm-Nd analysis on garnet, feldspar, monazite, and xenotime and by a chemical U-Th-Pb monazite age. On the basis of mineralogy, chemical composition, and crystallization ages, the evolution of the pegmatites is discussed in the framework of the geodynamic history of the Bohemian massif. The regional geology and a thorough description of the investigated pegmatites are presented.

Tables of data are presented for eight different tourmaline samples, including information concerning crystal structure and chemical composition. Tourmaline's composition is dependent on the temperature and pressure as well as the chemical composition of the magmatic or metamorphic environment where the tourmaline formed. The composition bears information that can resolve many petrological questions.

The study concludes that tourmaline is a common phase in the investigated pegmatites and that that the crystallization of tourmaline phases likely depleted the melt in boron, removing a fluxing component. This would initiate a rapid crystallization of the pegmatite components.

DAZ

Natural alexandrites and chrysoberyls from Madagascar with irregular and regular growth patterns. K. Schmetzer, *Australian Gemmologist*, Vol. 24, No 10, pp. 243–248.

Microscopic internal growth features commonly seen in synthetic alexandrite (grown using the floating zone method by the Japanese manufacturer Seiko) were also noted in natural samples reportedly from at least two localities in Madagascar (Ilakaka and Mananjary). Under crossed polarizers, an interference pattern showing multiple curved grain boundaries is considered diagnostic of synthetics grown by the floating zone method. A small sample (<10 stones) of natural alexandrites and chrysoberyls, displayed strikingly similar interference patterns. Unlike their synthetic counterparts, the natural samples also revealed plane parallel growth structures, associated with color zoning, that mimic crystal faces. These microscopic differences along with other analytical techniques should readily separate the natural from synthetic material. A larger sample size, particularly with precise details of provenance and sample acquisition, would lend support to these preliminary results.

KAM

Pressure-temperature-fluid constraints for the Emmaville-Torrington emerald deposit, New South Wales, Australia: Fluid inclusion and stable isotope studies. L. Loughrey, D. Marshall, P. Jones, P. Millsteed, and A. Main, Central *European Journal of Geosciences*, Vol. 4, No. 2, pp. 287–299.

This article presents two historic emerald mines in Australia. The Emerald mine is located near Emmaville in eastern Australia. It was formed in the Moule Granite stock, which is part of the New England fold and thrust belts. Emeralds were formed as "bunches" in pegmatite loads 50 mm to 1 m thick. They were found in cavities and associated with cassiterite, fluorite, arsenopyrite, wolframite, buebnerite, ferberite, and quartz. The Heffernan's Wolfram mine is located 5 km northwest of Torrington. Here, emeralds were formed in a decomposed pegmatite load 30 cm wide. These two mines are Type 1 deposits, in which metasediments are found at the contact zone.

Emeralds from these deposits show sharp color banding of green to greenish yellow and colorless parallel to the basal plane. They formed from a saline fluid composed of both liquid and vapor phases. Examination of fluid inclusions and chemical composition suggests that the green bands were precipitated from the liquid phase and the clear bands from the vapor phase. As the liquid-vapor interface shifted up and down repeatedly, the green and colorless bands occurred alternately. According to electron microprobe and cathodoluminescence (CL) analyses, the

green band was rich in Cr and V, while various Fe concentrations were detected across the color banding. The chemical plot of Cr, V, and Fe concentrations shows only a very slight difference compared to emeralds from worldwide. MgO and Na_2O values were extremely low, however. The process of emerald precipitation, dissolution, and subsequent re-precipitation was evident in the disrupted, irregular zones shown by backscatter electron and CL images. These images also revealed Brazil-law twinning. The Emmaville emeralds contained two- and three-phase inclusions along healed fractures, growth zones, or as isolated inclusions. Two-phase inclusions were originally trapped as vapor phase and three-phase inclusions as liquid phase. Two-phase inclusions (up to 210 microns in size) were composed of vapor and brine, and three-phase inclusions (up to 80 microns) contained brine, vapor bubble, and halite cube or solid. Three-phase inclusions were consistently found within Cr-rich zones. Similar fluid inclusions were also found in quartz associated with emeralds. Relative to SMOW (Standard Mean Ocean Water), the stable isotope values $\delta_{18}O$ and δD H_2O of fluids trapped in channel in the Emmaville samples were measured as 10.8 to 12.4‰ and –79 to –103‰, respectively. The microthermometric analysis of fluid inclusions revealed emerald formation pressure of >150 bars and temperature of >367°C, respectively. *KSM*

Sapphires related to alkali basalts from the Cerová Highlands, Western Carpathians (southern Slovakia): Composition and origin. P. Uher, G. Giuliani, S. Szakáll, A. Fallick, V. Strunga, T. Vaculovič, D. Ozdín, and M. Gregáňová, *Geologica Carpathica*, Vol. 63, No. 1, 2012, pp. 71–82, http://dx.doi.org/10.2478/v10096-012-0005-7.

This study presents a detailed description of the blue, gray-pink, and pink sapphires from the Cerová Highlands in the Western Carpathians (southern Slovakia), based on new analytical data (CL, LA-ICP-MS, EMPA, and oxygen isotopes). The sapphire occurs as (1) clastic heavy mineral in the secondary sandy filling of a Pliocene alkali basaltic maar at Hajná ka, and (2) crystals in a pyroxene-bearing syenite/anorthoclasite xenolith of Pleistocene alkali basalt near Gortva. The range and mean Fe/Ti, Cr/Ga, Ga/Mg, and Fe/Mg values plus the Fe. Ti, Cr, Ga, and Mg contents indicate bimodal origins with stronger affinity of blue sapphires (both Hajná ka and Gortva) to magmatic domain, and of grey-pink sapphires more related to the metamorphic one. The blue sapphires show similar $\delta_{18}O$ values: 5.1‰ in the Gortva xenolith, and 3.8 and 5.85‰ in the Hajná ka placer, which are comparable to those of mantle to lower crustal magmatic rocks. *GL*

Treasure Island: A mineralogical tour of Italy's Isle of Elba. E. A. Crawford, *Rock & Gem*, Vol. 42, No. 5, 2012, pp. 20–25.

Elba, the largest of seven islands in the Tuscan Archipelago, is also the most geologically diverse—nearly 200 mineral species are found here. The island is divided into three distinct regions: igneous rock in the west, metamorphic rock in the east, and sedimentary deposits of clay, sandstone, and limestone in the flat central region.

The author's tour of Elba begins in the west. Composed entirely of granite, Monte Capanne is the result of the largest igneous intrusion in western Tuscany. The mountain's pluton was fed by several veins of magma, one of them particularly rich in lithim and cesium. These additional elements permitted the formation of tourmaline. The island is best known for its elbaite, which was first discovered there in 1913. Rich in lithium, elbaite comes in various hues of pink, green, yellow, blue, and black. Schorl, a black tourmaline containing iron instead of lithium, is also common. Twenty species of beryl have been identified around the Monte Capanne area.

The rock of eastern Elba—composed primarily of gneiss, skarn, and marble—is metamorphic in origin, but there are distinct differences between the northern and southern regions. The southeastern peninsula is known for the prevalence of gneiss and a small but significant level of copper. Specimens of blue and green copper minerals have been found, including azurite, malachite, chrysocolla, and cuprite. Other minerals found in the area include magnetite, garnet, atacamite, brochantite, jarosite, gypsum, marcasite, galena, calcite, aragonite, siderite, dolomite, rhodochrosite, and smithsonite.

The town of Porto Azzurro marks the boundary between the northeastern and southeastern regions. The red, jasper-rich hills around Porto Azzurro are sedimentary, like much of central Elba. The eastern side of Cima del Monte, from Porto Azzurro to the northernmost town of Cavo, is the heart of Elba's mining culture. The hills are red with iron deposits that contributed to the success of the island's civilizations for thousands of years.

Minerals found in northeastern Elba include goethite, limonite, fluorite, calcite, aragonite, aurichacite, arsenopyrite (containing particles of gold, silver, and cobalt), diopside, sphalerite, galena, bismuthinite, gypsum, and chalcopyrite. *DAZ*

INSTRUMENTS AND TECHNIQUES

In situ analysis of garnet inclusion in diamond using single-crystal X-ray diffraction and X-ray micro-tomography. F. Nestola, M. Merli, P. Nimis, M. Parisatto, M. Kopylova, A. De Stephano, M. Longo, L. Ziberna, and M. Manghnani, *European Journal of Mineralogy*, Vol. 24, No. 4, 2012, pp. 599–606, http://dx.doi.org/10.1127/0935-1221/2012/0024-2212.

An innovative form of nondestructive analysis was performed on a microscopic garnet inclusion in a 0.001 ct dia-

mond from the Jericho kimberlite in Nunavut, Canada. First, X-ray computed microtomography (evolved from the "CAT scan") provided a 3D map of the inclusion, which measured only 0.1 mm in longest dimension. X-ray diffraction, accurately centered on the inclusion thanks to the 3D map, determined the inclusion's unit-cell parameters and fractional coordinates of oxygen atoms. This data was then inserted into a computer model based on multiple regression equations, assuming minimal residual pressure on the inclusion. The resulting garnet composition was within previously established limits determined by traditional destructive tests. Although still in its infancy, this technique holds considerable promise in accurately identifying other inclusions in diamonds and could aid aid in diamond exploration, provenance determination, and study of the earth's mantle. *KAM*

Spectroscopic identification of rubies. Y. Gayevsky, E. Grushinskaya, and E. Belichenko, *Russian Diamonds & Jewellery*, Winter 2012, pp. 12–14.

This study employed infrared spectroscopy along with X-ray fluorescence analysis to investigate 75 natural, lead glass–filled, and synthetic rubies (flux and Verneuil methods) ranging from 0.06 to 3.81 ct.

The natural ruby samples showed single peaks at 3309 and 3323 cm^{-1}, corresponding to the OH^- group and heat treatment. Impurity elements of Ti, Ga, and V were found. A piece of Mong Hsu rough showed peaks at 2125, 1990, and 1990 cm^{-1}, associated with the OH^- group present in boehmite.

The samples filled with lead glass revealed large quantities of Pb as well as the presence of Ti and Ga.

The Verneuil synthetic ruby samples showed infrared peak series 3419, 3278, and 3263 cm^{-1}; 3278, 3232, 3184, and 3164 cm^{-1}; and 3309, 3232, and 3184 cm^{-1} associated with the OH^- group. Diagnostic properties using X-ray fluorescence are not identified in these rubies.

The flux grown synthetic ruby samples show impurities of Pt, Bi, and Pb, but no diagnostic indications using infrared spectroscopy.

The authors conclude that infrared spectroscopy along with X-ray fluorescence analysis used together with standard gemological techniques enable a more precise identification of natural, lead glass-filled, and synthetic rubies. *ERB*

SYNTHETICS AND SIMULANTS

Photoluminescence studies of the 523.7 nm optical centre in HPHT synthetic diamond. W. Kaiyue, J. Steeds, and L. Zhihong, *Diamond and Related Materials*, Vol. 23, 2012, pp. 162–166, http://dx.doi.org/10.1016/j.diamond.2011.12.046.

The authors test the idea that the 523.7 nm optical center generally observed in electron-irradiated HPHT-grown synthetic diamond is associated with nitrogen interstitial complexes. This was the conclusion of absorption studies by A. T. Collins and S. Rafique (*Proceedings of the Royal Society of London A*, Vol. 367, No. 1728, 1979, pp. 81–97). This optical center is not observed in CVD-grown synthetic diamond with nitrogen contents up to 50 ppm. In the present work, the authors investigated HPHT synthetic diamonds, CVD synthetic diamonds, and ^{13}C- and ^{15}N-enriched materials using low-temperature photoluminescence (PL) techniques paired with irradiation and annealing experiments. To ensure they were studying the same optical center as Collins and Rafique, the authors borrowed some of the original samples from the earlier study.

Similar to Collins and Rafique, the authors found an increased intensity of the 523.7 nm emissions with increasing nitrogen content and an additional zero photon line (ZPL) emission at 626.3 nm. While the earlier absorption study showed reversible bleaching of the 523.7 nm center and increasing intensity of the 626.3 nm ZPL with exposure, the authors observed a reversible decrease in the 626.3 nm ZPL with an increase in 488 nm laser irradiation and no bleaching of the 523.7 nm center. Both groups noted the disappearance of the 626.3 nm center with annealing above 200°C. But whereas Collin and Rafique saw the 523.7 nm emission anneal out at 250°C, the present study did not observe this until above 750°C. The two sets of data—absorption and PL—actually obscure the origin of the 523.7 nm center in electron-irradiated synthetic diamond samples: The role of vacancies, nitrogen, or self-interstitials is still unresolved. *JS-S*

Star ruby. K. Schmetzer (SchmetzerKarl@hotmail.com) and T. Hainschwang (thomas.hainschwang@ggtl-lab.org), *Gems & Jewellery*, Winter 2011/2012, Vol. 20, No. 4, pp. 14–17.

A star ruby marketed as natural initially showed no natural inclusions, growth structures, concentrations of rutile needles, or the commonly observed curved striations of Verneuil synthetics. Chemical and spectroscopic examination by X-ray fluorescence (EDXRF) revealed strong peaks of chromium and titanium and weaker peaks assigned to iron and nickel. The presence of lamellar grain boundaries with interference colors under crossed polarizers, as well as a distinct strain pattern, indicated that the core consisted of Verneuil-grown synthetic corundum. This suggests the formation of a thin chromium and titanium layer by overgrowth of a corundum cabochon in a flux-bearing environment, and subsequent formation of rutile precipitates by exsolution at lower temperatures. The ruby was manufactured, cut as a cabochon, and then treated to improve its color and induce asterism. *GL*

Synthetic star alexandrite. K. Schmetzer (SchmetzerKarl@hotmail.com) and A. Hodgkinson (alan-hodgkinson@talktalk.net), *Gems & Jewellery*, Autumn

2011, Vol. 20, No. 3, pp. 9–11.

A piece of rough Czochralski-grown synthetic alexandrite produced by Kyocera yielded a cat's-eye and a six-rayed star cabochon. The first step in the growth process is the production of homogeneous single crystals containing titanium oxide as a dopant. In the second step, the crystal is annealed at elevated temperatures in an oxidizing atmosphere. The rutile needles precipitated are responsible for the chatoyant effect when the material is cut as a cabochon. Chemical analysis by LA-ICP-MS confirmed that TiO_2 was applied as a dopant to create chatoyancy and asterism in these synthetic alexandrites. In natural chatoyant chrysoberyl and alexandrite, the tiny needles or channels responsible for the light bands are always oriented parallel to the a-axis. This information is useful in separating natural chatoyant alexandrites from synthetics with that have needles parallel to the c-axis. *GL*

The wolf at the door. J. Ogden, *The Jeweller*, August/September, 2012, pp. 75–76.

Jack Ogden, the former CEO of Gem-A, discusses the threat of synthetic diamonds to the jewelry industry today. The key issue is the inability to routinely distinguish synthetic diamonds from their natural counterparts. This lack of a simple detection method, paired with the cost differential between natural diamonds and synthetics, has led to an alarming lack of disclosure. Laboratories can detect many of the synthetics, but stone dealers and retailers by and large cannot.

Synthetic diamonds larger than 0.75 ct are rare, but small ones have become increasingly common, both mounted in jewelry and sold as loose stones. Because lab reports are not cost effective for smaller diamonds, a dealer or retailer must assume that these goods are potentially synthetic and factor this into purchasing decisions related to price. As a buyer, it is prudent to work with trusted suppliers and have a relationship with a laboratory capable of detecting synthetics. Ogden's final advice is to remember that a lab report is an opinion, but any implication of natural origin from the seller is a guarantee. *JS-S*

TREATMENTS

Le traitement thermique de l'andradite [Heat treatment of andradite]. P.-Y. Chatagnier, *Revue de Gemmologie A.F.G.*, No. 180, June 2012, pp. 12–16 [in French].

Heat treatment to enhance the color of Russian demantoids was mentioned by J. Stephenson and N. Kouznetsov ("Major deposits of demantoid around the world," *InColor*, Summer 2009, pp. 16–20), but no details of the process were described. Because no Russian demantoids were available, the present author only tested samples from Namibia and Madagascar. The stones were examined first by standard methods and then heated at 100°C increments for two hours, from 300° to 1000°C. The results of two representative stones from Namibia and Madagscar are described in detail. While the color enhancement claimed for Russian demantoids could not be observed, all of the samples turned brown at 1000°C. They could not be distinguished from natural brown andradites. The authors describe possible charge transfer processes, mainly of Fe and Ti, as the cause of the color change. *RT*